# CONSTRUCTION OF TSUNAMI INUNDATION MAPS

# IN THE GULF OF MEXICO

## Report to the National Tsunami Hazard Mitigation Program

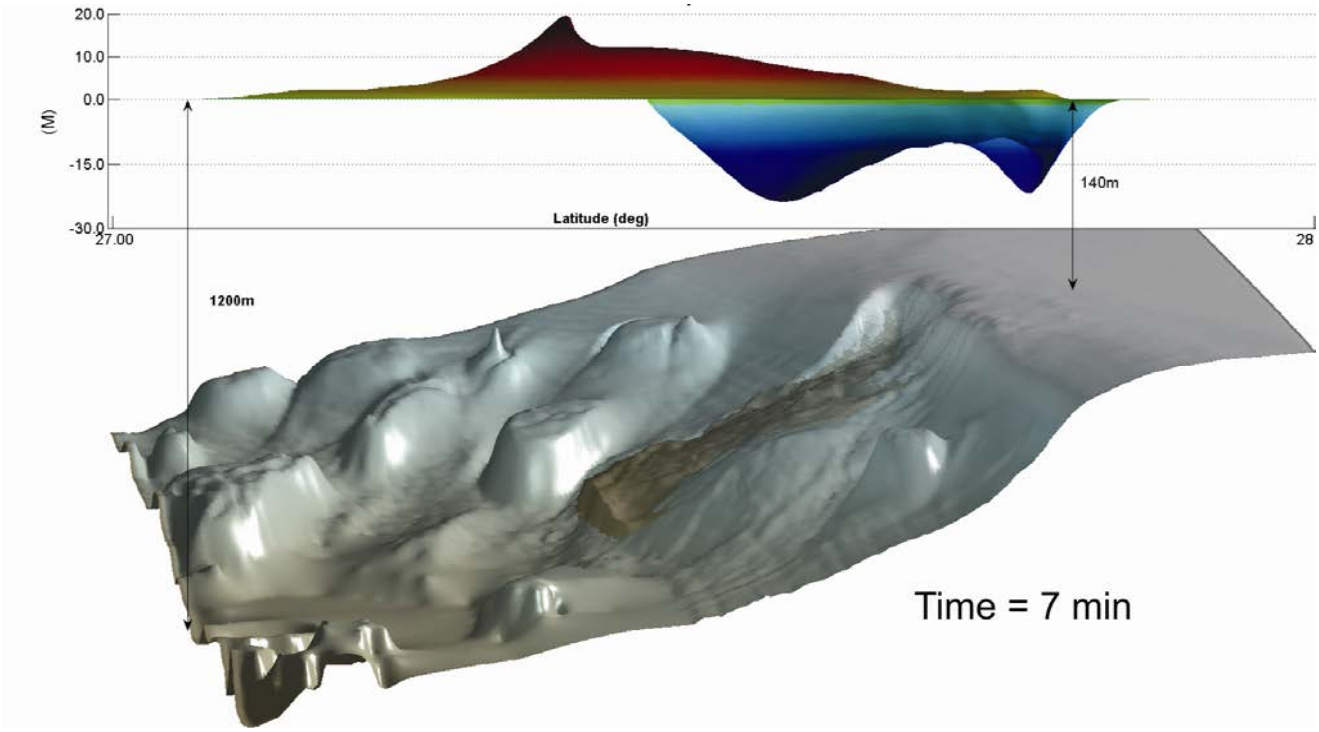


East Breaks Submarine Landslide -3D Numerical Simulation-

**Report of Investigation**

# CONSTRUCTION OF TSUNAMI INUNDATION MAPS IN THE GULF OF MEXICO

Report to the National Tsunami Hazard Mitigation Program

by:

**Juan J. Horrillo[1], Amanda L. Wood[1],**
**Charles Williams[2],**
**Ashwin Parambath[1] and Gyeong-Bo Kim[1]**

[1] Maritime Systems Engineering, Texas A&M University Galveston
[2] Preparedness Section Chief, Alabama Emergency Management Agency.

December 31/2010 Revision: 1

# Table of Contents

# Table of Figures

## Executive Summary

This study determines all elements necessary to construct the first tsunami inundation map to communities in the Gulf of Mexico (GOM) that will provide guidance to state emergency managers and optimize real-time tsunami warnings. Consequently, a detailed tsunami hazard assessment is presented for the selected community of Port Aransas, Texas. In addition, the study evaluates tsunami hazard for various coastal regions throughout the GOM.

Potential tsunami sources for the GOM are local submarine landslides, which have been examined by the Atlantic and Gulf of Mexico Tsunami Hazard Assessment Group , ten Brink et.al., 2009. In their findings, they stated that submarine landslides in the GOM are considered a potential tsunami hazard. However, the probability of tsunamis generated by large landslides are quite rare. This probability of occurrence is related to ancient and large landslides which were probably active prior to 7,000 years ago when large quantities of sediments were emptied into the Gulf of Mexico. Nowadays, sediment continues to empty into the Gulf of Mexico from the Mississippi River. This sediment supply contributes to slope steepening and increasing fluid pore pressure in sediments, which may lead to further landslide activity. Hence, the reason for the study on potential tsunami hazard effects in the Gulf of Mexico.

The construction of the first tsunami map is based on these identified ancient events of local submarine landslides. In order to estimate the extent and magnitude of the inundation by tsunami waves generated from local landslide sources, 3D and 2D numerical models have been used. Several tsunami scenarios were investigated, resulting in tsunami waves generated by three ancient underwater landslides: the East-Breaks, Mississippi Canyon and West Florida. Tsunami flooding inland-extent, maximum inundation depth, maximum inundation elevation and maximum momentum flux and direction were determined within the hazard areas of Port Aransas. Our study has confirmed that these landslide scenarios have indeed the potential to cause severe flooding and damage to the GOM coastal

communities. It is proved that such landslide sources can flood the entire town of Port Aransas with an average water elevation of 7 - 13ft (2.1 - 3.9m) or average water depth of 3 -8ft (0.9 - 2.4m). The tsunami flooding generated by these events is comparable to the maximum possible flooding that can be generated by hurricanes of category 2 to 4. Tsunami energy focusing is identified in several regions along the US GOM coastline, as well. Regions most impacted are located at the southern tip of South Padre Island, TX., Grand Island, LA, Fort Walton Beach-to-Cape San Blas, FL, and the northern region of the state of Tamaulipas, Mexico.

The results of the tsunami numerical modeling along with the regional historic observations are intended to provide guidance to local emergency management with evacuation planning and public education on reduction of potential tsunami hazards.

# Introduction

Gulf of Mexico (GOM) coasts were included to the U.S. Tsunami Warning System in January 2005. The main purpose of the warning system is local emergency management's capability to act in response to warnings. To plan for the warning response, emergency managers must understand what specific areas within their jurisdictions are threatened by tsunamis. Hazard areas can be determined by historical events or by modeling potential tsunami events (worst case scenario) or by using a probabilistic approach. As the GOM has no significant recent historic tsunamis records, numerical modeling must be used to determine coastal hazard zones. Potential tsunami sources for the GOM are local submarine landslides and earthquakes along the Caribbean plate boundary faults. Preliminary modeling of potential tsunami sources outside the GOM by Knight, (2006) indicated a very low threat and may not pose a tsunami hazard to the GOM coastal communities; however, ancient submarine landslides within the GOM may have generated tsunamis as examined by the Atlantic and Gulf of Mexico Tsunami Hazard Assessment Group (THAG), ten Brink *et.al*., 2009. In their findings, they stated that submarine landslides in the GOM are considered a potential tsunami hazard for the following reasons:

1. Some dated submarine landslides in the GOM have a post-glacial age
2. Large landslides in the GOM have been found in the submarine canyons and fan provinces extending from present Mississippi and other former large rivers that emptied into the GOM These large submarine landslides were probably active before 7500 years ago
3. Recent suggestions from seismic records of small-scale energetic submarine landslides in the GOM indicate that there is a probability of recurrence

Therefore, this study aims to verify if an event of such characteristic might certainly be a threat to the GOM's communities, and if so, what would be its effect in terms of inundation.

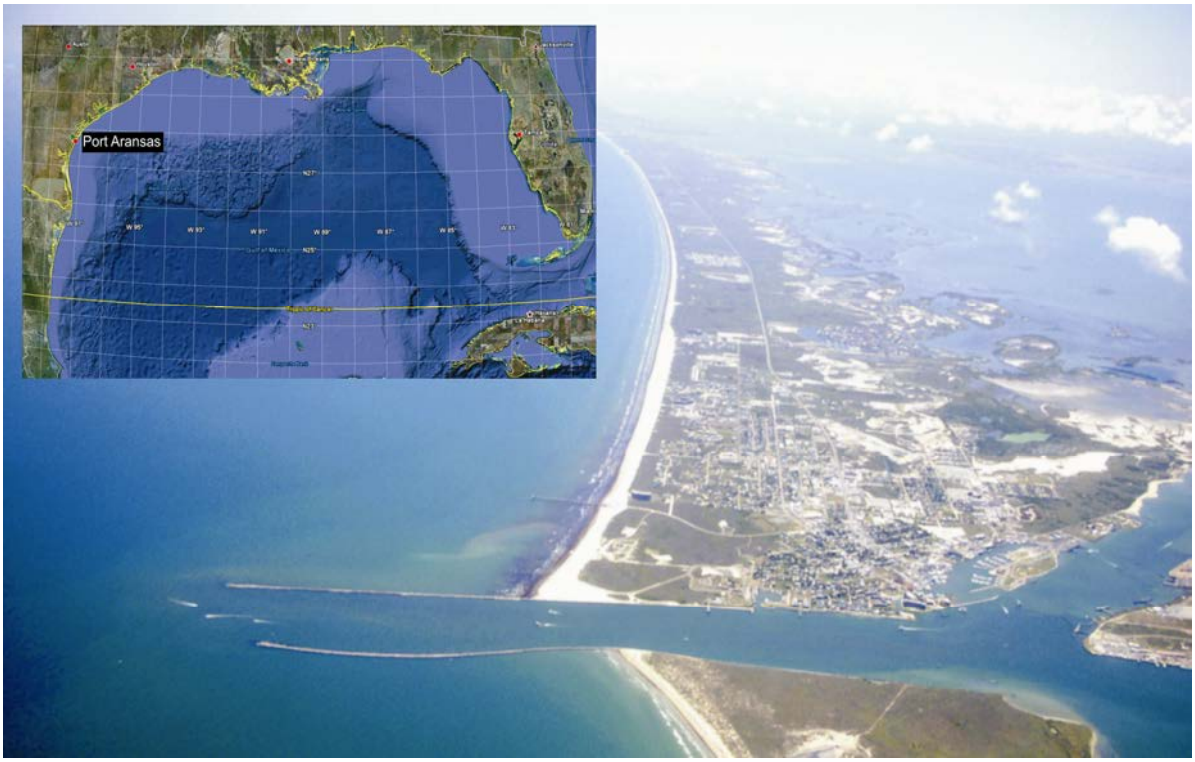


**Figure 1.** Aerial view of Port Aransas, Texas. Upper-left corner, location of Port Aransas, (source Google Earth).

This study determines all elements necessary to construct the first tsunami inundation map that will provide guidance to state emergency managers and optimize real-time tsunami warnings to communities on the GOM coastline. The construction of the first tsunami map is based on identified ancient events of local submarine landslides as described by THAG. The community selected to generate the first tsunami map is Port Aransas, Texas, see Figure 1. The selection of Port Aransas was made according to a preliminary study aiming to determine vulnerable areas for these identified past events. The selection was based on the proximity of ancient submarine landslides, tsunami energy focusing, affected community population (size) and the quality of existing local bathymetric and topographic data (DEM available). Tsunami flooding inland-extent, maximum inundation depth, maximum inundation elevation and maximum momentum flux and direction were determined within the hazard areas of Port Aransas.

## Regional and Historical Context

Port Aransas, Texas is a resort and fishing community on Mustang Island, located 24 miles northeast of Corpus Christi in the northeastern corner of Nueces County. Port Aransas was originally occupied by the Karankawa Indians who led a nomadic existence, migrating from the mainland of Texas to the coast (Kuehne, 1973). It was not until 1519 that the first Anglo-European stepped foot on the coast of Port Aransas, which up until 1833, was called Sand Point. Port Aransas' early economic reliance was on ranching, but as time progressed the town became more reliant on tourist attractions such as fishing and beaches.

Port Aransas was almost completely wiped out by the 1919 hurricane, which came on land between Brownsville and Corpus Christi. A storm surge of approximately 20 ft (6 m) high passed over the town wiping out most of the buildings and the dune systems (Myers, Butman, & Brown, 2006). Many of the residents, who survived the hurricane, left Port Aransas. It took many years for the islanders to rebuild the town. According to the report written by Myers, *et al.* (2006), the 1925 census shows that the Port Aransas population grew to 250 permanent residents. Since then, many hurricanes have come and gone. One of the largest hurricanes to hit Port Aransas was Hurricane Carla, which came ashore in 1961, causing massive destruction to the island, see Figure 2. Many other hurricanes had cause severe inundation and destruction; once again, rebuilding Port Aransas was a slow process.

Port Aransas currently remains as a relatively small community with a total population of 3,370 per the census 2000 demographic profile obtained from U.S. Census Bureau data ("2000 Census Data," 2010). However, during the summer months the population grows significantly to well over 20,000 during peak tourism.

### Tsunamis in the Gulf of Mexico

Usually the Gulf-coast communities are impacted by surges generated from hurricanes rather than tsunamis. The first recorded hurricane to impact Port Aransas was in June 1902. After that time, eleven

hurricanes passed over Port Aransas. The famous 1919 hurricane landed ashore between Brownsville and Corpus Christi; however, it caused the destruction of almost every building in Port Aransas.

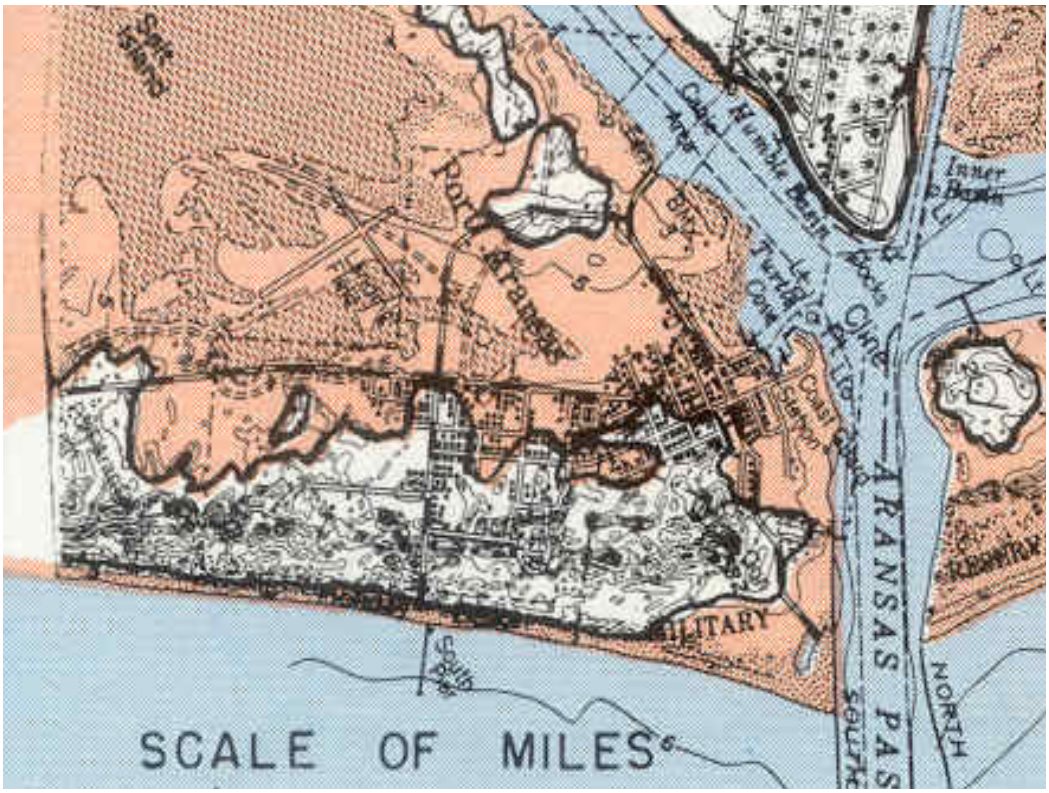


**Figure 2** . Port Aransas inundation due to hurricane Carla 1961. Dunes were not breached. Hurricane Carla's surge elevation ranges 8-9 ft. Pink solid hatch indicates inundated areas.

In August 1970, the first recorded hurricane named Celia passed directly over Port Aransas and the surge went directly into Corpus Christi Bay (Watson, 2009). According to a hurricane flood map produced by the U.S. Army Corps of Engineers (*Limits of Flooding City of Port Aransas*, 1971) the tide gauge just off the west side of Aransas Pass recorded a high water elevation of 8.0ft (2.4m), see Figure 3. The tide gauge located on the beach in Port Aransas recorded a crest high water elevation of 9.2ft (2.8m). The debris or drift-line elevation was recorded at 9.9ft (3.0m). The still high water mark elevation on the Corpus Christi Bay side of Port Aransas was measured at 8.9ft (2.7m) and 7.3ft (2.2m) just on shore. The still high water mark inland recorded an elevation of 8.5 ft (2.6 m). All recordings were measured from

the mean sea level datum. In all these hurricane events the dune systems were not breached; but, as it usually happens on communities that are settled close to a waterway access and protected by man-made/natural systems, most of the surge flood is generated from the lee part of the barrier island.

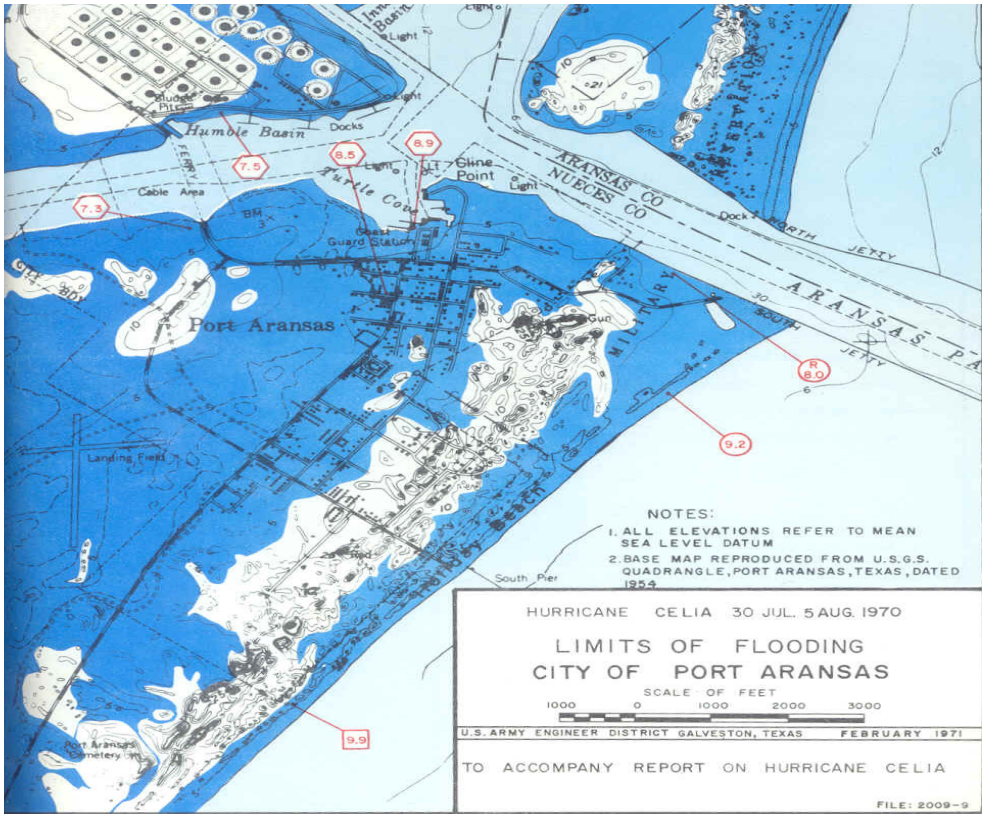


**Figure 3.** Port Aransas inundation due to hurricane Celia 1970. Dunes were not breached, Hurricane Celia's surge elevation was about 10 feet (3.0m). Blue solid hatch indicates inundation extent.

Hurricanes have greatly impacted Port Aransas and their likelihood is well documented. Using the numerical model SLOSH (Thomas LeBlanc personal communication) the maximum water elevation (Maximum of Maximum Envelope of Water (MEOW), MOM with respect to tide level -zero/high-) that can be expected from hurricanes in Port Aransas, TX. is shown in Table 1. This information has been provide as a frame of reference for comparison with tsunami numerical results.

**Table 1.** Maximum Water Elevation for hurricane of a given category in Port Aransas TX.

| Hurricane Category | Maximum Water Elevation Range (ft) | Maximum Water Elevation Range (m) |
|---|---|---|
| 1 | 4.3-4.9 | 1.31-1.49 |
| 2 | 7.3-7.6 | 2.22-2.31 |
| 3 | 9.6-10.3 | 2.92-3.14 |
| 4 | 13-13.2 | 3.96-4.02 |
| 5 | 16.3-16.6 | 4.97-5.06 |

The impact a tsunami might have on Port Aransas or coastline communities within the Gulf of Mexico is rare but not improbable. Recently, a national assessment of tsunami potential was performed by Dunbar and Weaver in 2008. In addition, a thorough review, performed by THAG, of the historical record regarding tsunamis in the Gulf of Mexico revealed that during the 20$^{th}$ century there have been three events consisting of tsunamis and seismic seiches measured and observed. The first event occurred on October 1918 when a seismogenic tsunami of small indeterminate amplitude originating west of Puerto Rico was recorded at the Galveston tide gauge station. The second event was on May 2, 1922, a tidal gauge station in Galveston recorded a 2.1 ft (0.64 m) amplitude wave, which was thought to have been generated by an earthquake in Vieques, Puerto Rico. However, THAG surmised that it was more likely a result of a source local to the Gulf of Mexico and Galveston. According to THAG, the third event resulting in seismic seiche waves, originating from the March 27, 1964 Gulf of Alaska earthquake, which reached a height of 0.6 ft (0.18 m) at the Freeport tide gauge station. These historical records of -small size tsunami amplitude- match very well the preliminary numerical modeling results of potential tsunami sources outside the GOM by Knight, 2006. The numerical results indicated a very low threat due to outside tsunami sources and they may not pose a tsunami hazard to the GOM coasts.

Port Aransas is protected by a wide band of strong and highly vegetated dune systems. The dunes, which are natural and man-made, act as a natural barrier to storm surges and alike; for instance, tsunamis. Tsunami period ranges around 10-30 minutes in contrast with storm surges that can last few hours (or few fraction of tide periods). During a storm surge, sealevel may change gradually, allowing beach storm

erosional processes to act along the dune system for an extended period. On the other hand, a tsunami wave has a relative short period, if it is comprared with a storm surge, but it has a steeper wave front with greater momentum which is more effective to produce substantial runups and therefore dune overtopping. Based on field visual inspection and numerical model results in Port Aransas, breaches (direct access from roads, homes or businesses onto the beach) and low elevation spots along the dune system crests are potential locations where tsunami may channel into the town. Figure 4 shows a typical example of a dune breach that has direct asccess to the beach.

Another example of a typical man-made breach in the dune system is shown in Figure 5. These types of breaches occur frequently throughout the dune systems. These breaches offer a great source of concern because weaken the dune systems by providing a source of access for storm surges and alike behind the dunes.

**Figure 4.** Dunes with a typical driveway breach and home behind

**Figure 5.** Dunes with breach along Port Aransas beach

## Landslide Hazard in the Gulf of Mexico

According to THAG there are no records which accurately date when landslides occurred in the past in order to determine what environmental or temporal conditions caused them. However, there are many temporally varying factors and geological characteristics which influence submarine slope stability in general. A few common causes of landslides include:

The location of the sediment deposits, particularly the slope of the sediment deposit.

Sediment deposits, which are relatively weak and produce a thick sediment layer in a short lapse of time over the continental slope (overpressure due to rapid accumulation of sedimentary deposit) have a greater chance for producing slope failures.

Earthquake or storm wave loading due to hurricane or extreme weather condition can build up soil pore pressure or cause gas hydrate dissociation.

The sea level plays a crucial role in increasing the chance for producing slope failures especially if the sea level is lowered near the shelf break.

Changes in seismicity related to isostatic loading or unloading of coastal and near-coastal regions by ice.

Changes in groundwater flow conditions within the continental slope and shelf.

The THAG concluded that the dominant factor which influences the times of occurrence of significant landslides is glaciation. The report also specified three geological provinces in the GOM that are likely to be the origin of submarine landslides. These provinces feature three major ancient scarps or excavations with their respective sediment depositions down slope that were capable to generate large tsunamis in the past. They are recognized as the East Breaks, Mississippi Canyon and the West Florida submarine landslides, see Figure 6.

The East Breaks landslide, which lies offshore of the Rio Grande River system is located in the salt province in the north-western part of the GOM. The East Breaks landslide occurred during the last lowstand of sea level and was the result of the failure of the shelf edge delta, which had accumulated sediment from the Rio Grande River over time. The Mississippi Canyon landslide is the largest and youngest of the landslides and is located in the canyon/fan province, which is at the outflow of the Mississippi River. The West Florida landslide is located in the West Florida Margins carbonate provinces, which rims the eastern side of the GOM. The landslide excavation is located on a gentler slope above the Florida Escarpment and it is sourced in Tertiary and Quaternary carbonate deposits. The most relevant information for the three submarine landslides is shown in Table 2.

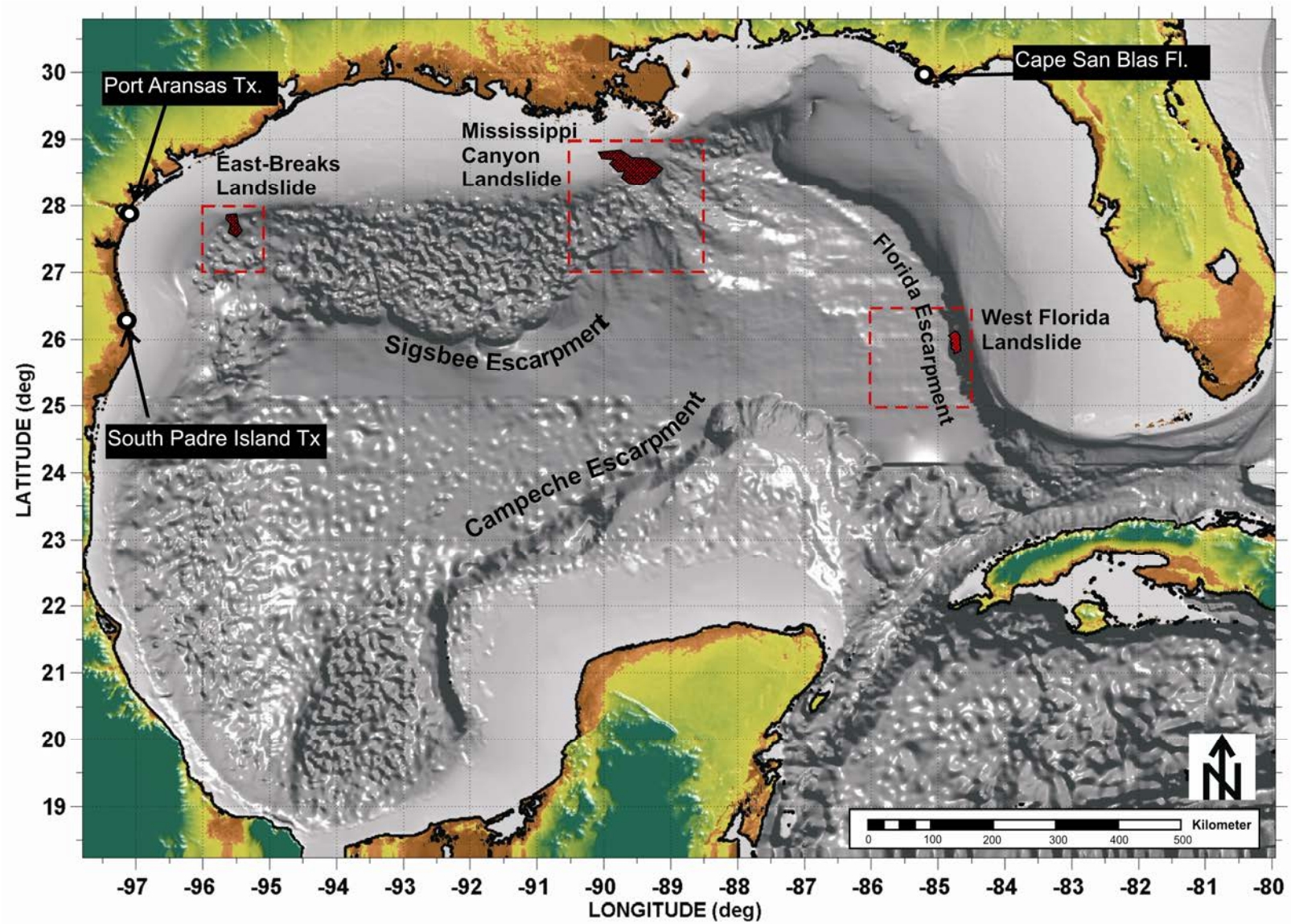


**Figure 6.** GOM's bathymetry and location of submarine landslides (in red) used to determine tsunami inundation in Port Aransas, TX. The landslides description and characteristics can be found in the Regional Assessment of Tsunami Potential in the Gulf of Mexico by ten Brink et.al., 2009. Bathymetry is derived from ETOPO1 (60 arc-seconds resolution), Amante and Eakins (2008). Dashed-red rectangles indicate domain with 15 arc-seconds resolution used for numerical calculation of the submarine landslide.

# Description of Numerical Models Used for Landslide Generation, Tsunami Waves Propagation and Inundation

For the construction of tsunami inundation maps in the GOM two numerical models are used:

1. The landslide generation (tsunami source) is taken by the 3D Navier-Stokes model developed by the University of Alaska Fairbanks (UAF) and Texas A&M University at Galveston (TAMUG) dubbed TSUNAMI3D for **T**sunami **S**olution **U**sing **N**avier-Stokes **A**lgorithm with **M**ultiple **I**nterfaces.
2. The tsunami wave propagation and inundation is carried out by the 2D non-hydrostatic/hydrostatic model developed by the University of Alaska Fairbanks (UAF) and the University of Hawaii (UH), NEOWAVE for **N**on-hydrostatic **E**volution of **O**cean **WAVE**.

## TSUNAMI3D Model

TSUNAMI3D code solves transient fluid flow with free surface boundaries, based on the concept of the fractional volume of fluid (VOF). The code uses an Eulerian mesh of rectangular cells having variable sizes. The fluid equations solved are the finite difference approximation of the Navier-Stokes and the continuity equations. The basic mode of operation is for single fluid calculation having multiple free surfaces. TSUNAMI 3D can also be used for calculations involving two fluids separated by a sharp or no-sharp interface, for instance, water and mud. In either case, the fluids may be treated as incompressible.

Table 2. GOM's Submarine Landslide Data (ten Brink, *et al.*, 2009)

| **East Breaks Landslide** | |
|---|---|
| Geologic Setting: | Shelf-edge delta |
| Post Failure Sedimentation: | Canyon appears to be partially filled) predominantly failure deposits with some post-failure sedimentation) |
| Age: | 10,000-25,000 years |
| Maximum Credible Single Event: | Max: Volume: 21.95 $km^3$<br>Area: 519.52 $km^3$ |
| Other Reported Volumes: | 50 – 60 $km^3$ |
| Excavation Depth: | ~160 m (shelf to base of headwall scarp) |
| Runout Distance: | 91 km from end of excavation and 130 km from headwall based on GLORIA mapping |
| Other Reported Runout Distance | 160 km |
| **Mississippi Canyon Landslide** | |
| Geologic Setting: | Shelf-edge delta and fan system |
| Post Failure Sedimentation: | Canyon appears to be partially filled (failure deposits or post-failure sedimentation) |
| Age: | 7,500 to 11,000 years |
| Maximum Credible Single Event: | Volume: 425.54 $km^3$ |
| Other Reported Volumes: | 1750 $km^3$<br>1500-2000 $km^3$ |
| Area: | 3687.26 $km^2$ |
| Excavation Depth: | ~300 m (in the upper canyon) |
| Runout Distance: | 297 km from toe of excavation area and 442 km from the headwall scarp |

| Florida Margin Landslide (Table 1 continuation) | |
|---|---|
| Geologic Setting: | Edge of a carbonate platform |
| Post Failure Sedimentation: | None visible on multi-beam images or on available high-resolution seismic profiles |
| Age: | Early Holocene or older |
| Maximum Credible Single Event: | Volume: 16.2 $km^3$ |
| Area: | 647.57 $km^2$ |
| Excavation Depth: | ~150 m, but quite variable |
| Runout Distance: | Uncertain. The landslide deposit is at the base of the Florida Escarpment buried under younger Mississippi Fan deposits |

Internal fixed or moving obstacles (bathymetry/objects) are defined by blocking out fully or partially any desired combination of cells in the mesh. The hydrodynamic (nonhydrostatic) pressure field is solved using the incomplete Choleski conjugated gradient method.

The 3D code was exclusively developed for tsunami purposes, under the supervision of Professor Zygmunt Kowalik, UAF, and several contributions from Bill Knight, West Coast & Alaska Tsunami Warning Center (WC/ATWC) and Ed Kornkven Arctic Region Supercomputing Center (ARSC). The code is based on the development originated in Los Alamos National Laboratory (LANL) during the 70's which traces its history to the work done by C. W. Hirt and a group of collaborators and researchers, including among others A. A. Amsden, T. D. Butler, L. D. Cloutman, B. J. Daly, R. S. Hotchkiss, C. Mader, R. C. C. Mjolsness, B. D. Nichols, H. M. Ruppel, M. D. Torrey and more recently D.B. Kothe.

The current TSUNAMI3D code has undergone dramatic changes from their original conception, Horrillo's thesis, 2006. In particular, the VOF algorithm for tracking the movement of a free surface interface between two fluids or fluid-void has been simplified specially for the 3D mode of operation to account for the horizontal distortion of the computational cells with respect of the vertical scale which is proper in the construction of efficient 3D grids for tsunami simulations. In Addition, the pressure term

has been split in two components, hydrostatic and non-hydrostatic. The splitting of the pressure term permits obtain hydrostatic solution by merely switching off the non-hydrostatic pressure terms. Therefore, TSUNAMI3D can be used to discern non-hydrostatic effects of the hydrostatic solution yet keeping the three dimensional structure.

TSUNAMI3D model is suitable for complex tsunami wave generation due to: 1) moving or deformable objects capability; 2) subaerial/subsea landslide including simplified soil rheology and 3) complex vertical or lateral bottom deformation.

Although TSUNAMI3D code has the capability of variable grids (1D telescoping), It does not comprise the nesting capability (2D telescoping); therefore, for construction of inundation maps a symbiosis is needed between TSUNAMI3D and NEOWAVE, specially when simulating landslide or complex bottom deformation on a very large domain. TSUNAMI3D is in constant development and it requires FORTRAN and MATLAB (for post-processing) programming skills to put it to work. Usually a 3D landslide case required a large amount of computer memory and CPU wall time to obtain the solution. Few subroutines, the most computational demanding, are parallelized using OPENMP directives. In the 2D mode of operation, the code uses PETSC-MPI library to solve the pressure field.

### NEOWAVE Model

NEOWAVE is built on the nonlinear shallow-water equations with a non-hydrostatic pressure term to describe weakly dispersive waves. The model is equivalent to existing models based on the classical Boussinesq equations. In addition, the code features a momentum conserved advection scheme that enables the modeling of breaking waves without the aid of analytical solutions for bore approximation or empirical equations for energy dissipation. An upwind scheme extrapolates the free-surface elevation instead of the flow depth to provide the flux in the momentum and continuity equations. This scheme greatly improves the model stability, which is essential for computation of energetic breaking waves and runups. The pressure term is split into hydrostatic and non-hydrostatic components

as well, and the vertical velocity is introduced in response to the non-hydrostatic pressure through the three dimensional continuity equation. NEOWAVE is a final product of the University of Hawaii (UH), that has is origin by the work done by professor Zygmunt Kowalik, University of Alaska Fairbanks (UAF) and several contributions from Paul Whitmore, Bill Knight, West Coast Alaska Tsunami Warning Center (WC/ATWC) and Tom Logan, UAF Arctic Region Supercomputing Center (ARSC). The program was greatly enhanced having in mind a final product for practical tsunami application by Yoshiki Yamazaki and Fai Cheung, UH. The result of this effort consisted in: a) developing a more robust momentum conservation scheme; b) including the nesting capability necessary for construction of tsunami inundation maps; c) considering the breaking and shock wave discontinuity; d) developing a faster linear equation solver and e) a more friendly user input interface.

NEOWAVE has shown very good agreement (see Yamazaki, Kowalik and Cheung, *et.al*, 2009) with the benchmark cases for tsunami model validation and verification described in the report OAR PMEL-135, Synolakis, *et.al,* 2007. Since the numerical scheme for the momentum and continuity equations remains explicit, the implicit non-hydrostatic solution is applicable to the existing hydrostatic model by switching off this term.

### Coupling TSUNAMI3D and NEOWAVE

Firstly, TSUNAMI3D is used to model the landslide induced tsunami waves. The 3D tsunami generation-domain size is determined according to the landslide volume, extent and orientation of the seabottom failure or scarp. The boundaries of the generation domain must extend enough to assure that the tsunami created by the landslide is fully developed before it leaves the generation boundaries. After the landslide has transferred most of its energy into the generation domain, TSUMAMI3D model passes averaged field variables along water column to the 2D depth integrated model NEOWAVE. Three dimensional field variables namely, the velocity vector and the non-hydrostatic pressure $q$ are depth integrated, averaged and passed along the water surface elevation to the 2D depth integrated model.

These field variables are then the initial condition for NEOWAVE which is the responsible for the propagation and runup of the tsunami waves toward the area of interest.

## TSUNAMI3D Governing Equations

The governing equations to describe the flow of two incompressible Newtonian fluids (eg.,water and mud) in a domain $\Omega(t)$, are given by the equation of conservation of mass

$$\frac{\partial u}{\partial x}+\frac{\partial v}{\partial y}+\frac{\partial w}{\partial z}=0 \tag{1}$$

and the conservative equation of momentum given by:

**A-** water:

$$\frac{\partial u}{\partial t}+\frac{\partial uu}{\partial x}+\frac{\partial uv}{\partial y}+\frac{\partial uw}{\partial z}$$
$$=-\mathrm{g}\frac{\partial \eta_1}{\partial x}-\frac{1}{\rho_1}\frac{\partial q}{\partial x}+\frac{\partial}{\partial x}\left[\frac{\mu_1}{\rho_1}\left(2\frac{\partial u}{\partial x}\right)\right]+\frac{\partial}{\partial y}\left[\frac{\mu_1}{\rho_1}\left(\frac{\partial u}{\partial y}+\frac{\partial v}{\partial x}\right)\right]$$
$$+\frac{\partial}{\partial z}\left[\frac{\mu_1}{\rho_1}\left(\frac{\partial u}{\partial z}+\frac{\partial w}{\partial x}\right)\right] \tag{2}$$

$$\frac{\partial v}{\partial t}+\frac{\partial uv}{\partial x}+\frac{\partial vv}{\partial y}+\frac{\partial vw}{\partial z}$$
$$=-\mathrm{g}\frac{\partial \eta_1}{\partial y}-\frac{1}{\rho_1}\frac{\partial q}{\partial y}+\frac{\partial}{\partial x}\left[\frac{\mu_1}{\rho_1}\left(\frac{\partial v}{\partial x}+\frac{\partial u}{\partial y}\right)\right]+\frac{\partial}{\partial y}\left[\frac{\mu_1}{\rho_1}\left(2\frac{\partial v}{\partial y}\right)\right]$$
$$+\frac{\partial}{\partial z}\left[\frac{\mu_1}{\rho_1}\left(\frac{\partial v}{\partial z}+\frac{\partial w}{\partial y}\right)\right] \tag{3}$$

$$\frac{\partial w}{\partial t}+\frac{\partial uw}{\partial x}+\frac{\partial vw}{\partial y}+\frac{\partial ww}{\partial z}$$
$$=-\frac{1}{\rho_1}\frac{\partial q}{\partial z}+\frac{\partial}{\partial x}\left[\frac{\mu_1}{\rho_1}\left(\frac{\partial w}{\partial x}+\frac{\partial u}{\partial z}\right)\right]+\frac{\partial}{\partial y}\left[\frac{\mu_1}{\rho_1}\left(\frac{\partial w}{\partial y}+\frac{\partial v}{\partial z}\right)\right]$$
$$+\frac{\partial}{\partial z}\left[\frac{\mu_1}{\rho_1}\left(2\frac{\partial w}{\partial z}\right)\right] \tag{4}$$

where, $u(x,y,z.t), v(x,y,z,t)$ and $w(x,y,z,t)$ are the velocity components along the coordinate axes of the fluid at any point $\boldsymbol{x}=x\hat{\imath}+y\hat{\jmath}+z\hat{k}$ at time $t$, $\eta_1(x,y,t)$ is the water-surface elevation measured from a vertical datum, $\rho_1$ is the density of the fluid, $q$ is the nonhydrostatic pressure, $\mu_1/\rho_1$

can be related to the water eddy viscosity and $g$ is the acceleration due to gravity. The total pressure, $p = p_{hyd} + q$, has been divided into a hydrostatic pressure $p_{hyd} = \rho_1 g(\eta_1 - z)$ and a dynamic pressure $q$ such that $\partial p_{hyd}/\partial z = -g$.

The velocities $u, v \; and \; w$ associated with a computational cell is located at the right, back and the top face of the cell respectively and the non-hydrostatic pressure $q(x, y, z, t)$ is located at the cell center.

For the simulation of landslide induced tsunami waves an additional set of equations are needed to include the second fluid or the mud-landslide with density $\rho_2$. Here, the mud is considered as a Newtonian fluid with a given eddy viscosity related to $\mu_2/\rho_2$. The set of governing equations for the momentum in the second layer or mud are given by:

**B-** mud:

$$\frac{\partial u}{\partial t} + \frac{\partial uu}{\partial x} + \frac{\partial uv}{\partial y} + \frac{\partial uw}{\partial z}$$
$$= -\mathrm{g}\left(\alpha \frac{\partial \eta_1}{\partial x} + (1-\alpha)\frac{\partial \eta_2}{\partial x}\right) - \frac{1}{\rho_2}\frac{\partial q}{\partial x} + \frac{\partial}{\partial x}\left[\frac{\mu_2}{\rho_2}\left(2\frac{\partial u}{\partial x}\right)\right]$$
$$+ \frac{\partial}{\partial y}\left[\frac{\mu_2}{\rho_2}\left(\frac{\partial u}{\partial y} + \frac{\partial v}{\partial x}\right)\right] + \frac{\partial}{\partial z}\left[\frac{\mu_2}{\rho_2}\left(\frac{\partial u}{\partial z} + \frac{\partial w}{\partial x}\right)\right] \quad (5)$$

$$\frac{\partial v}{\partial t} + \frac{\partial uv}{\partial x} + \frac{\partial vv}{\partial y} + \frac{\partial vw}{\partial z}$$
$$= -\mathrm{g}\left(\alpha \frac{\partial \eta_1}{\partial y} + (1-\alpha)\frac{\partial \eta_2}{\partial y}\right) - \frac{1}{\rho_2}\frac{\partial q}{\partial y} + \frac{\partial}{\partial x}\left[\frac{\mu_2}{\rho_2}\left(\frac{\partial v}{\partial x} + \frac{\partial u}{\partial y}\right)\right]$$
$$+ \frac{\partial}{\partial y}\left[\frac{\mu_2}{\rho_2}\left(2\frac{\partial v}{\partial y}\right)\right] + \frac{\partial}{\partial z}\left[\frac{\mu_2}{\rho_2}\left(\frac{\partial v}{\partial z} + \frac{\partial w}{\partial y}\right)\right] \quad (6)$$

$$\frac{\partial w}{\partial t} + \frac{\partial uw}{\partial x} + \frac{\partial vw}{\partial y} + \frac{\partial ww}{\partial z}$$
$$= -\frac{1}{\rho_2}\frac{\partial q}{\partial z} + \frac{\partial}{\partial x}\left[\frac{\mu_2}{\rho_2}\left(\frac{\partial w}{\partial x} + \frac{\partial u}{\partial z}\right)\right] + \frac{\partial}{\partial y}\left[\frac{\mu_2}{\rho_2}\left(\frac{\partial w}{\partial y} + \frac{\partial v}{\partial z}\right)\right]$$
$$+ \frac{\partial}{\partial z}\left[\frac{\mu_2}{\rho_2}\left(2\frac{\partial w}{\partial z}\right)\right] \quad (7)$$

Again, here $u(x,y,z.t), v(x,y,z,t)$ and $w(x,y,z,t)$ are the velocity components along the coordinate axes in the mud domain at time $t$, $\eta_2(x,y,t)$ is the mud-surface elevation measured from a vertical datum, $\rho_2$ is the density of the mud, $\alpha$ is the fluid-mud density ratio given by $\alpha = \rho_1/\rho_2$ and $\mu_2/\rho_2$ is a expression that can be related to the mud eddy viscosity. The total pressure, $p = p_{hyd} + q$, has been divided into a hydrostatic pressure $p_{hyd} = g[\rho_1(\eta_1 - \eta_2) + \rho_2(\eta_2 - z)]$ and the dynamic pressure $q$.

Both interfaces, water surface elevation (water-void) and mud surface elevation (fluid-mud or mud-void) are traced using a simplified VOF method based on the donor-acceptor algorithm, Hirt and Nichols, 1981. The simplified VOF method features a scalar function $F_{1,2}(x,y,z,t)$ to define the water/mud region in space and time. Here, sub-indices 1 and 2 indicate scalar function for water and mud respectively. The $F$ function accounts for the fractional volume of fluid/mud contained into the cell (concentration). A unit value for $F$ corresponds to a fluid cell totally filled with water/mud, while a value of zero indicates an empty cell (no water or mud). Therefore, cells with $F$ value between zero and one indicates a surface cell or interface cell. The equation describing the $F$ function is given by

$$\frac{dF_{1,2}}{dt} = \frac{\partial F_{1,2}}{\partial t} + \frac{\partial uF_{1,2}}{\partial x} + \frac{\partial vF_{1,2}}{\partial y} + \frac{\partial wF_{1,2}}{\partial z} = 0 \tag{8}$$

which states that $F_{1,2}$ propagates with the fluid velocities $u, v \; and \; w$. Physical properties in each cell element, *i.e.*, the density and eddy viscosity, can be weighted in term of the $F_{1,2}(x,y,z,t)$ function. For example, a general expression for density is determined by the following equation and condition,

$$\rho(x,y,z,t) = \rho_1(F_1 - F_2) + \rho_2 F_2 \tag{9}$$

Equation (9) indicates that advection or transportation of the second fluid (mud) requires the existence of fluid (water) in the cell such that $F_1 >= F_2$ (condition). This technique greatly simplify calculations of both free surfaces, since the advection algorithm for the second fluid (mud) is an external procedure that it is completed once the advection of the first fluid (water) is done.

As the non-hydrostatic pressure $q$, the scalar function $F$ is located at cell center. Equation (8) can only be solved in the water and mud domains. The water and mud surface elevations $\eta_{1,2}(x, y, t)$ are a mere byproduct of $F_{1,2}$ and they are calculated by integrating the scalar function $F_{1,2}(x, y, z, t)$ along the water/mud column at each $x, y$ location.

The governing equations are solved by using the standard volume difference scheme starting with field variables such as $u, v, w, q \; and \; F$ are known at time $t = 0$. Nonlinear terms are approximated using up-wind down-wind approach up to the third order. The governing equations then are solved by discretisizing them spatially and temporally to obtain the field variables in the domain at any required time.

Turbulence closure approximations are not considered, instead a general eddy viscous formulation is employed as depicted in the momentum equation. At the water-mud interfaces the equivalent viscosity is calculated using a weighting function similar to the expression and condition indicated in equation 9, which reads

$$\mu/\rho(x, y, z, t) = \mu_1/\rho_1(F_1 - F_2) + \mu_2/\rho_2(F_2) \tag{10}$$

## NEOWAVE Governing Equations

In this section is summarized the formulation and assumptions of the governing equations for the depth-integrated, non-hydrostatic NEOWAVE model. The governing equations are derived from the incompressible Navier-Stokes equation and the continuity equation in the spherical coordinates system $(\lambda, \phi, z)$ in which $\lambda$ is longitude, $\phi$ is latitude, and z denotes normal distance from the still water level as described in great detail in Yamazaki, Kowalik and Cheung, 2009.

The resulting momentum equations along $\lambda, \phi, z$ directions and the continuity equation are :

$$\frac{\partial U}{\partial t}+\frac{U}{R\cos\phi}\frac{\partial U}{\partial \lambda}+\frac{V}{R}\frac{\partial U}{\partial \phi}-\left(2\Omega+\frac{U}{R\cos\phi}\right)V\sin\phi=-\frac{g}{R\cos\phi}\frac{\partial \zeta}{\partial \lambda}$$

$$-\frac{1}{2}\frac{1}{R\cos\phi}\frac{\partial q}{\partial \lambda}-\frac{1}{2}\frac{q}{DR\cos\phi}\frac{\partial(\zeta-h+\eta)}{\partial \lambda}-n^2\frac{g}{D^{1/3}}\frac{U\sqrt{U^2+V^2}}{D} \tag{11}$$

$$\frac{\partial V}{\partial t}+\frac{U}{R\cos\phi}\frac{\partial V}{\partial \lambda}+\frac{V}{R}\frac{\partial V}{\partial \phi}+\left(2\Omega+\frac{U}{R\cos\phi}\right)U\sin\phi=-\frac{g}{R}\frac{\partial \zeta}{\partial \phi}$$

$$-\frac{1}{2}\frac{1}{R}\frac{\partial q}{\partial \phi}-\frac{1}{2}\frac{q}{DR}\frac{\partial(\zeta-h+\eta)}{\partial \phi}-n^2\frac{g}{D^{1/3}}\frac{V\sqrt{U^2+V^2}}{D} \tag{12}$$

$$\frac{\partial W}{\partial t}=\frac{q}{D} \tag{13}$$

$$\frac{\partial(\zeta-\eta)}{\partial t}+\frac{1}{R\cos\phi}\frac{\partial(UD)}{\partial \lambda}+\frac{1}{R\cos\phi}\frac{\partial(V\cos\phi D)}{\partial \phi}=0 \tag{14}$$

where $U, V$ and $W$ are depth-averaged velocity components in the $\lambda, \phi$ and $z$ directions respectively; $t$ is time, $\zeta$ is the free surface elevation, $R$ is the earth's radius, $\Omega$ is the earth's angular velocity, $\rho$ is water density, $q$ is non-hydrostatic pressure, $g$ is gravitational acceleration and $n$ is Manning's coefficient for the sea-bottom friction. The vertical velocity $W$ is assumed to have a linear distribution along the water column; therefore the vertical velocity component $W$ is simply the average value of the vertical velocity at the free surface and the seafloor. The total depth is defined as $D = \zeta + (h - \eta)$ where $h$ is the water depth and $\eta$ is seafloor deformation.

A detailed discussion of NEOWAVE numerical scheme and capability can be found in great detail in Yamazaki, Kowalik and Cheung, 2009.

## TSUNAMI3D Model Validation

It is considered important for any tsunami numerical model to be evaluated against standard benchmarking cases suggested by NOAA and NTHMP. Herein two experimental landslide cases have

been chosen to validate the TSUNAMI3D code for tsunami generation caused by sub-aerial and sub-sea landslides. The two test cases are:

1- Tsunami generation and runup due to 3D landslide

2 -Tsunami generation and runup due to 2D landslide

The first experiment compares TSUNAMI3D numerical results with laboratory data obtained in a series of 3D experiments carried out at Oregon State University (OSU) by Synolakis and Raichlen, 2003; Raichlen and Synolakis, 2003.

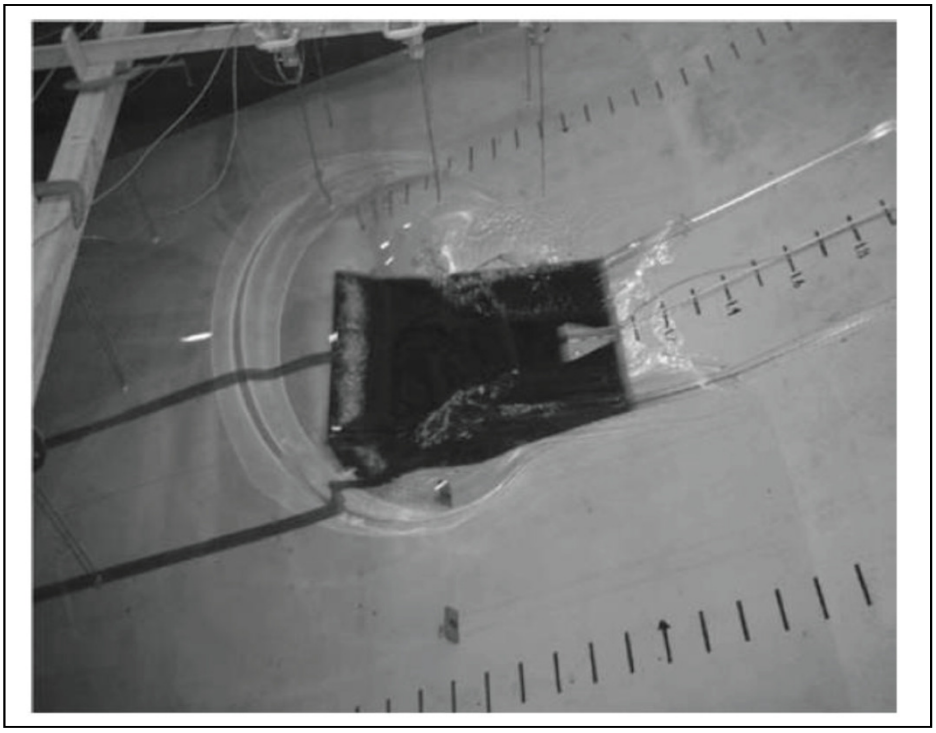

**Figure 7.** Experiment of a solid wedge induced waves. "Tsunami generation and runup due to three-dimensional landslide", Synolakis *et al.*, (2007), OAR PMEL-135.

In the physical 3D experiment a solid wedge was used to represent the landslide induced waves, see Figure 7. Detailed information and data of the physical experiment are found in the tsunami benchmark "*Tsunami Generation and Runup Due to Three-dimensional Landslide*", Synolakis *et al.* 2007, OAR PMEL-135. Figure 8 shows a qualitative snapshot of 3D numerical result which illustrates the numerical

domain dimensions, free surface elevation and velocity vectors at a given time. For numerical efficiency, just half domain is used in the simulation which has an axis of symmetry.

TSUNAMI3D's results are portrayed against the experimental in Figure 9. Overall numerical results agree fairly well with the experimental results. The rebound wave (second wave recorded by gage 1) resulting from the drag of the solid wedge is slightly overestimated by the model. Similar overestimation in the rebound wave has been reported by Abadie and Grilli, 2010, as well. The high nonlinearity of the generated waves is evident; this type of wave cannot be reproduced by depth integrated models.

The normalized root mean square deviation (NRMSD) is used to measure model deviation or precision. The MRMSD is defined as:

$$NRMSD(t)\% = \frac{1}{\zeta_{e,max} - \zeta_{e,min}} \sqrt{\frac{\sum_{i=1}^{n(t)} (\zeta_{e,i} - \zeta_{m,i})^2}{n(t)}} \tag{15}$$

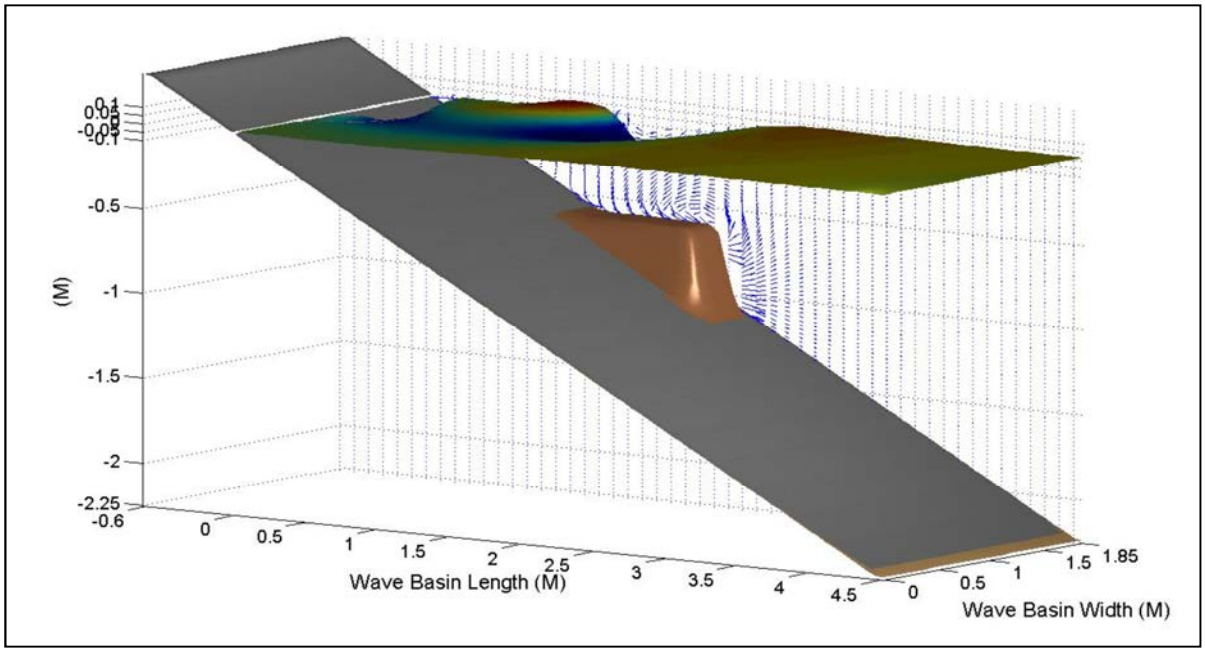


**Figure 8**. TSUNAMI3D's snapshot of the solid wedge induced waves.

NRMSD measures the differences between values predicted by the model $(\zeta_m)$ and the values actually observed in the physical experiment $(\zeta_e)$. Variable $n(t)$ is the number of observed points at a

given time. This graphical technique plotted in time permits to measure model precision for the first, second and subsequent waves as it is shown in Figure 9. NRMSD is a good measurement of the dispersion of individual differences or deviations.

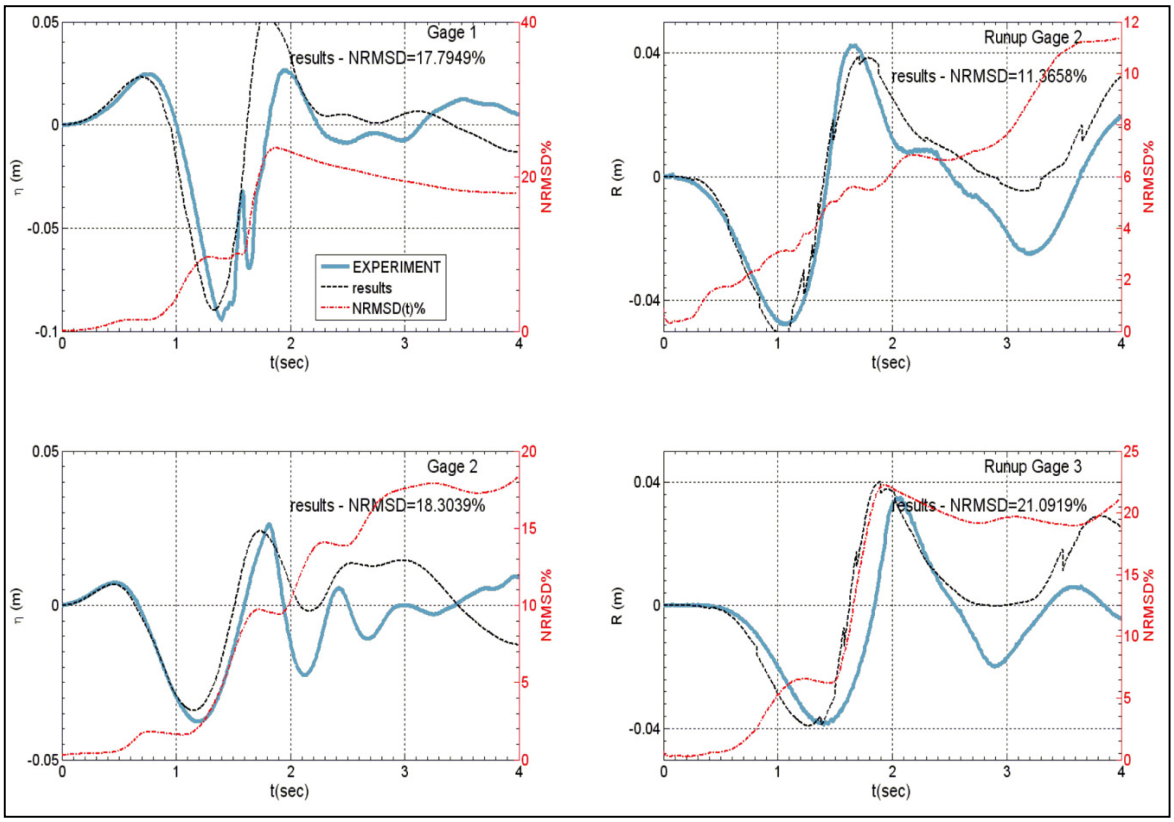


**Figure 9.** Comparison of TSUNAMI3D numerical result (black broken line) Against experiment. "Tsunami generation and runup due to three-dimensional landslide", Synolakis *et al*., (2007), OAR PMEL-135. Red line is the normalized root mean square deviation plotted in time.

The second experiment aims to predict the free surface elevation and runup associated with a 1D translating Gaussian shaped mass which is initially at the shoreline, Synolakis *et al.* (2007). In dimensional form the seafloor deformation can be described by

$$\eta(x,t) = H(x) + \eta_o(x,t) \tag{16}$$

where

$$H(x) = x\ tan(\beta) \tag{17}$$

$$\eta_o(x,t) = \delta\ exp\left(-\left(2\sqrt{\frac{x\mu^2}{\delta\ tan(\beta)}} - \sqrt{\frac{g}{\delta}}\mu t\right)^2\right) \tag{18}$$

where $\eta_o$ is the slide thickness, $\delta$ is the maximum slide thickness, $\mu = \delta/L$ is the thickness slide length ratio, $\beta$ is the slope angle and $L$ is the slide length. Once in motion, the landslide mass moves at constant acceleration. This test case along with a linear analytical solution is described in great detail in Liu, Lynett and Synolakis, 2003.

The benchmark problem presents two cases, A and B. Case B has been chosen to test TSUNAMI3D model because it offers higher nonlinearity than its counterpart case A. For this test, TSUNAMI3D model has been activated to the 2D mode to carry out the experiment. The experimental setup information for case B follows.

CASE B: $tan\beta/\mu = 1, \quad \beta = 5.7^o,\ \delta = 1\text{m}, \mu = 0.1$; and the free surface locations are determined at selected times according to: $\sqrt{\frac{g}{\delta}}\mu t = \ 0.5,\ 1.0,\ 2.5, 4.5$ (non-dimensional time).

To solve numerically the benchmark problem two additional 1D approaches other that TSUNAMI3D-2D (2D mode on) have been considered to compare with the linear analytical solution and to withdraw some conclusions. The two methods selected are the 1D linear and the nonlinear shallow water depth integrated methods, LSW and NLSW respectively. It is expected that the linear analytical solution will match the LSW approach but mismatch the NLSW method. On the other hand, TSUNAMI3D-2D approach is nonlinear and two dimensional. Since TSUNAMI3D-2D includes the vertical component of velocity and acceleration (nonhydrostatic and dispersive) some differences are expected as the numerical result is compared with the linear analytical solution, LSW and NLSW which are in principle depth integrated methods. The finite difference solution of momentum equation for the LSW and NLSW

approaches is solved on a staggered grid using the original depth integrated code (an early version of NEOWAVE), see Kowalik and Murty, 1993. The nonlinear term for the NLSW method has second order approximation in space and first order in time.

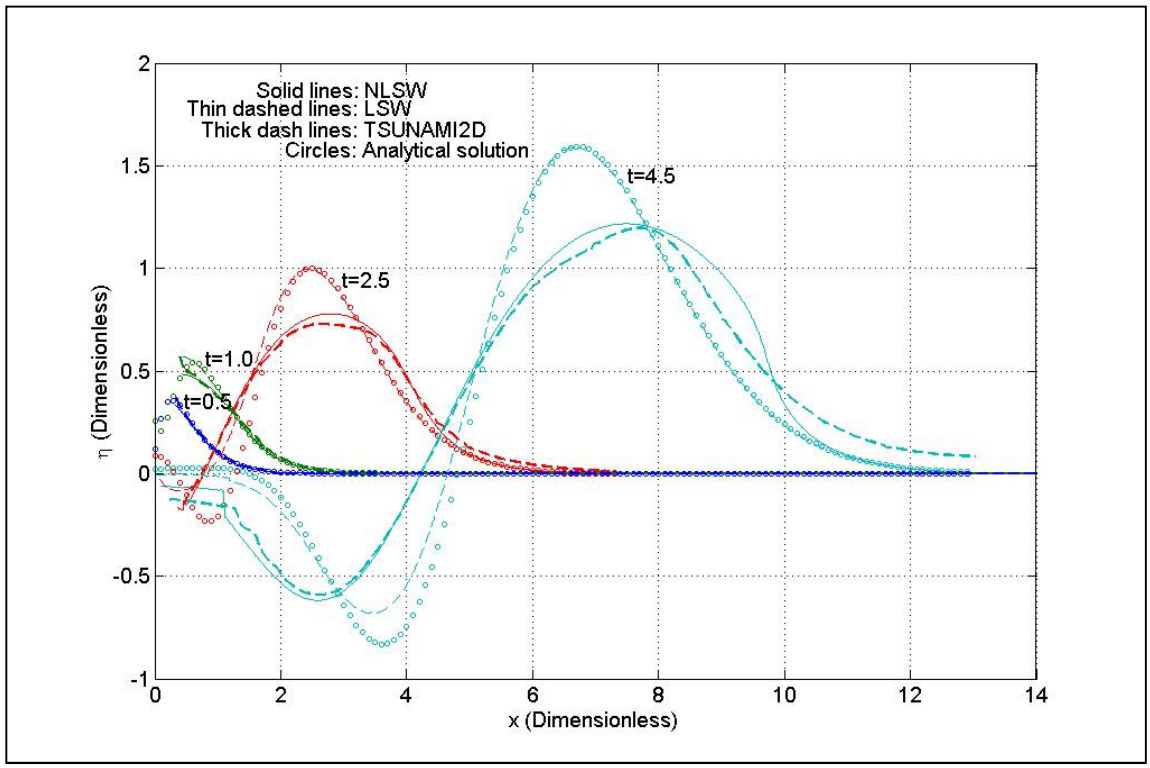


**Figure 10.** Comparison of TSUNAMI3D's numerical result against analytical solution, nonlinear and linear shallow water approaches. Benchmark "Tsunami generation and runup due to two-dimensional landslide", Synolakis *et al*. (2007), OAR PMEL-135.

In this experiment TSUNAMI3D-2D model has been extended to deal with deformable moving objects in the computational domain. As can be gleaned from Figure 10 and Figure 11, TSUNAMI3D-2D's results agreed very well with 1D NLSW approach. However, some differences are evident, like the wave skewness and the location of the shoreline. It is important to mention that TSUNAMI3D-2D solves the full 2D Navier-Stokes equations with the vertical and horizontal velocities being variables along the water column, while the shallow water (SW) approximation used in the analytical solution, assumes constant horizontal velocity and no vertical velocity. The SW approaches (analytical and numerical) missed the physics caused by the vertical acceleration or the non-hydrostatic effect. It is then suggested,

that the TSUNSMI3D-2D solution is ideally suited for this case, where relatively high vertical acceleration occurs. In this particular nonlinear case, TSUNAMI3D-2D predicts a wave more elongated, skewed and less tall than the 1D NLSW approach for later time, *i.e.*, $\sqrt{\frac{g}{\delta}}\mu t = 2.5$ and $\sqrt{\frac{g}{\delta}}\mu t = 4.5$. When nonlinearity is not strong, all numerical models agreed very well with the analytical solution at earlier time, *i.e.*, $\sqrt{\frac{g}{\delta}}\mu t = 0.5$ and $\sqrt{\frac{g}{\delta}}\mu t = 1.0$.

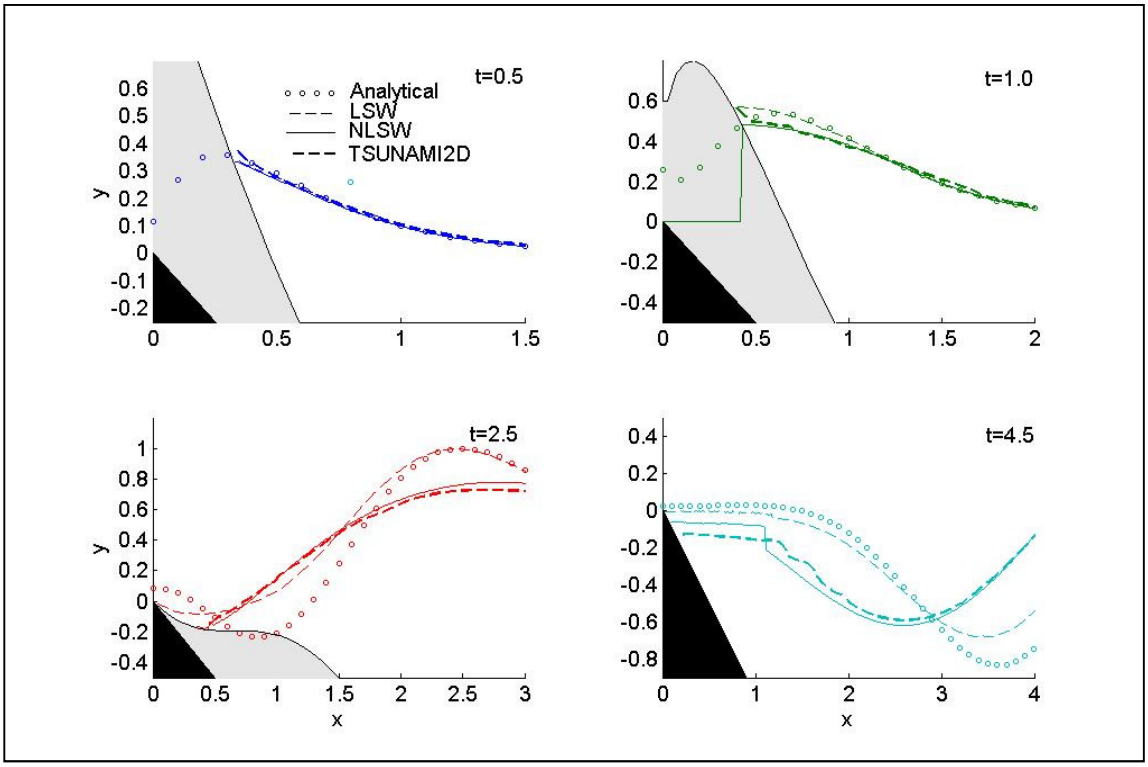


**Figure 11.** Comparison of the TSUNAMI3D (2D mode) numerical result (thick broken line) against the analytical solution and the nonlinear and linear shallow water approaches. "Tsunami generation and runup due to two-dimensional landslide", Synolakis *et al.* (2007), OAR PMEL-135.

In practical 3D numerical simulation of a typical submarine landslide scenario in the GOM requires a relative low resolution to circumvent computer overload and obtains a reasonable convergence and efficient solution. Physical properties tend to diffuse faster in low resolution, *e.g.*, density; so it is alleged, that keeping a sharp interface between mud-water would minimize the excessive diffusion problem originated by the low resolution. To validate TSUNAMI3D code performance in real landslide cases and

verify the model capability in dealing with sharp versus diffusive interface, an experiment is carried and compared with results obtained by using the commercial package, FLOW3D. It is advisable to mention that FLOW3D can be run in the two dimensional mode as well (FLOW3D-2D).

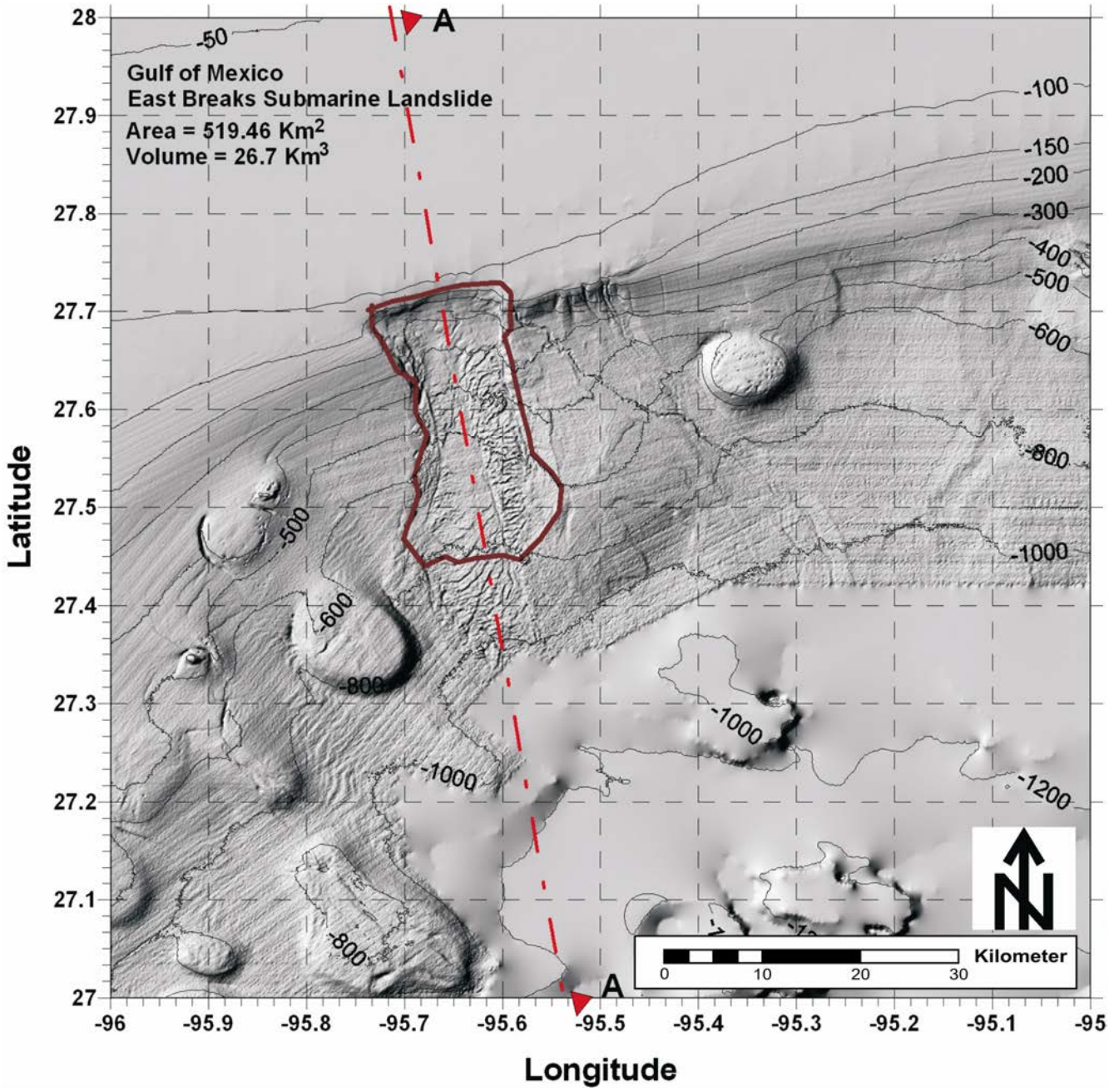


**Figure 12.** Gulf of Mexico East Breaks submarine landslide scarp location and bathymetry. Transect A-A indicates cross-section used for the 2D model setups. Bathymetry is given in meters.

The experiment uses the East Breaks landslide scenario. Figure 12 shows the bathymetry of the northwest corner of the GOM that surrounds the East Breaks scarp. Transect A-A indicates the location of the cross section used by TSUNAMI3D and FLOW3D numerical models with the 2D mode activated. As it is seen, transect A-A bisects the East-Breaks scarp in the direction of the landslide propagation.

To facilitate models comparison, a juxtaposed sequence of free surface elevation and mud interface configuration derived from models results is shown in Figure 13.

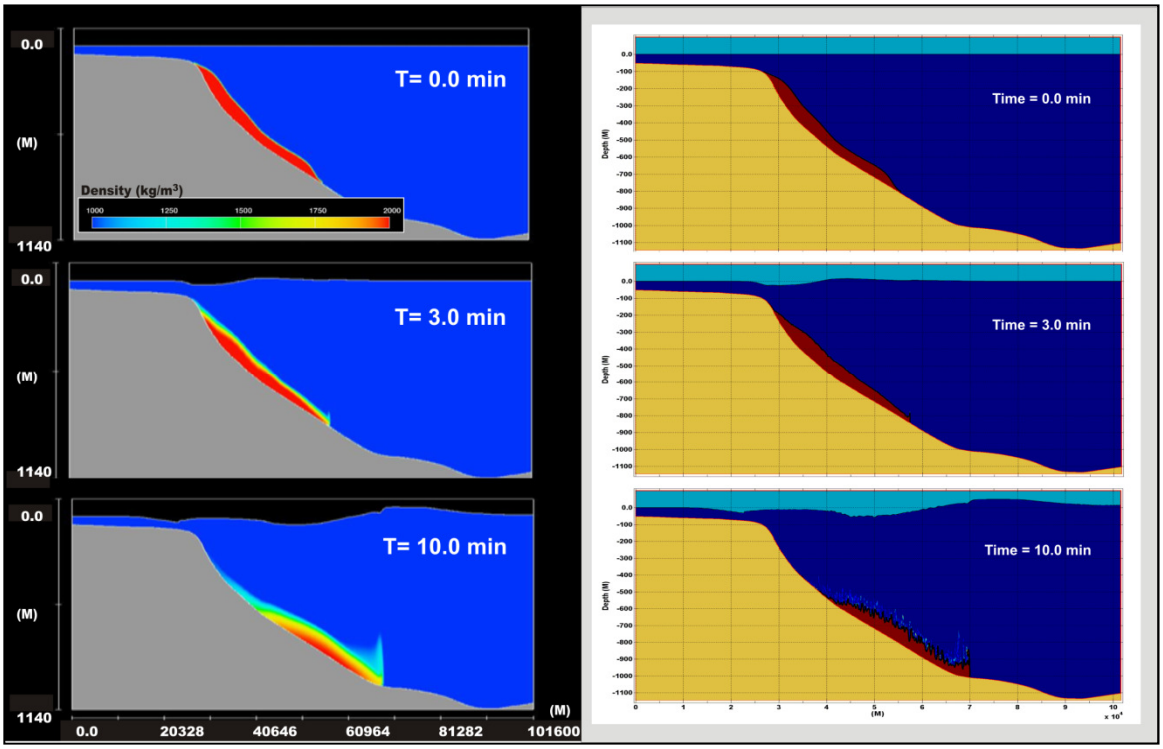


**Figure 13.** Snapshots comparison for the 2D East Breaks submarine landslide experiment along transect A-A. Left side, FLOW3D results; right side, TSUNAMI3D results**.**

The excessive diffusion of the mud into the water column due to the low resolution required for practical tsunami application is evident in the FLOW3D result. As it is observed, FLOW3D-2D diffuses the mud quite high in the water column. On the other hand, TSUNAMI3D-2D features ripples on the water-mud interface which are product of two-layers with different velocity and physical properties, named Kelvin-Helmholtz instability (Chandrasekhar 1961). In this particular case, the Kelvin-Helmholtz instability causes the immediate mud surface waves to change into high-frequency components due to the

sharp gradient of density and viscosity, Gisler, 2006. Nevertheless, the free surface results obtained by both methods, see upper plot in Figure 14, match very well. No shown here by tested in this study, less viscous slides produce larger tsunami waves, while more viscous slides produce modest ones. Less viscous slides also produce longer runouts, but at the same time leave more deposits from the turbidity currents that result in the interchange and mutual entrainment between slide material and water, Gisler, 2006, and Abadie and Grilli, 2010. This reasoning implies, that mud slide with a sharp interface will propagate faster and probably will generate slightly large wave at early stage of wave evolution as it is seen in Figure 14. However, for this particular real size case, it seems that selecting a sharp or diffusive mud-water interface does not affect notoriously the outcome (size) of the generated waves.

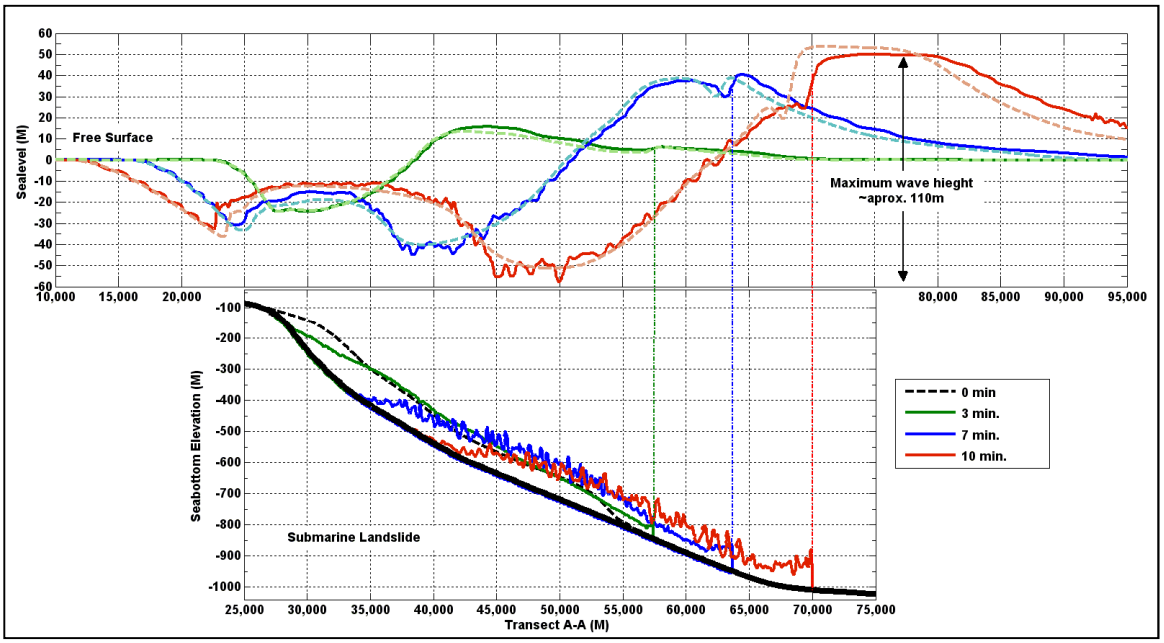


**Figure 14.** Snapshot for the 2D East-Breaks submarine landslide along transect A-A taken at 0, 3, 7 and 10 minutes. Top graph, free surface elevation comparison of FLOW3D (broken line) versus TSUNAMI3D (Solid line). Bottom graph, TSUNAMI3D's mud surface sequence.

Performing 3D tsunami calculation in domains comparable to the GOM landslide size is usually prohibitive due to the large amount of memory and computer time required. However, TSUNAMI3D code performed relatively efficient for the given landslide domain sizes. For instance, a typical GOM's

landslide required a domain of 2x2 degree in size to fully develop a tsunami wave. Typically, model horizontal resolution is 15 sec and vertical resolution (variable) is in the order of 0.5m to 20m. The finer vertical resolution is restrained in the water free surface and water-mud interface region; the coarser vertical resolution is confined in the deeper water region. A representative total number of cells is about 15 millions. Computer time required to simulate 30 minutes of landslide is around 100 CPU hours. TSUNAMI3D code can handle relatively high resolution but obviously with a high computational cost. Entering the complex geometry to represent the surrounding bathymetry and the 3D landslide configuration is a challenging process too, and it requires automatization.

Submarine landslide simulations using 2D (vertical and horizontal) or 1D (depth integrated model) could be misleading. Such numerical simulation will reproduce larger and faster waves than its 3D counterpart due to the lateral confinement that restrain lateral radiation.

### NEOWAVE Model Validation

The 2D depth integrated model numerical scheme and validation to meet tsunami model standards according to National Tsunami Hazard Mitigation Program (NTHMP) are found in great detail in Yamazaki, *et.al*, 2009.

## Methodology and Data

### Grid Development and Data Sources

Preliminary numerical simulations were carried out over the entire GOM in order to identify tsunami energy focusing along the GOM's coastline, shallow and deep water regions. Three tsunami sources (submarine landslides described by THAG) were used to calculate maximum wave amplitude and arrival time for the entire GOM. A foremost coarse grid of 60 arc-seconds was used for the entire GOM domain (Figure 6) and a finer grid of 15 arc-seconds for the tsunami generation regions, dashed-red rectangles in Figure 6. Table 3 shows the coordinates limits for the foremost or primary domain (60 arc-seconds) and

Tables 4, 5 and 6 summarize coordinate limits for the tsunami source domains (15 arc-seconds), East-Breaks, Mississippi Canyon and West Florida respectively.

This preliminary set of numerical simulations facilitated the selection of the community of Port Aransas for construction of the first tsunami inundation map. For the selection of the community several factors were considered: 1) the proximity of submarine landslides; 2) tsunami energy focusing (maximum surface elevation); 3) the quality of the existing local bathymetric/topographic data (DEM available) and the size of the community and infrastructure.

**Table 3.** Coordinate limits for the Gulf of Mexico foremost domain. Tsunami simulation for maximum wave amplitude and arrival time

| Gulf of Mexico Grid. Resolution (60 arc-seconds | |
|---|---|
| Foremost Domain | Degree |
| Longitude Left | -97.90 |
| Lower Latitude | 18.1333 |
| Longitude Right | 80.05 |
| Upper Latitude | 30.6833 |

**Table 4**. Coordinate limits for the East Breaks landslide-domain. Tsunami simulation for maximum wave amplitude and arrival time.

| East Breaks Grid. Resolution (15 arc-seconds) | |
|---|---|
| Tsunami Source Domain | Degree |
| Longitude Left | -96.00 |
| Lower Latitude | 27.00 |
| Longitude Right | -95.20 |
| Upper Latitude | 28.00 |

**Table 5.** Coordinate limits for the Mississippi Canyon landslide-domain. Tsunami simulation for maximum amplitude and arrival time.

| Mississippi Canyon Grid. Resolution (15 arc-seconds) | |
|---|---|
| Tsunami Source Domain | Degree |
| Longitude Left | -90.50 |
| Lower Latitude | 27.00 |
| Longitude Right | -88.50 |
| Upper Latitude | 29.00 |

**Table 6.** Coordinate limits for the West Florida landslide-domain. Tsunami simulation for maximum amplitude and arrival time.

| West Florida Grid. Resolution (15 arc-seconds) | |
|---|---|
| Tsunami Source Domain | Degree |
| Longitude Left | -86 |
| Lower Latitude | 25 |
| Longitude Right | -84.5 |
| Upper Latitude | 26.5 |

The foremost 60 arc-seconds grid was obtained from the National Geophysical Data Center's publicly available ETOPO1, Amante and Eakins, (2009). The ETOPO1 is a 1 arc-minute global relief of the Earth's surface, which was designed to support tsunami forecasting, and ocean circulation modeling. The data spatial horizontal resolution is approximately 1690 m (latitude 24°) and these data sets were shifted to common horizontal and vertical datum. The topographic data sets were obtained from NASA, NGDC and the National Snow and Ice Data Center (Amante & Eakins, 2009). The specifications for ETOPO1 are shown in Table 7.

The 15 arc-seconds grid for the tsunami generation regions (East Breaks, Mississippi Canyon and West Florida, dashed-red rectangles in Figure 6) was obtained from publicly available data on the National Geophysical Data Center's U.S. Coastal Relief Model website which integrates offshore bathymetry data with land topography data.

**Table 7**. Specifications for ETOPO 1 (Amante & Eakins, 2009)

| | |
|---|---|
| Versions | Ice Surface, Bedrock |
| Coverage Area | Global: -180 to 180 , -90 to 90 |
| Coordinate System | Geographic decimal degrees |
| Horizontal datum | World Geodetic System of 1984 (WGS 84) |
| Vertical Datum | Sea Level |
| Vertical Units | Meters |
| Cell Size | 1 arc-minute |
| Grid Format | Multiple: netCDF, g98, binary float, tiff, xyz |

The bathymetric data sources include:

The U.S. National Ocean Service Hydrographic Database

The U.S. Geological Survey (USGS)

The Monterey Bay Aquarium Research Institute

The U.S. Army Corps of Engineers

The bathymetric contour data source is from the International Bathymetric Chart of the Caribbean Sea and the Gulf of Mexico project ("U.S. Coastal Relief Model," 2010). The vertical datum source is based on the mean low water elevation and the mean lower-low water elevation. The topographic data source is referenced to NAVD88. The data spatial resolution is approximately 423 m (latitude 24°) and these data sets were shifted to common horizontal and vertical datum.

Figure 15 shows the 15 arc-seconds bathymetry of the northwest corner of the GOM that surrounds the East-Breaks scarp. Likewise, Figure 16 and Figure 17, show the 15 arc-seconds bathymetry for the Mississippi Canyon and West Florida respectively. Red polygons on figures, delimit the excavation regions used to determine landslide volumes and areas which are needed as input for numerical calculations of submarine landslide induced tsunami waves. Tsunamis generated from these domains are used as model initial conditions for calculation of maximum wave amplitude, arrival time and the inundation of Port Aransas.

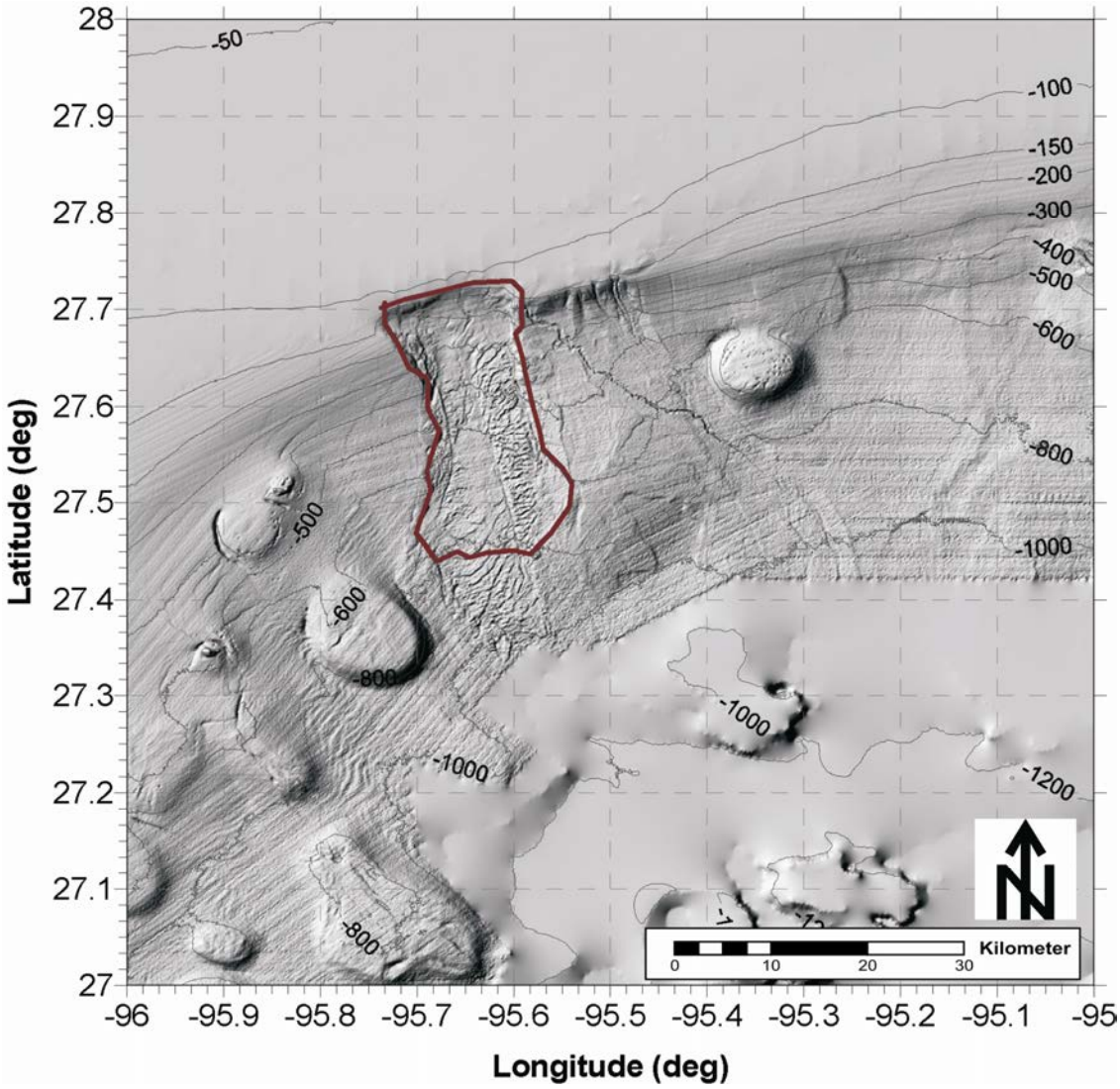


**Figure 15.** East-Breaks submarine landslide location, excavation limits and surrounding bathymetry (in meters).

Based on the preliminary numerical simulation results obtained on the entire GOM, *e.g.*, location of tsunami maximum amplitude, finer grids were used over the northern portion of Gulf of Mexico to solve with better detail the impact the tsunami has on Port Aransas. In the new set of numerical simulations with finer grids, the foremost domain has a horizontal resolution of 15 arc-seconds with finer grids nested or embedded. Embedding grids consists of placing a small relatively fine mesh, covering the Port Aransas coastal region, within a sequentially larger and more coarse mesh, ultimately encompassing the northern portion of the Gulf of Mexico of 15 arc-seconds resolution. This embedding procedure is an

important factor because it enables the propagation of waves generated from distant or local sources using a coarse resolution for efficient purpose. In addition it solves the waves height, runup and extent of inundation with higher resolution in the location of interest.

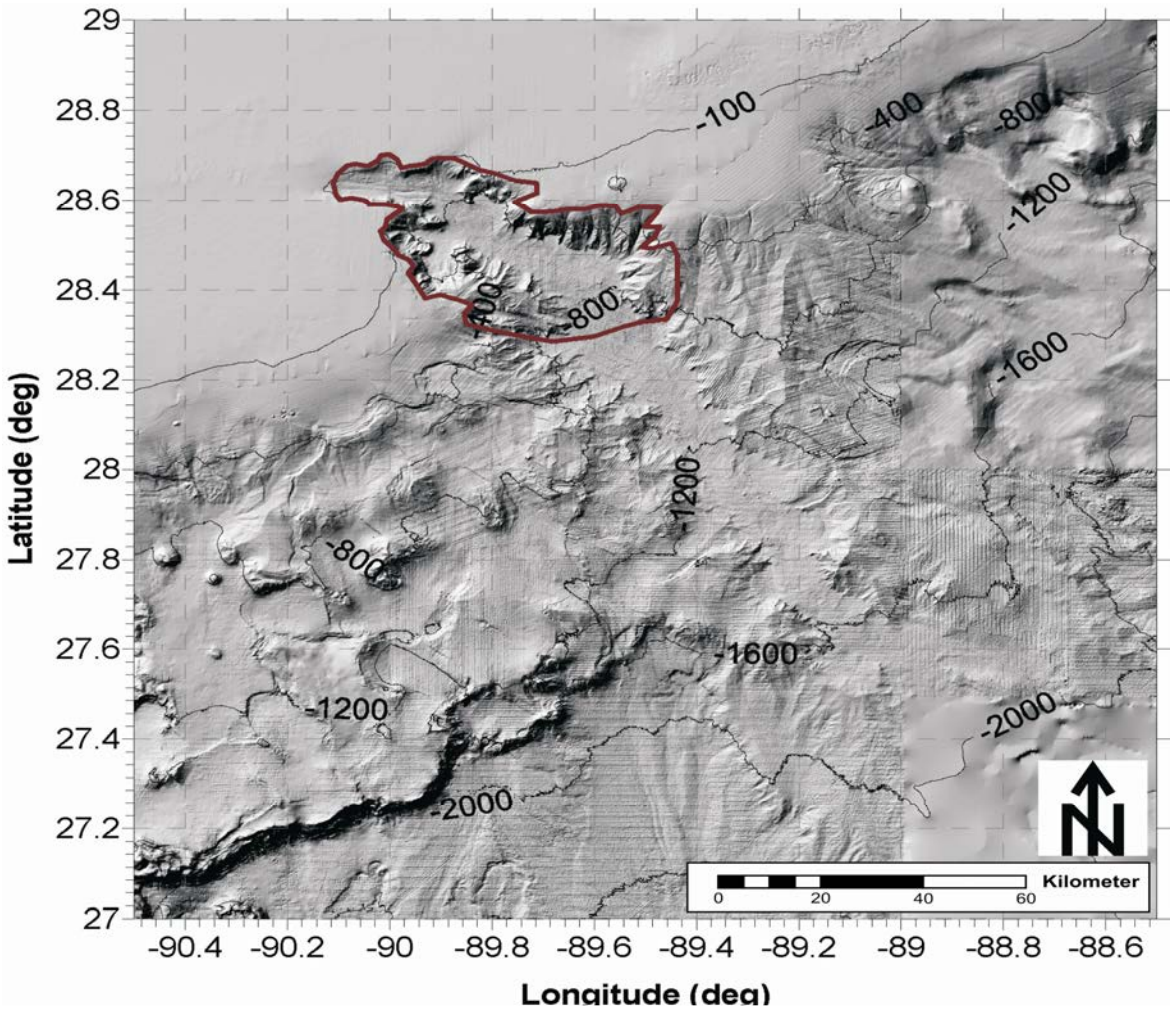


**Figure 16.** Mississippi Canyon submarine landslide, excavation limits and surrounding bathymetry (in meters).

The finer domains utilized a series of nested telescoping grids. In general, three nested grids were used for modeling and generating the tsunami inundation map. The horizontal resolution of these nested grids are 3, 1 and 1/3 arc-seconds, with a telescoping ratio of 5:3:3. The extent of the landslide source, foremost and nested domains for the East Breaks and Mississippi Canyon landslide events used for Port Aransas inundation mapping are shown in Table 8 and Table 9 respectively.

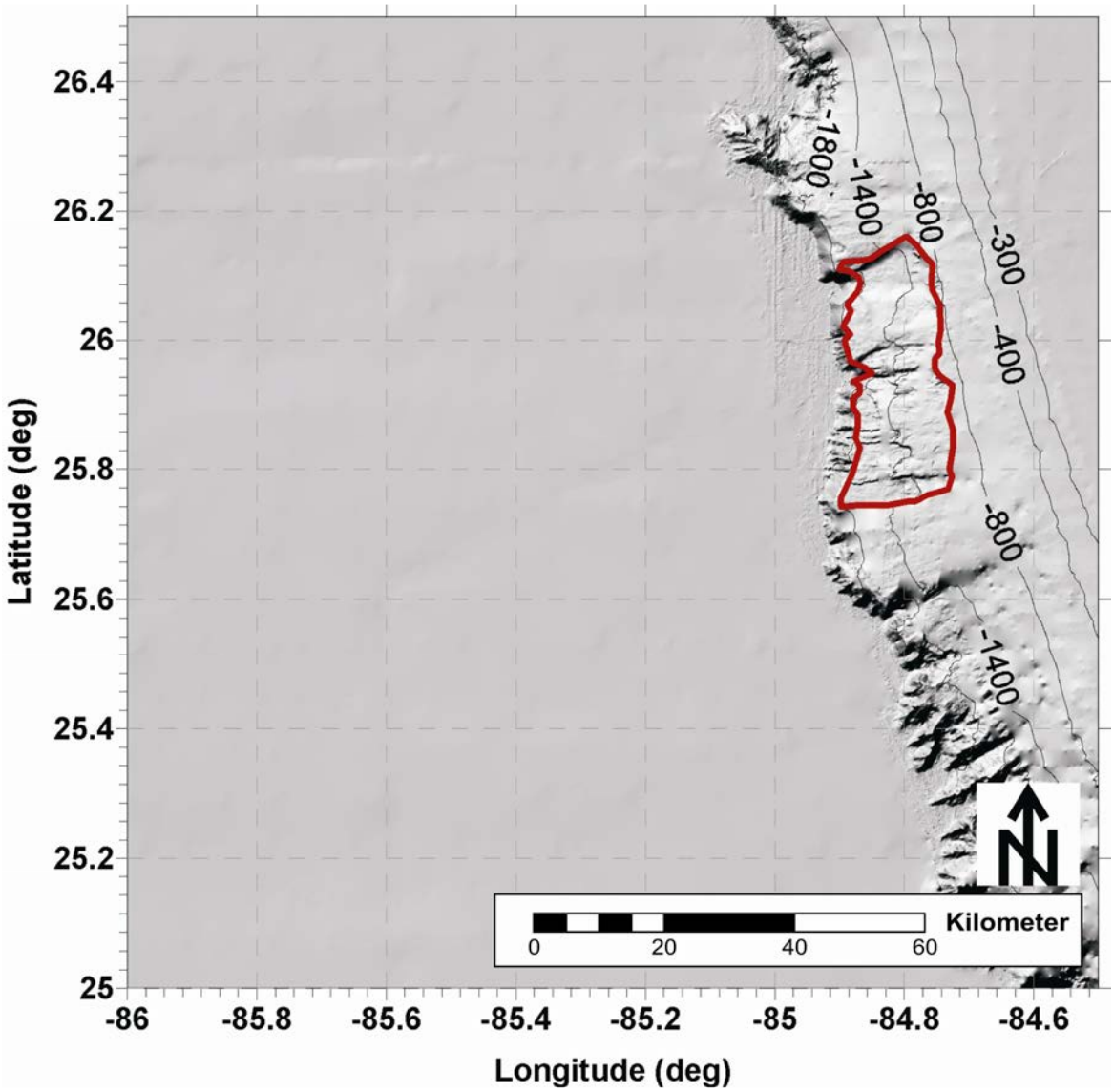


**Figure 17.** West Florida submarine landslide location, excavation limits and surrounding bathymetry (in meters).

It is important to point out in advance that the West Florida landslide was not considered in the new set of numerical simulations with finer grids since its impact is minuscule and hardly noticeable; so an events of similar magnitude, location and characteristic do not represent a tsunami hazard for the community and infrastructure of Port Aransas.

**Table 8**. Coordinate limits for the East Breaks scenario.
Tsunami simulation for construction of inundation maps.

| East Breaks Generated Tsunami | |
|---|---|
| Tsunami Source. Resolution (15 arc-seconds) | |
| Longitude Left | -96.00 |
| Lower Latitude | 27.00 |
| Longitude Right | -95.20 |
| Upper Latitude | 28.00 |
| Foremost Domain. Resolution (15 arc-seconds) | |
| Longitude Left | -97.58333333 |
| Lower Latitude | 25.0 |
| Longitude Right | -93.00 |
| Upper Latitude | 30.00 |
| First Nested Grid. Resolution (3 arc-seconds) | |
| Longitude Left | -97.53333 |
| Lower Latitude | 27.50 |
| Longitude Right | -96.90 |
| Upper Latitude | 28.11666 |
| Second Nested Grid. Resolution (1 arc-seconds) | |
| Longitude Left | -97.1666 |
| Lower Latitude | 27.70 |
| Longitude Right | -96.95 |
| Upper Latitude | 27.98333 |
| Third Nested Grid. Resolution (1/3 arc-seconds) | |
| Longitude Left | -97.11666 |
| Lower Latitude | 27.7991666 |
| Longitude Right | -97.02666 |
| Upper Latitude | 27.8825 |

Figure 18 and Figure 19 depict the nested telescoping grids used to model the East Breaks and Mississippi Canyon landslide respectively.

The domain which has the finer mesh or highest resolution is the 1/3-arc-seconds grid, which covers Port Aransas and surrounding coastal regions. This particular grid has combined bathymetric and topographic data, which allows for the calculation of tsunami inundation onto previously dry land.

**Table 9**. Coordinate limits for the Mississippi Canyon scenario. Tsunami simulation for construction of inundation maps.

| Mississippi Landslide Generated Tsunami | |
|---|---|
| Tsunami Source. Resolution (15 arc-seconds) | |
| Longitude Left | -90.50 |
| Lower Latitude | 27.00 |
| Longitude Right | -88.50 |
| Upper Latitude | 29.00 |
| Foremost Domain. Resolution (15 arc-seconds) | |
| Longitude Left | -97.58333333 |
| Lower Latitude | 25.00 |
| Longitude Right | -87.00 |
| Upper Latitude | 30.00 |
| First Nested Grid. Resolution (3 arc-seconds) | |
| Longitude Left | -97.53333 |
| Lower Latitude | 27.50 |
| Longitude Right | -96.90 |
| Upper Latitude | 28.11666 |
| Second Nested Grid. Resolution (1 arc-seconds) | |
| Longitude Left | -97.1666 |
| Lower Latitude | 27.70 |
| Longitude Right | -96.95 |
| Upper Latitude | 27.98333 |
| Third Nested Grid. Resolution (1/3 arc-seconds) | |
| Longitude Left | -97.11666 |
| Lower Latitude | 27.7991666 |
| Longitude Right | -97.02666 |
| Upper Latitude | 27.8825 |

The finer grids used in the numerical simulation were obtained from two sources:

a) The 1/3 arc-seconds grid, which is a bathymetric-topographic digital elevation model (DEM) developed by Taylor, *et.al.* (2008), was downloaded from publicly available data on the National Geophysical Data Center's U.S. Coastal Relief Model website. The DEM includes the communities of Corpus Christi, Port Aransas , Aransas Pass, Ingleside, Portland and Rockport. It includes Corpus Christi Bay, Aransas Bay, Nueces Bay, Copano Bay, Padre, Mustang, San Jose islands and the northern portion of Baffin Bay. The specifications for the DEM are shown in Table 10. The data sources were obtained from NOAA's National Ocean Service (NOS), the National Geospatial-Intelligence Agency, and the USGS. The 1/3 arc-seconds data was used to generate the 1 arc-seconds and 3 arc-seconds grids.

**Table 10**. Specifications for the Corpus Christi, Texas DEM (Taylor, *et al.*, 2008)

| Grid Area | Corpus Christi, Texas |
|---|---|
| Coverage Area | 96.65 to 97.7 W; 27.3 to 28.15 N |
| Coordinate System | Geographic decimal degrees |
| Horizontal Datum | World Geodetic System 1984 (WGS84) |
| Vertical Datum | Mean High Water (MHW) |
| Vertical Units | Meters |
| Grid Spacing | 1/3 arc-seconds |
| Grid Format | ESRI ASCII raster grid |

b) The 15 arc-seconds grid was downloaded from publicly available data on the National Geophysical Data Center's U.S. Coastal Relief Model website which integrates offshore bathymetry data with land topography. The bathymetric contour data source is from the International Bathymetric Chart of the Caribbean Sea and the Gulf of Mexico project ("U.S. Coastal Relief Model," 2010). The vertical datum source is based on the mean low water elevation and the mean lower-low water elevation. The topographic data source is referenced to NAVD88.

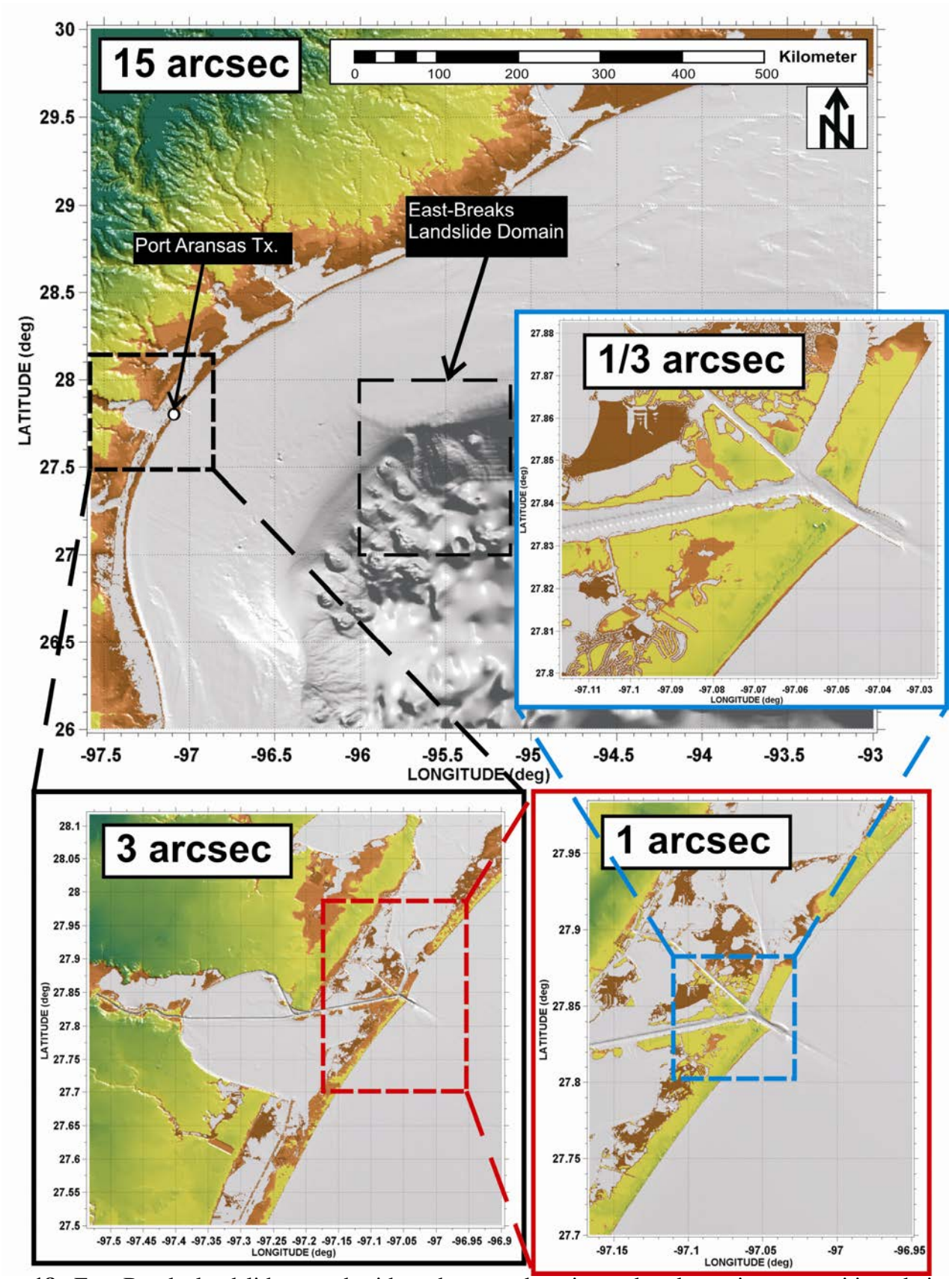


**Figure 18.** East-Breaks landslide nested grids and source domain used to determine tsunami inundation in Port Aransas.

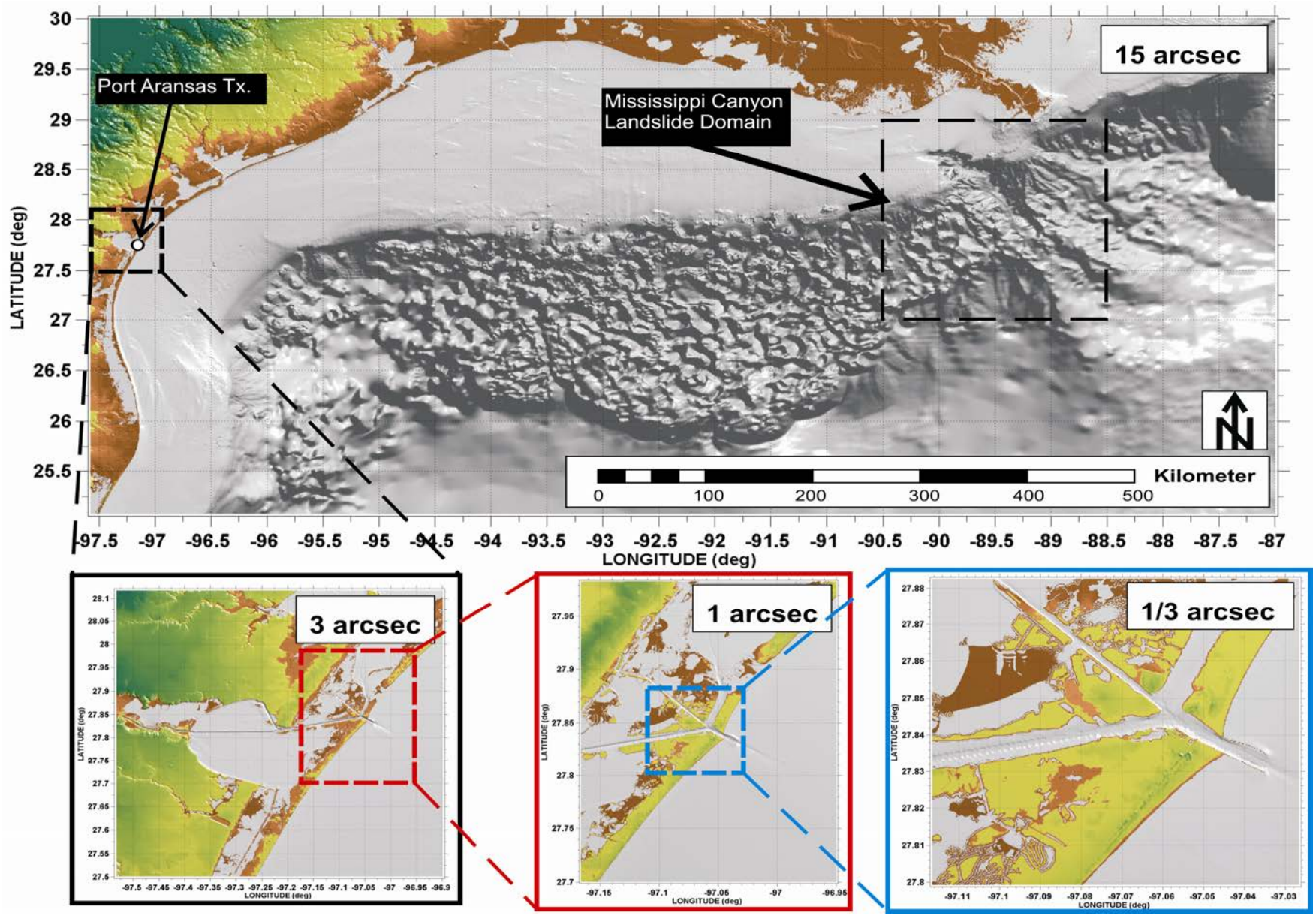


**Figure 19.** Mississippi Canyon landslide nested grids and source domain used to determine tsunami inundation in Port Aransas.

The vertical datum source for the finer grid DEM's are referenced to the mean high water elevation; whereas, the coarser grid is referenced to the mean lower-low water elevation and mean low water elevation. The range of tide variation in Port Aransas is approximately 0.88 ft (0.27m). The measured elevations at station 8775237 in Port Aransas are shown in Table 11.

**Table 11.** Elevations on datum at Tidal Station 8775237 in Port Aransas, TX.

| Elevations on Station Datum<br>National Ocean Service (NOAA) | | |
|---|---|---|
| Station: 8775237 | | |
| Name: Port Aransas, Texas | | |
| Datum | Value (ft) | Description |
| MHHW | 5.55 | Mean Higher-High Water |
| MHW | 5.52 | Mean High Water |
| DTL | | Mean Diurnal Tide Level |
| MTL | 5.12 | Mean Tide Level |
| MSL | 5.17 | Mean Sea Level |
| MLW | 4.72 | Mean Low Water |
| MLLW | 4.57 | Mean Lower-Low Water |

## Model Results

First set of numerical simulation was carried out using TSUNAMI3D to determine the tsunami source caused by each of the three submarine landslide scenarios described by THAG. The submarine landslide scenarios are: East Breaks, Mississippi Canyon and West Florida.

The submarine landslide dimensions were based on the volume of material removed from the excavation region using a technique similar to that applied by ten Brink *et al.* (2006). The technique uses the surrounding bathymetry to outline the extent of the excavation where a discontinuity of isobaths is observed, then, the pre-landslide slope surface is reconstructed by interpolating the nearby existing

isobaths to create a smooth surface and thus estimate a pre-landslide configuration. The reconstructed surface is subtracted from the existing seafloor surface to obtain the submarine landslide volume. The area is estimated based on the volume projection in the horizontal plane.

It is important to mention there are some slightly differences between the volumes/areas determined in this study and the reported by the THAG. The landslide pre-failure configurations used in this study are compared against the reported by the THAG in Table 12.

**Table 12.** Submarine landslide volume/area comparison

| Submarine Landslide | This study | THAG |
|---|---|---|
| **East Breaks** | | |
| Area ($Km^2$) | 519.46 | 519.52 |
| Volume ($Km^3$) | 26.70 | 21.95 |
| **Mississippi Canyon** | | |
| Area ($Km^2$) | 2153.00 | 3687.26 |
| Volume ($Km^3$) | 425.00 | 425.54 |
| **West Florida** | | |
| Area ($Km^2$) | 647.00 | 647.57 |
| Volume ($Km^3$) | 18.40 | 16.20 |

The volume estimates are considered conservative, as the estimates obtained in this study are slightly above the volume estimates reported by the THAG. Likewise, the area estimate for the Mississippi Canyon (2153 $Km^2$ versus 3687.26 $Km^2$) is considered conservative as well, since it is below the reported by the THAG. Replacing the Mississippi Canyon volume of 425$Km^3$ by using the same technique described in ten Brink *et al.* (2006) fills up mostly the upper part of the excavation with an estimated area of 2153 $Km^2$. This landslide volume is localized mostly in upper part of the shelf break slope (in the shallow water region of the excavation area. This arrangement makes this submarine landslide more efficient in generating a large tsunami because the water depth is shallower.

The first set of numerical simulations (which determined the tsunami source for each case scenario) was used as input to NEOWAVE to generate a second set of numerical simulations but using this time a

coarser grid on the entire GOM to determine maximum wave amplitude and tsunami arrival time. Finally, a set of numerical simulations was carried out using nested grids with finer resolution to obtain maximum inundation depth , maximum water elevation, and maximum momentum flux and direction in Port Aransas. A detailed description and discussion of numerical results are presented below for each landslide scenario.

### East Breaks Submarine Landslide Model Results

Figure 20 depicts qualitatively TSUNAMI3D numerical results for the East Breaks initial tsunami source by using a sequence of snapshots. Model parameters, physical properties and computer performance used in the numerical simulation are given in Table 13.

**Table 13.** East Break submarine landslide source model information

| Model Domain | |
|---|---|
| Number of Cells $x$-Direction | 192 |
| Number of Cells $y$-Direction | 240 |
| Number of Cells $z$-Direction | 125 |
| Total Number of Cells | 5'760,000 |
| $dx$ | 422 m |
| $dy$ | 464 m |
| $dz$ | Variable (minimum 4 m) |
| $dt$ | Variable (maximum 0.5 sec) |
| Physical Properties | |
| Water Density | 1025 Kg/ $m^3$ |
| Mud Density | 2000 kg/$m^3$ |
| Mud Angle of Repose | 0° |
| Slip Condition | Yes |
| Eddy Viscosity | 1e-5 $m^2$/sec |
| Computer Info. | |
| CPU Time | 48 hours |
| # of Processors | 4 |

A quantitative plot of the East Breaks initial tsunami source is portrayed in Figure 21. As it can be gleaned from Figure 21, a maximum wave of approximately 144ft (44m) high is recorded after 7 minutes of the slide initiation. The outgoing positive wave with amplitude of 66ft (20m) is followed by a negative

wave or initial surface depression of 78ft (~24m) caused by the landslide down slope motion. Notice that a rebounding wave is emerging from the surface depression between the outgoing and negative backgoing wave. The rebounding wave does not evolve as a massive wave, instead, as a short and dispersive wave, which is believed to be a consequence of the landslide motion in the subcritical regime ($F_R = U_m/\sqrt{gD} \ll 1$, where: $U_m$ is the averaged mud velocity, $D$ is the water depth and $g$ is the gravitational acceleration).

Using the previous 3D results as an input on a coarse grid of 60 arc-seconds, a preliminary numerical simulation was carried out over the entire GOM to identify the effects of the East Break submarine landslide along GOM's coastline, shallow and deep water regions. Maximum wave amplitude and tsunami arrival time for the entire GOM domain were calculated. Model parameters, physical properties and computer performance used in the numerical simulation are given in Table 14. The same GOM's domain size was used to calculate the effect of the tsunami caused by the Mississippi Canyon and West Florida scenarios using their respective landslide configurations/volume as indicated in Table 12.

**Table 14.** East Breaks/Mississippi Canyon/West Florida numerical model information. Maximum wave amplitude and tsunami arrival time for the entire GOM.

| Model Domain | |
|---|---|
| Number of Cells $x$-Direction | 1072 |
| Number of Cells $y$-Direction | 754 |
| Total Number of Cells | 808,288 |
| $dx$ | 60 arc-seconds |
| $dy$ | 60 arc-seconds |
| $dt$ | 2.0 sec) |
| Model or Simulation Time | 4 hours |
| Physical Properties | |
| Water Density | 1000 Kg/ $m^3$ |
| Bottom Friction | 0.025 |
| Computer Info. | |
| CPU Time | <30 min |
| # of Processors | 4 |

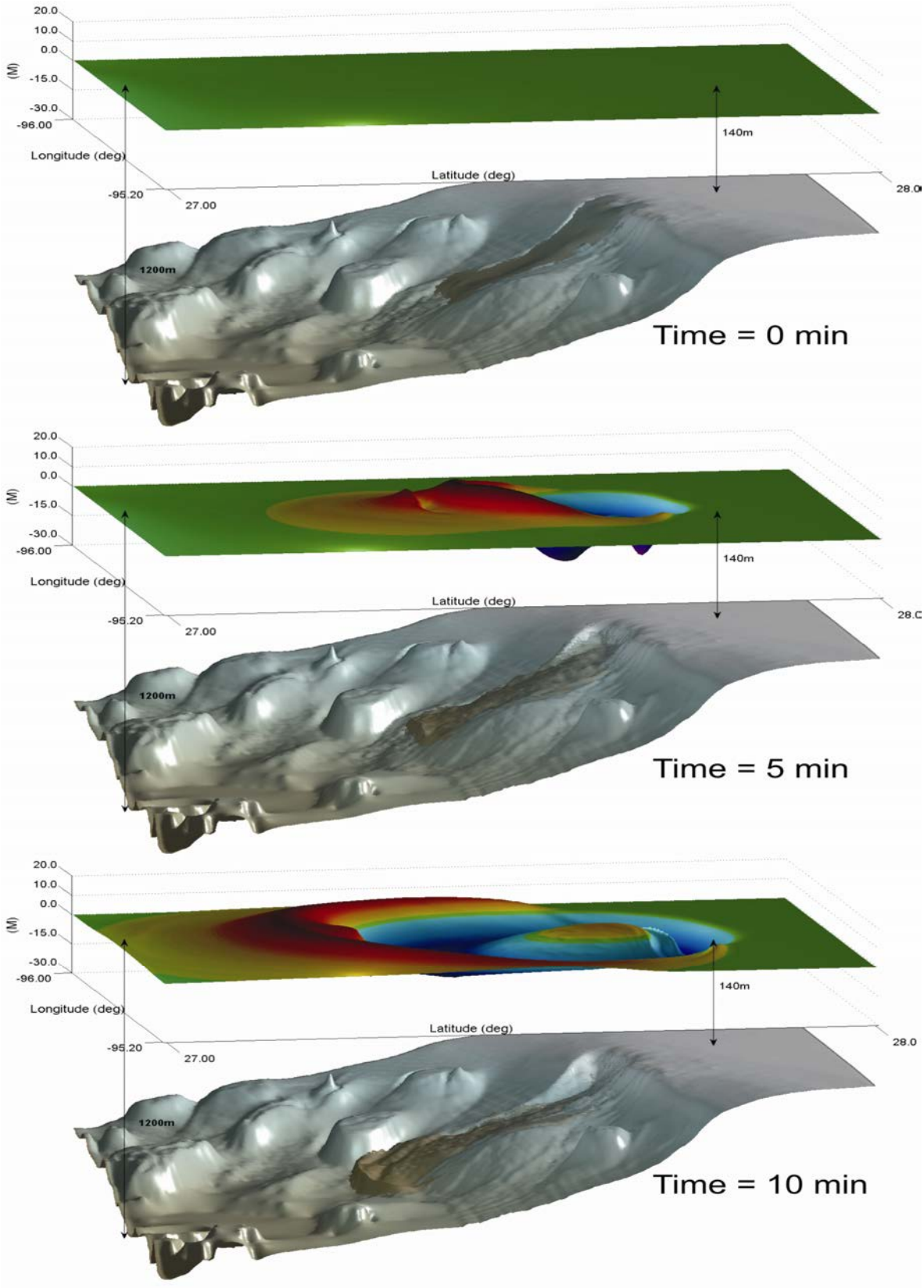


**Figure 20.** Sequence in perspective-view. TSUNAMI3D's numerical result for the determination of the initial tsunami source caused by the East Breaks submarine landslide.

Figure 22 shows East-Breaks landslide maximum wave amplitude recorded after 4 hours of tsunami propagation. Tsunami waves of 10ft (3m) of amplitude are observed very close to the shoreline of Port Aransas. Tsunami energy amplifications on shallow coastal regions are observed in South Padre Island, TX., Cape San Blas, FL., and in the northern region of the state of Tamaulipas, Mexico**.**

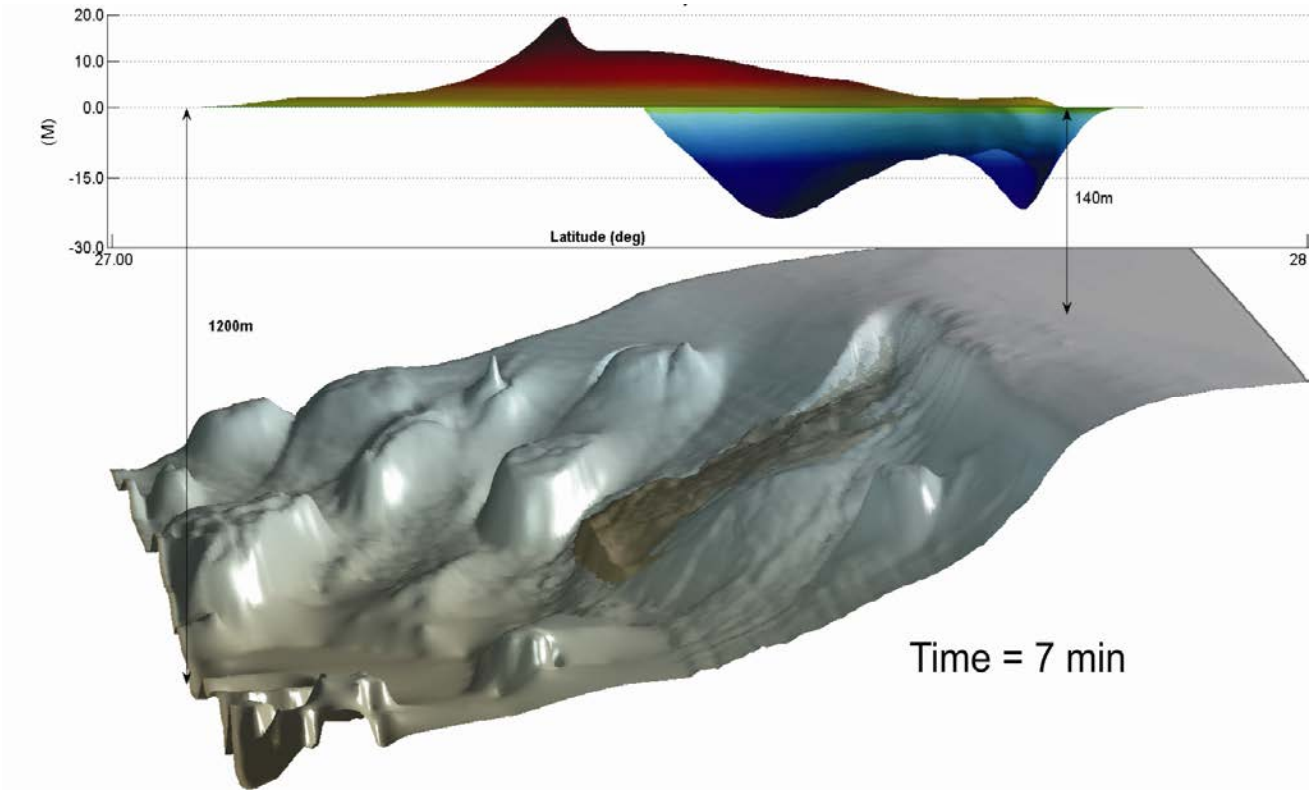


**Figure 21.** TSUNAMI3D's numerical result side-view for the East Breaks submarine landslide. Maximum wave height recorded at 7 minute after the landslide initiation.

Wave-guides are observed along the Sigsbee Escarpment, Mississippi Canyon and other small canyon morphologies along the US and Mexican shelf breaks. The Sigsbee escarpment seems to play an important role as it is believed to be responsible for tsunami wave enhancement in the coastal region around Cape San Blas, FL. On the western side of the GOM, as the tsunami wave propagates parallel or along the Western shelf break slope, wave energy is refracted against the coasts and redirected into South

Padre Island, TX (wave amplitude 16ft or 5m), and the northern region of the state of Tamaulipas, Mexico (wave amplitude 13ft or 4m).

Figure 23 shows tsunami arrival time for the East Breaks landslide scenario. The East Breaks scarp is approximately located at 87 miles (140 Km) east of Port Aransas and the tsunami arrival time is estimated between 1.5 to 2 hours after the submarine landslide initiation. It is important to bring into consideration that after 2.5 hours of the landslide initiation, Cuba which is located 780 miles (1256km) apart from the landslide source is reached almost at the same time that Galveston, TX., which is just located at 125 miles (200 km). The slower tsunami propagation toward Galveston coastline is owed to the shallow water and wider shelf the tsunami encounters as it propagates.

Finally, nested-finer grid simulations were carried out to obtain maximum water depth, maximum water elevation, and maximum momentum flux and direction in Port Aransas.

Figure 24. shows tsunami maximum wave amplitude obtained in the foremost domain (15 arc-seconds) of the nested grid simulation. The finer resolution result matches very well the previous solution obtained using a lower resolution of 60 arc-seconds (see Figure 22 and Figure 24 for comparison). Figure 25 and Figure 26.give an indication of the maximum inundation depth or water depth ($h = \zeta - d$ where $\zeta$ is the sealevel and $d$ is the land elevation. Both quantities are referred to MHW) caused by the East-Breaks landslide in Port Aransas. It is important to point out, that inundation depth shallower than 1ft (0.30m) is not plotted on figures, this means, that flooding regions with water depth lower than one foot are not seen, implying, that the East-Breaks landslide nearly flooded the entire town. Maximum water depth in the populated area (excluding dune system areas) of Port Aransas ranges from 1 to 6ft (0.30 - 1.8m), with an average water depth of ~3ft (~0.9m). Figure 27 shows maximum water elevation or sealevel elevation with respect to MHW. Maximum water elevation in the populated area (excluding dune system areas) of Port Aransas ranges from 6 to 12ft (1.80 - 3.6m), with an average water elevation of ~7ft (~2.1m). The tsunami flooding generated by this event is comparable to the maximum flooding that can

be generated by the storm surge of a hurricane of category 2, see Table 1. These estimations are practical for construction of flood zones maps and flood insurance rate maps.

Figure 28 illustrates the magnitude and direction of the inundation at maximum momentum flux. This quantity is valuable for visualization of the flood or runup direction at maximum tsunami energy. It can be used to estimate forces on structures in Port Aransas. A complete discussion of tsunami forces acting on structures can be found in Yeh, 2007. From Figure 28, it can be gleaned that most of the water entering the town is the result of tsunami overtopping through the dune system of Port Aransas. The momentum flux in the populated area of Port Aransas ranges from 3 to 9 $m^3/s^2$per unit mass and per unit breath. These calculations are important for engineering design purposes, and they can be valuable in the process of determining structures capable to resist tsunami loads. In addition, they can assist coastal managers in quickly assessing the relative vulnerability of a dune system, identifying the nature and location of the dunes weaknesses.

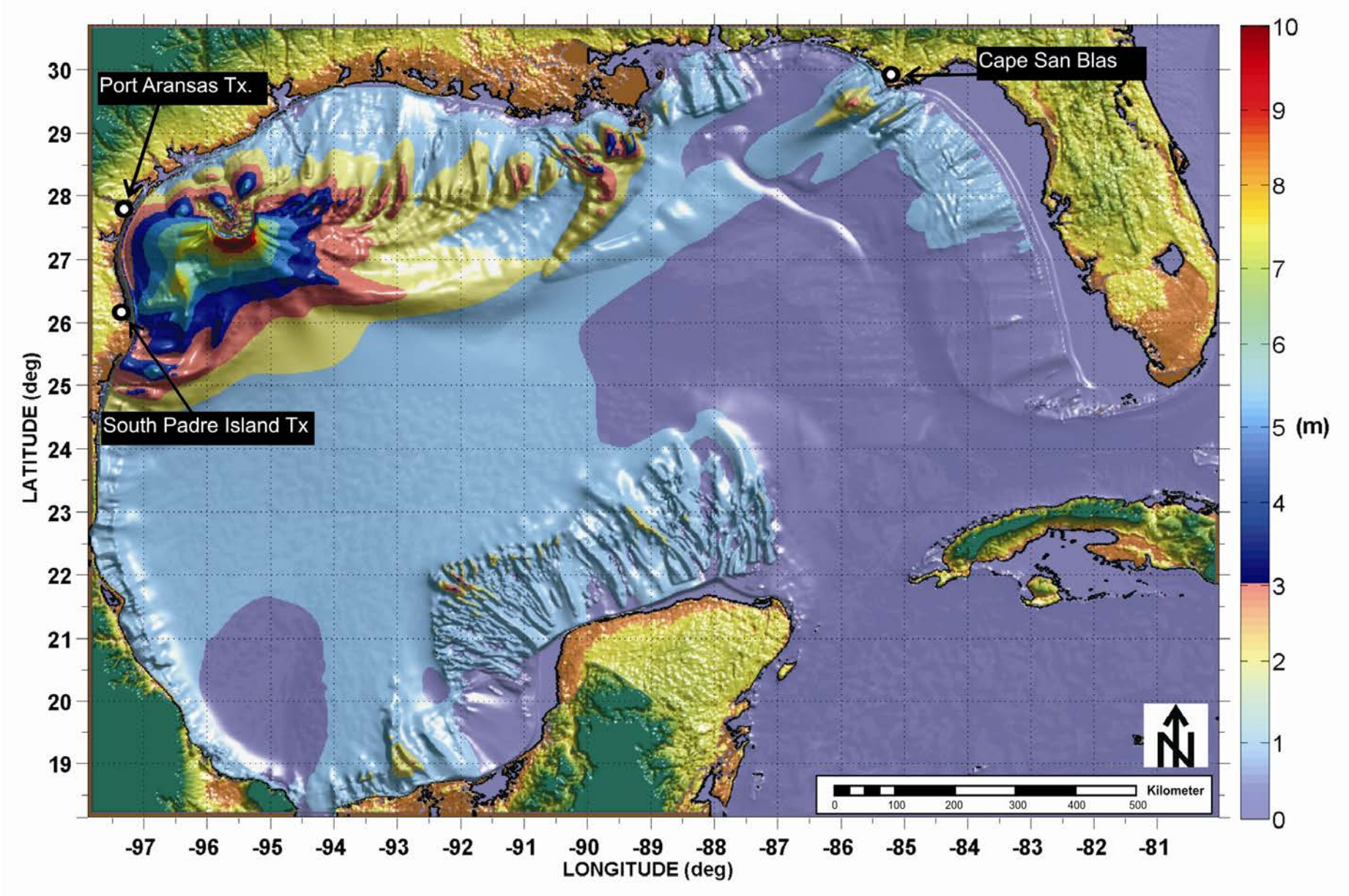


**Figure 22.** East-Breaks landslide maximum wave amplitude using 60 arc-seconds grid resolution.

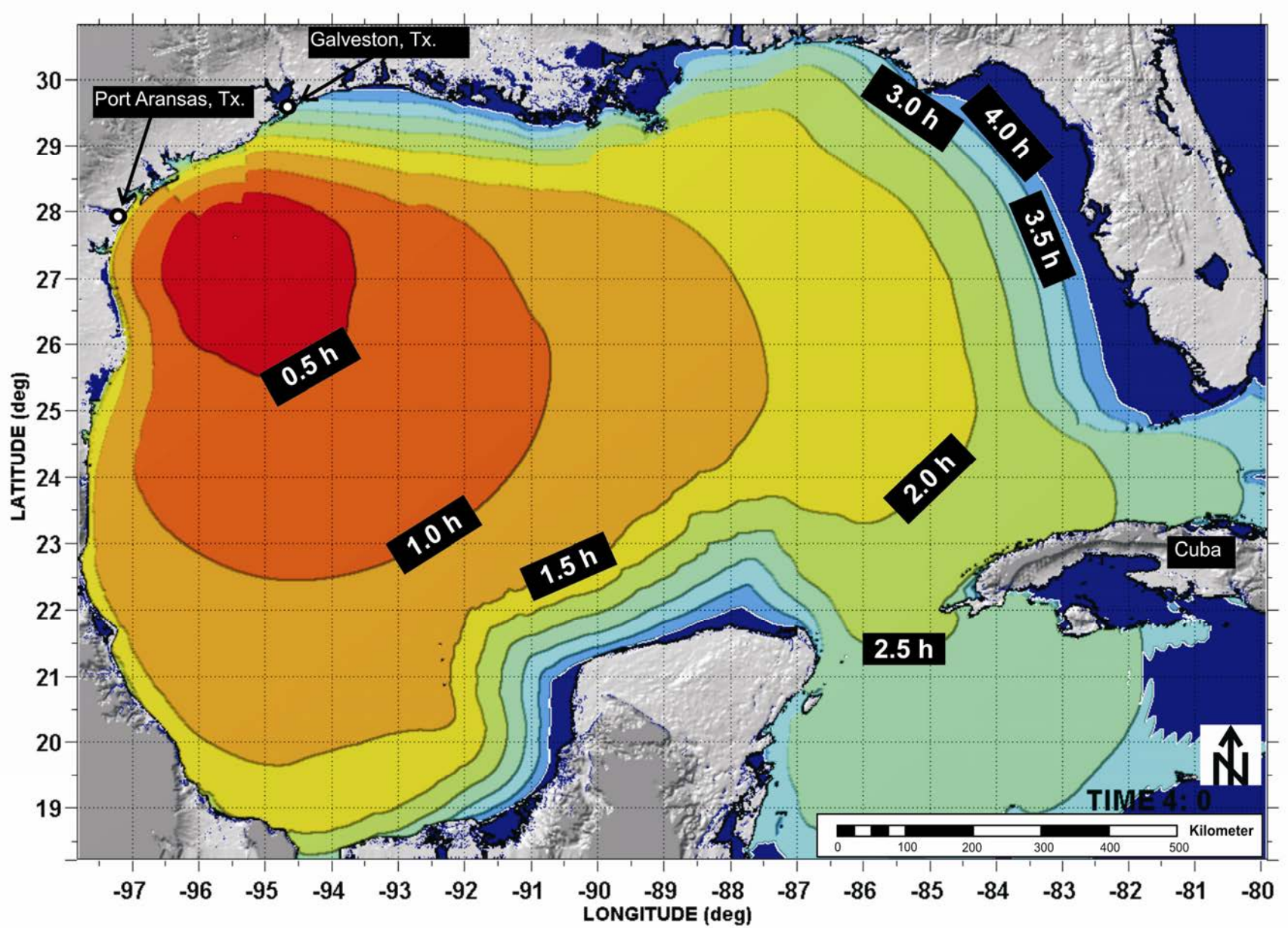


**Figure 23.** Tsunami arrival time for the East Break landslide.

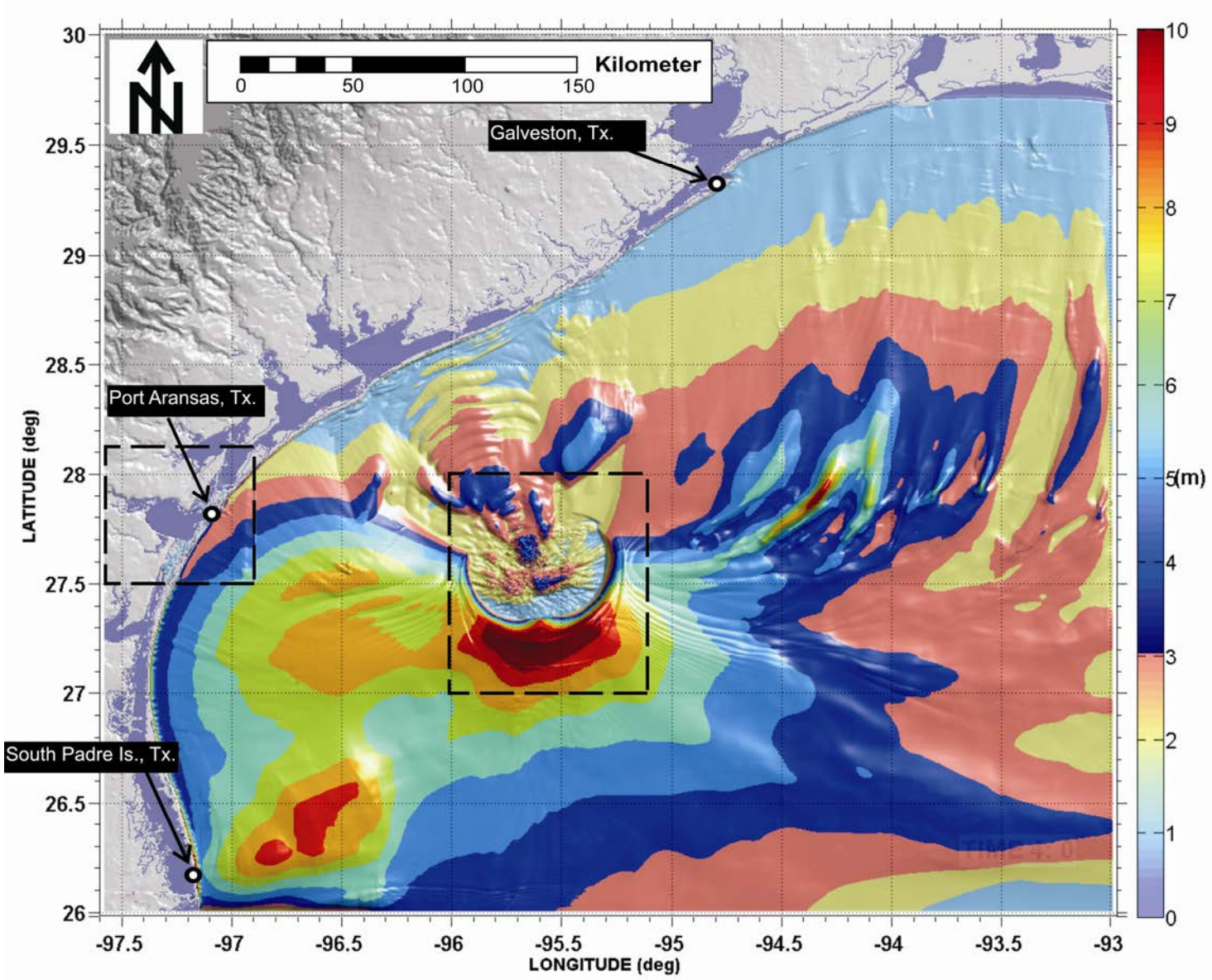


**Figure 24.** East-Breaks landslide maximum wave amplitude using 15 arc-seconds grid resolution. Rectangles indicate domain limits of the first nested grid and landslide source domain.

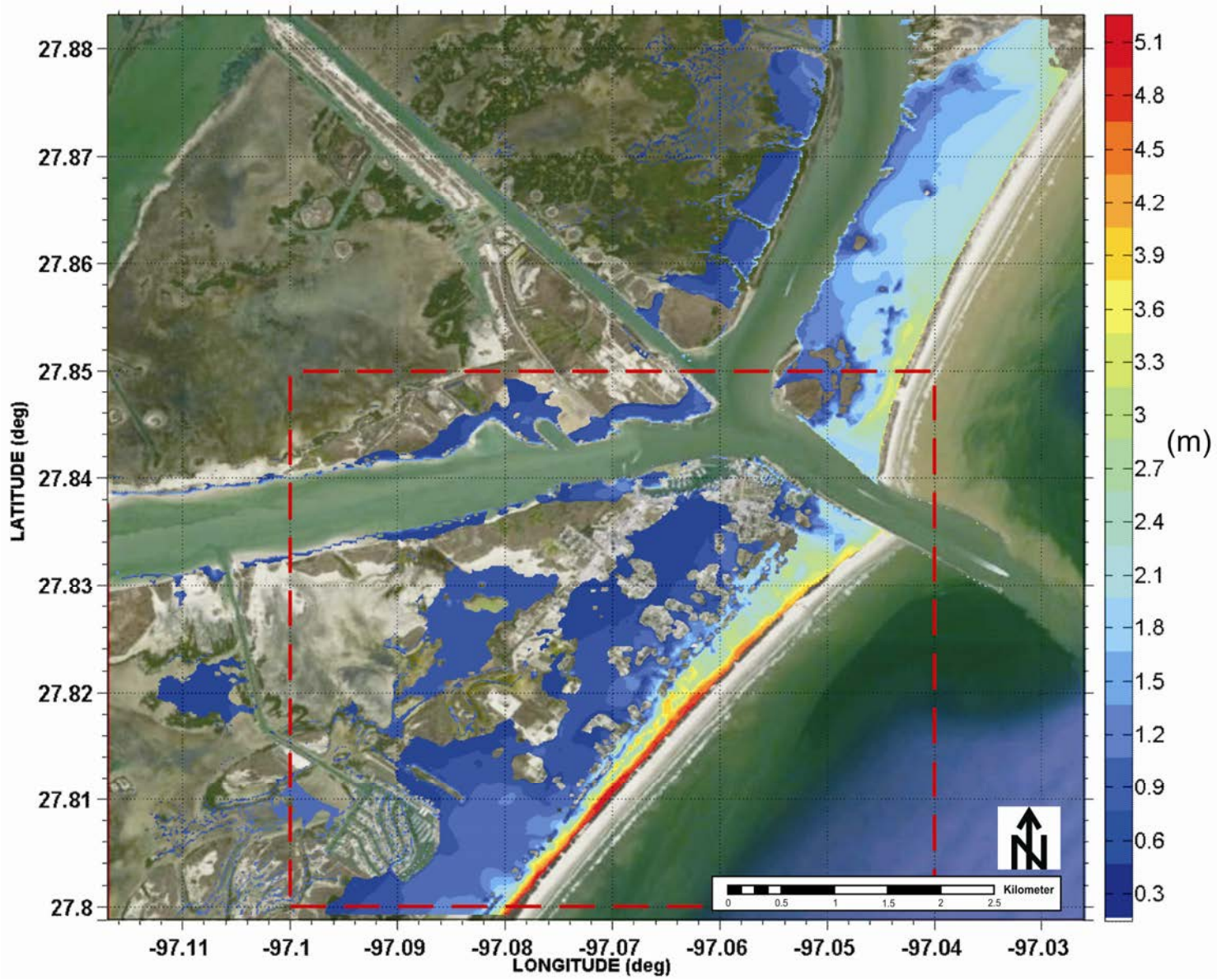


**Figure 25.** Tsunami inundation (water depth) caused by the East-Breaks landslide in Port Aransas. Red rectangle encloses the populated area of Port Aransas.

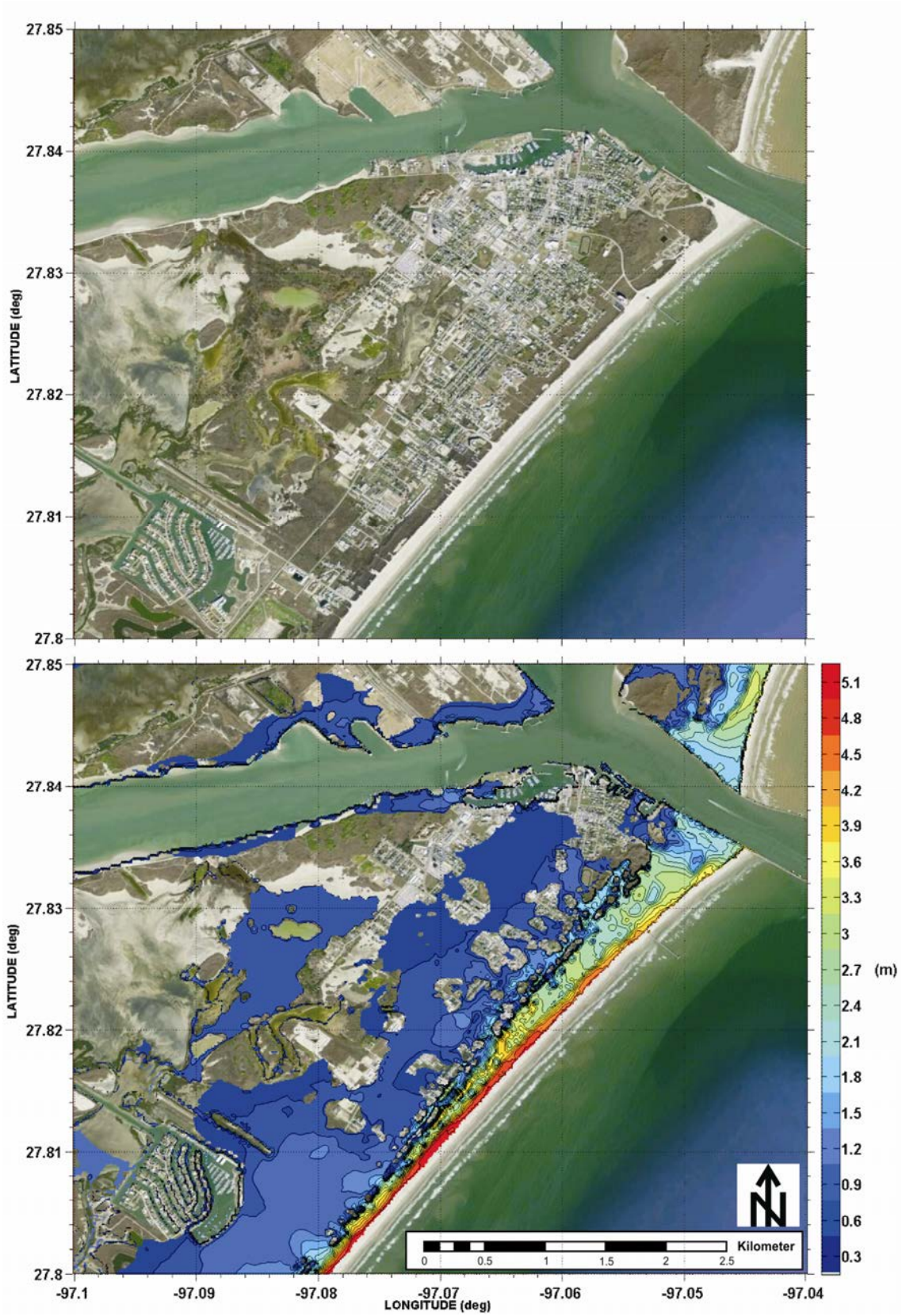


**Figure 26.** Zoom-in from Figure 25. Maximum water depth caused by the East-Breaks landslide in Port Aransas

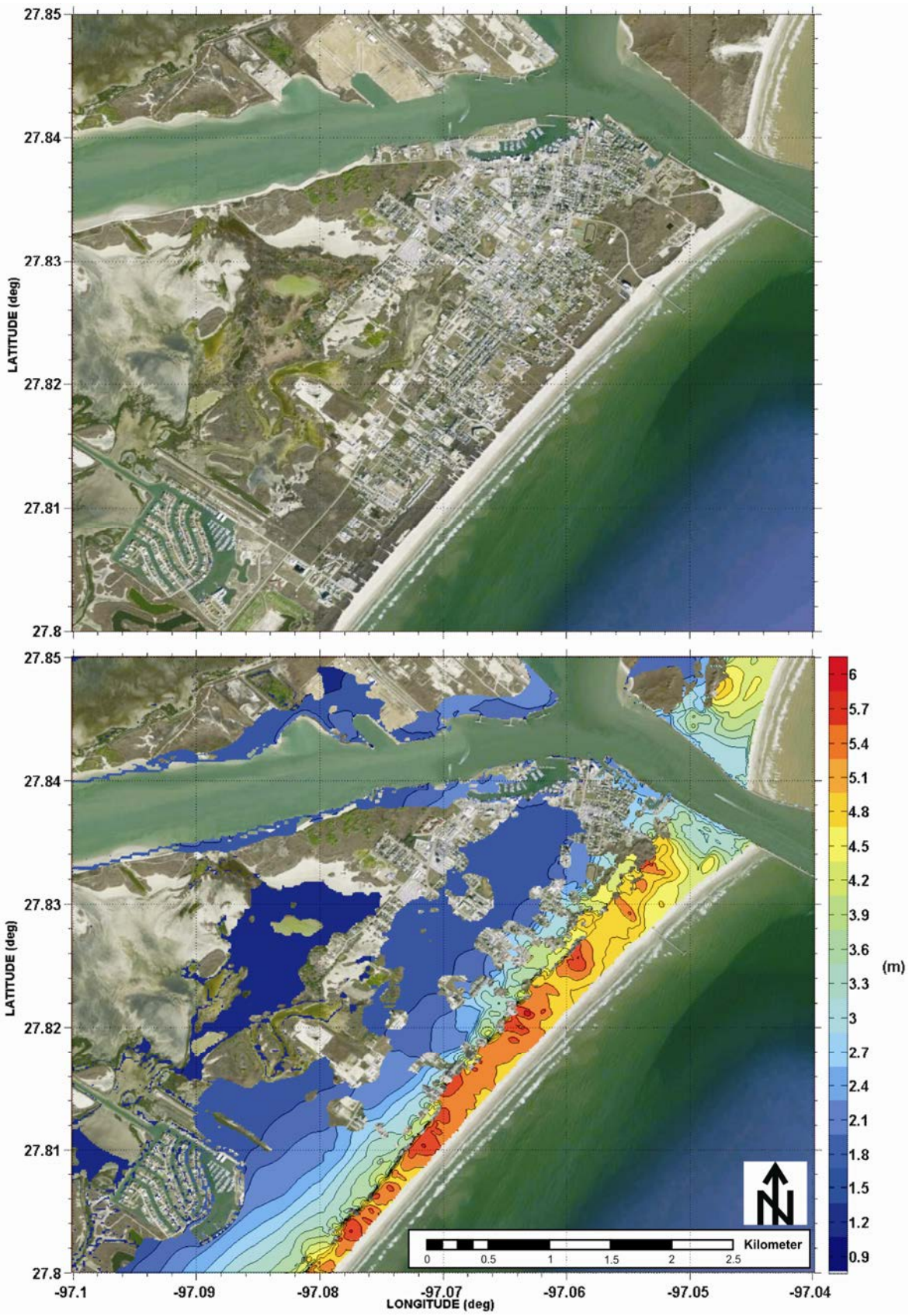


**Figure 27.** Maximum water elevation caused by the East-Breaks landslide in Port Aransas.

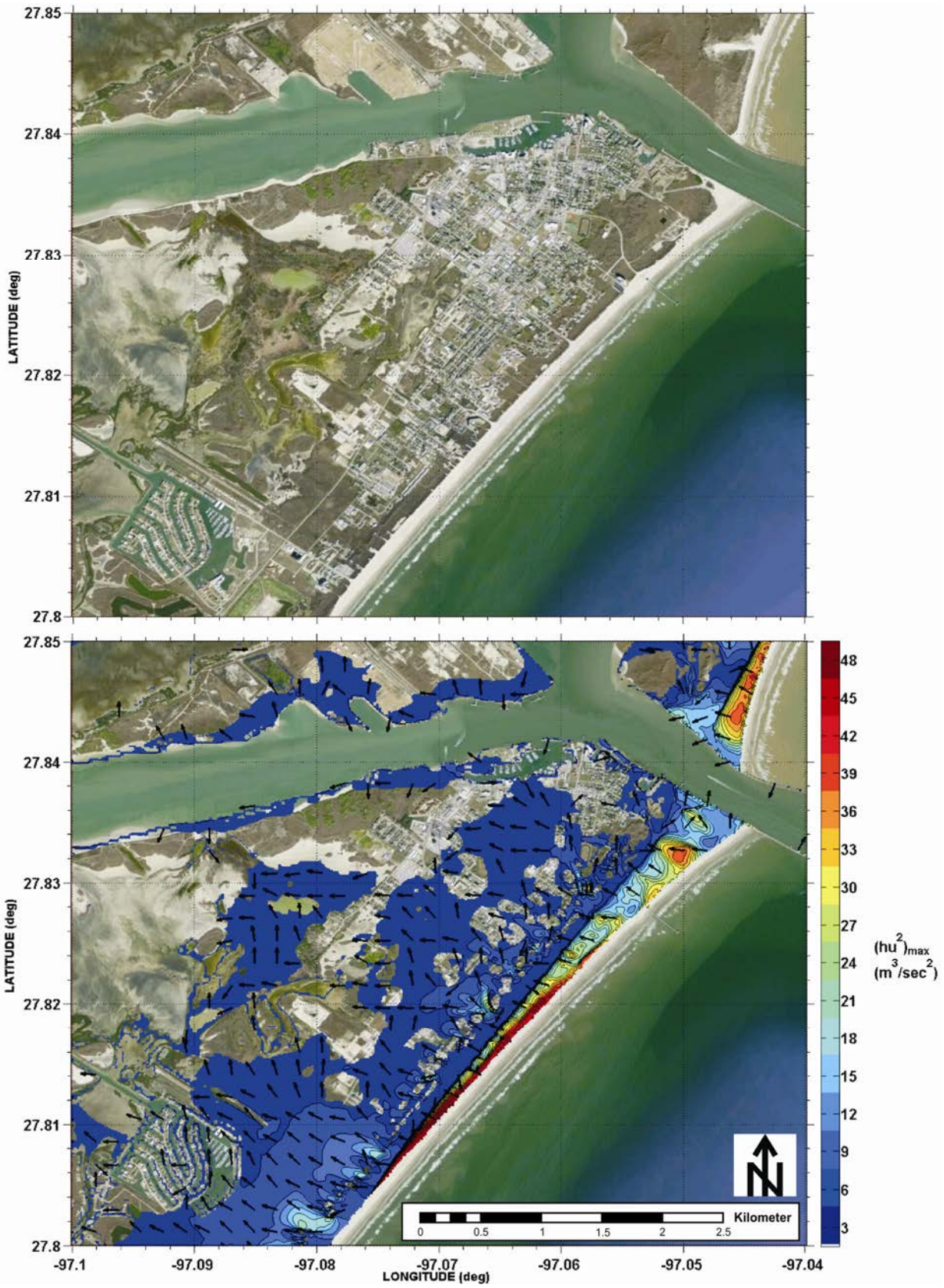


**Figure 28.** Maximum tsunami momentum flux caused by the East-Breaks landslide in Port Aransas. Arrows represent momentum flux direction.

### Mississippi Canyon Submarine Landslide Model Results

Figure 20 depicts qualitatively TSUNAMI3D numerical results for the Mississippi Canyon initial tsunami source by using a sequence of snapshots. Model parameters, physical properties and computer performance used in the numerical simulation are given in Table 15.

**Table 15**. Mississippi Canyon submarine landslide source model information

| Model Domain | |
|---|---|
| Number of Cells $x$-Direction | 480 |
| Number of Cells $y$-Direction | 480 |
| Number of Cells $z$-Direction | 75 |
| Total Number of Cells | 17'280,000 |
| $dx$ | 410 m |
| $dy$ | 464 m |
| $dz$ | Variable (minimum 4 m) |
| $dt$ | Variable (maximum 0.5 sec) |
| Physical Properties | |
| Water Density | 1025 Kg/ $m^3$ |
| Mud Density | 2000 kg/$m^3$ |
| Mud Angle of Repose | 0° |
| Slip Condition | Yes |
| Eddy Viscosity | 1e-5 $m^2$/sec |
| Computer Info. | |
| CPU Time | ~160 hours |
| # of Processors | 4 |

A quantitative plot of the Mississippi Canyon initial tsunami source is portrayed in Figure 30. As it can be gleaned from Figure 30, a maximum wave of approximately 426ft (130m) high is recorded after 8 minutes of the slide initiation. The outgoing positive wave with amplitude of 210ft (64m) is followed by a negative wave or initial surface depression of 216ft (66m) caused by the landslide down slope motion.

Using the previous 3D results as an input on a coarse grid of 60 arc-seconds, a preliminary numerical simulation was carried out over the entire GOM to identify the effects of the Mississippi Canyon submarine landslide along GOM's coastline, shallow and deep water regions. Maximum wave amplitude

and tsunami arrival time for the entire GOM domain were calculated. Model parameters, and physical properties used in the numerical simulation are given in Table 14.

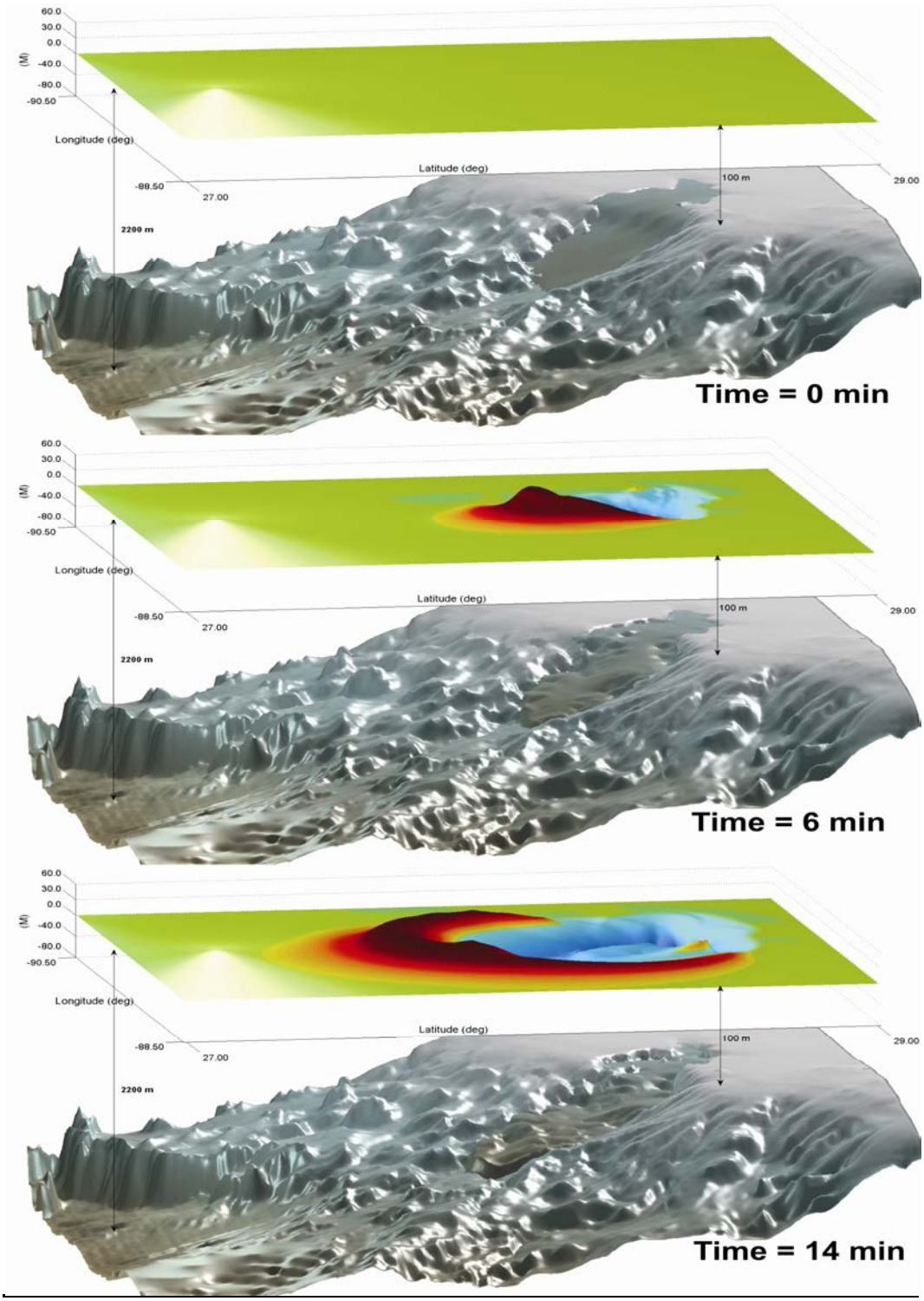


**Figure 29.** Sequence in perspective-view. TSUNAMI3D's numerical result for the determination of the initial tsunami source caused by the Mississippi Canyon submarine landslide.

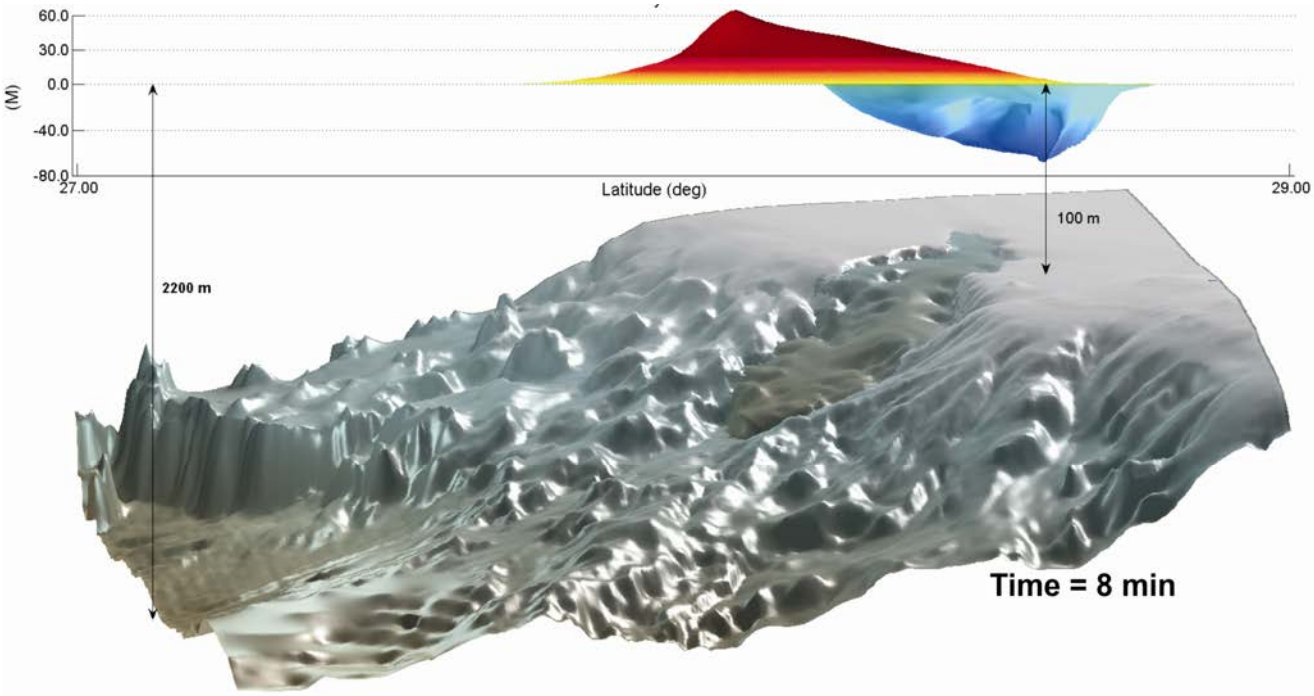


**Figure 30.** TSUNAMI3D's numerical result side-view for the Mississippi Canyon submarine landslide. Maximum wave height recorded at 8 minutes after the landslide initiation.

Figure 31 shows Mississippi Canyon landslide maximum wave amplitude recorded after 4 hours of tsunami propagation. From Figure 31, tsunami waves of 16ft (5m) of amplitude are observed on the shoreline of Port Aransas. Tsunami energy amplifications are observed on coastal shallow regions of Port Aransas and South Padre Island, TX., Fort Walton Beach-to-Cape San Blas, FL. and Cuba. Offshore wave amplifications are notorious on the northern shelf of the Yucatan Peninsula, Mexico, and along of the US-GOM's shelf breaks. Wave-guides are observed along the Sigsbee Escarpment, Mississippi Canyon and other small canyon morphologies along the US and Mexican shelf breaks. Again, the Sigsbee escarpment seems to be responsible for tsunami wave enhancement in Port Aransas coastal region and Cape San Blas, FL. Wave amplitude of 20ft (6m) high is observed on the shoreline of South Padre Island, TX and the northern region of the state of Tamaulipas, Mexico.

Figure 32 shows tsunami arrival time for the Mississippi Canyon submarine landslide scenario. The Mississippi Canyon scarp is approximately located at 443 miles (713 Km) east of Port Aransas and the tsunami arrival time is estimated between 3.0 to 3.5 hours after the submarine landslide initiation.

Figure 33 shows tsunami maximum wave amplitude obtained in the foremost domain (15 arc-seconds) for the nested grid numerical simulation. Tsunami waves of 38ft (~12m) of amplitude are observed on the shoreline of Grand Island, LA. Notice on figure that wave amplitude greater than 15m (50ft) cannot be discerned in the plot. This is intended to visualize regions that tsunami waves surpass the required deck height (50ft) of most offshore platforms in the GOM. The result gives an indication that such an event ($425Km^3$) may put in danger the integrity of oil production in the GOM.

Figure 34 and Figure 35 show maximum inundation depth caused by the Mississippi Canyon landslide in Port Aransas. The Mississippi Canyon landslide catastrophically flooded the entire town by overtopping the dune system. Maximum water depth in the populated area (excluding dune system areas) of Port Aransas ranges from 4 to 11ft (1.2 - 3.3m) with an average water depth of ~8ft (~2.4m). Figure 36 shows maximum water elevation in the populated area of Port Aransas with respect to MHW. Water elevation ranges from 11 to 18ft (3.3 - 5.4m) with an averaged water elevation of ~13ft (~3.9m). The tsunami flooding generated by this event is comparable to the maximum flooding that can be generated by the storm surge of a hurricane of category 4, see Table 1.

Figure 37 illustrates the magnitude and direction of the inundation at maximum momentum flux. From Figure 37 can be gleaned that most of the water entering the town is the result of tsunami overtopping the dune system of Port Aransas. The momentum flux average in the populated area of Port Aransas is around $25m^3/s^2$per unit mass and per unit breath. This quantity is important for engineering design purposes, and it can assist coastal managers in quickly assessing the relative vulnerability of a dune system.

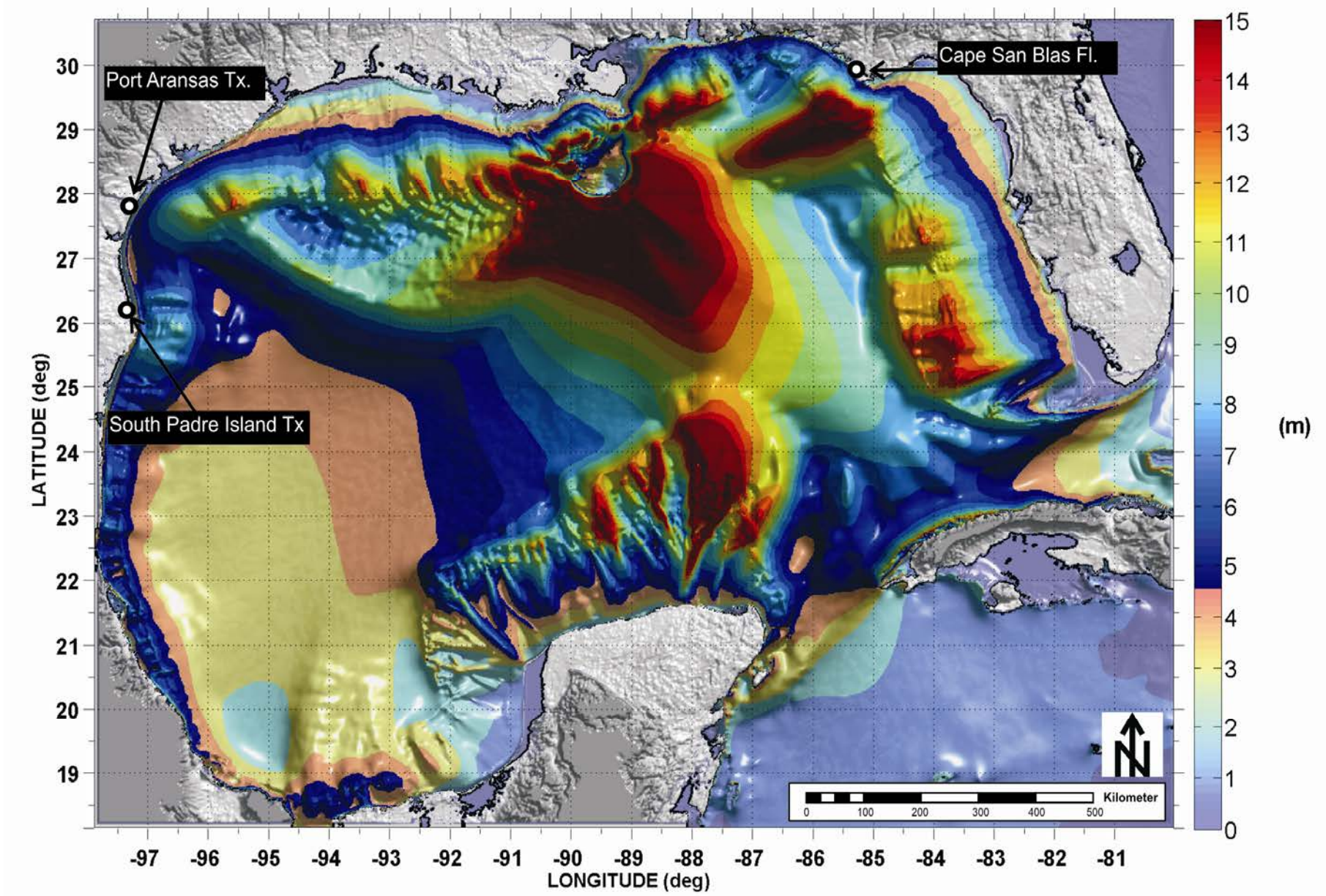


**Figure 31.** Mississippi Canyon landslide maximum wave amplitude using 60 arc-seconds grid resolution.

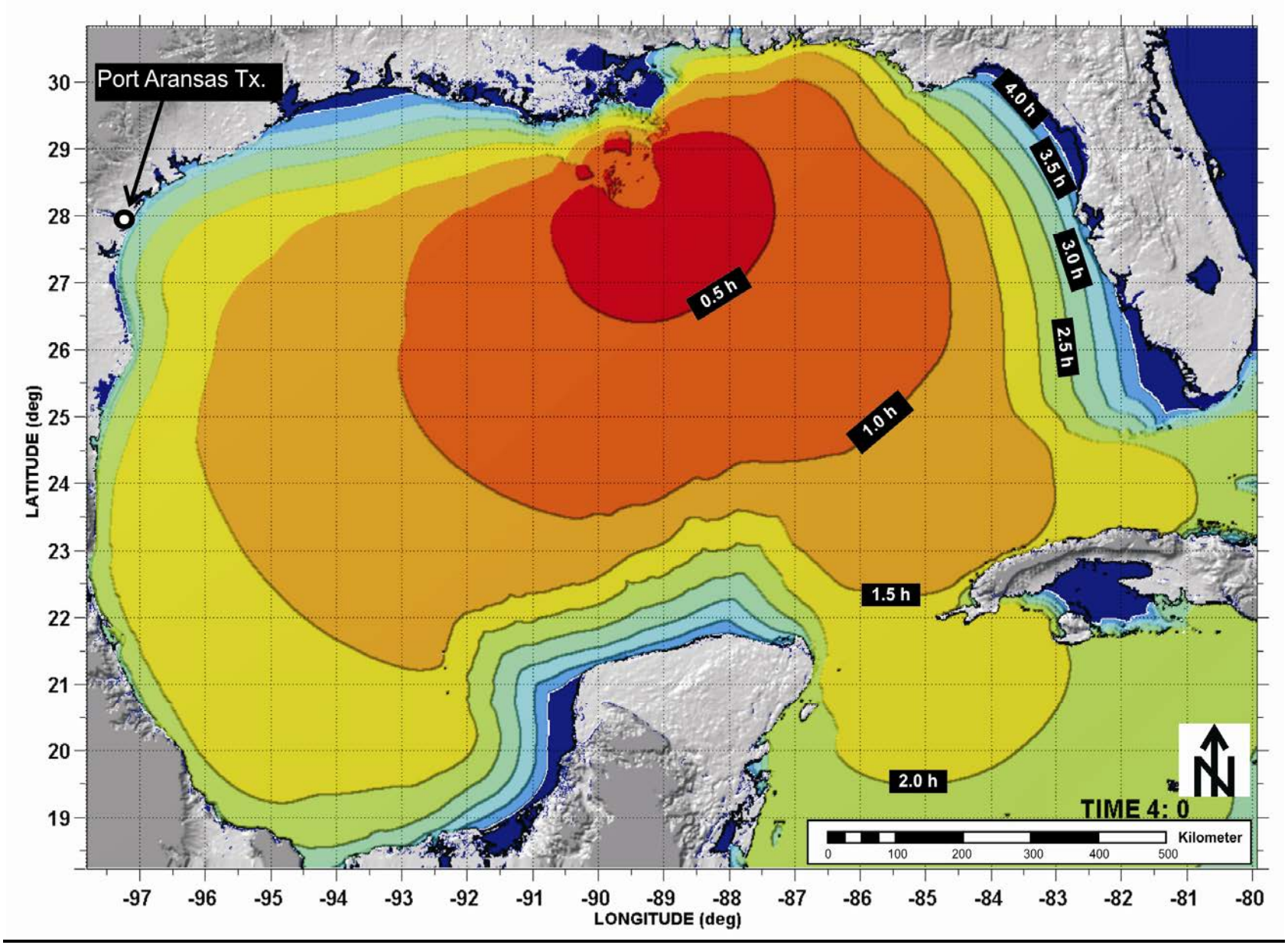


**Figure 32.** Tsunami arrival time for the Mississippi Canyon landslide.

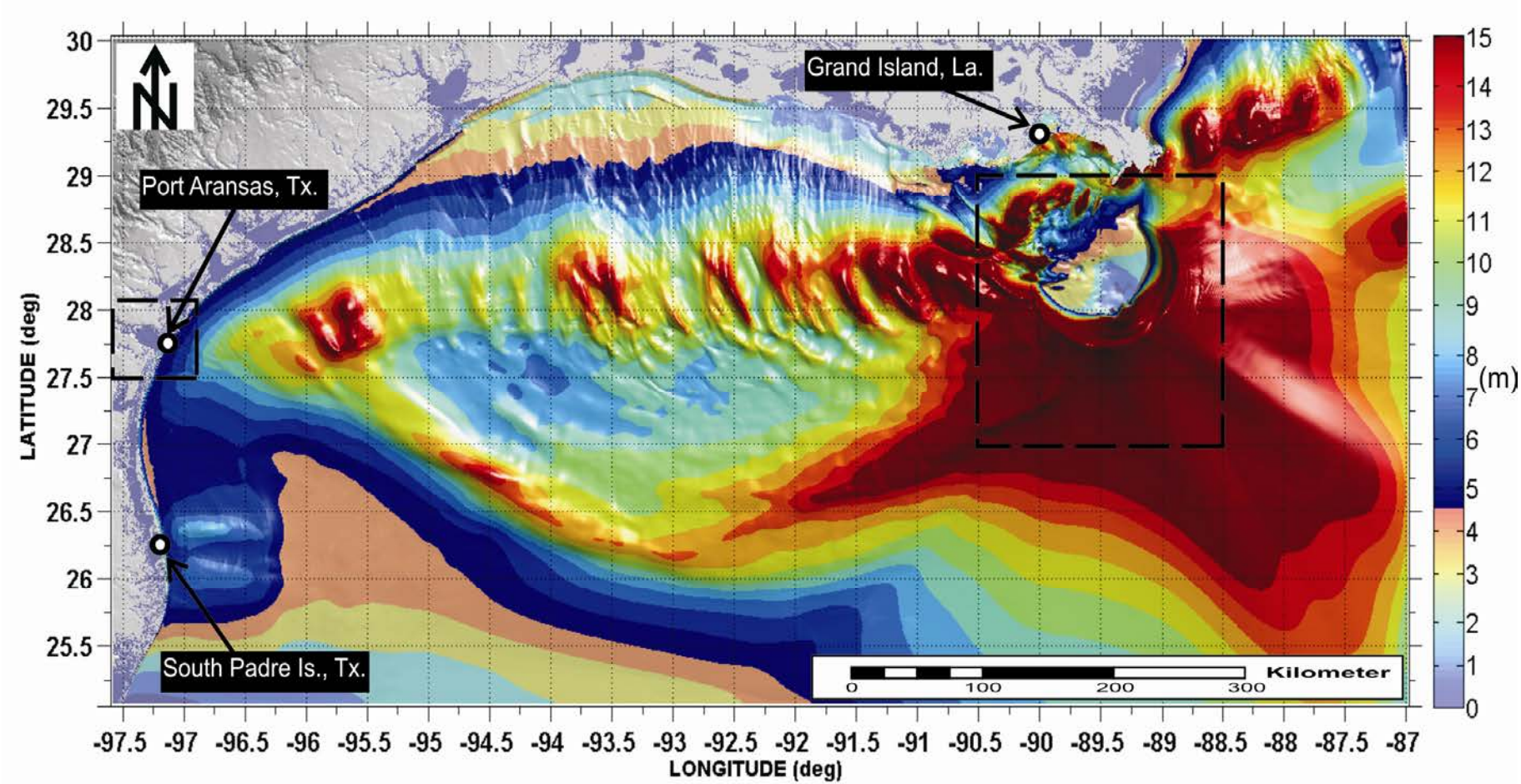


**Figure 33.** Mississippi Canyon landslide maximum wave amplitude using 15 arc-seconds grid resolution. Rectangles indicate domain limits of the first nested grid and landslide source domain.

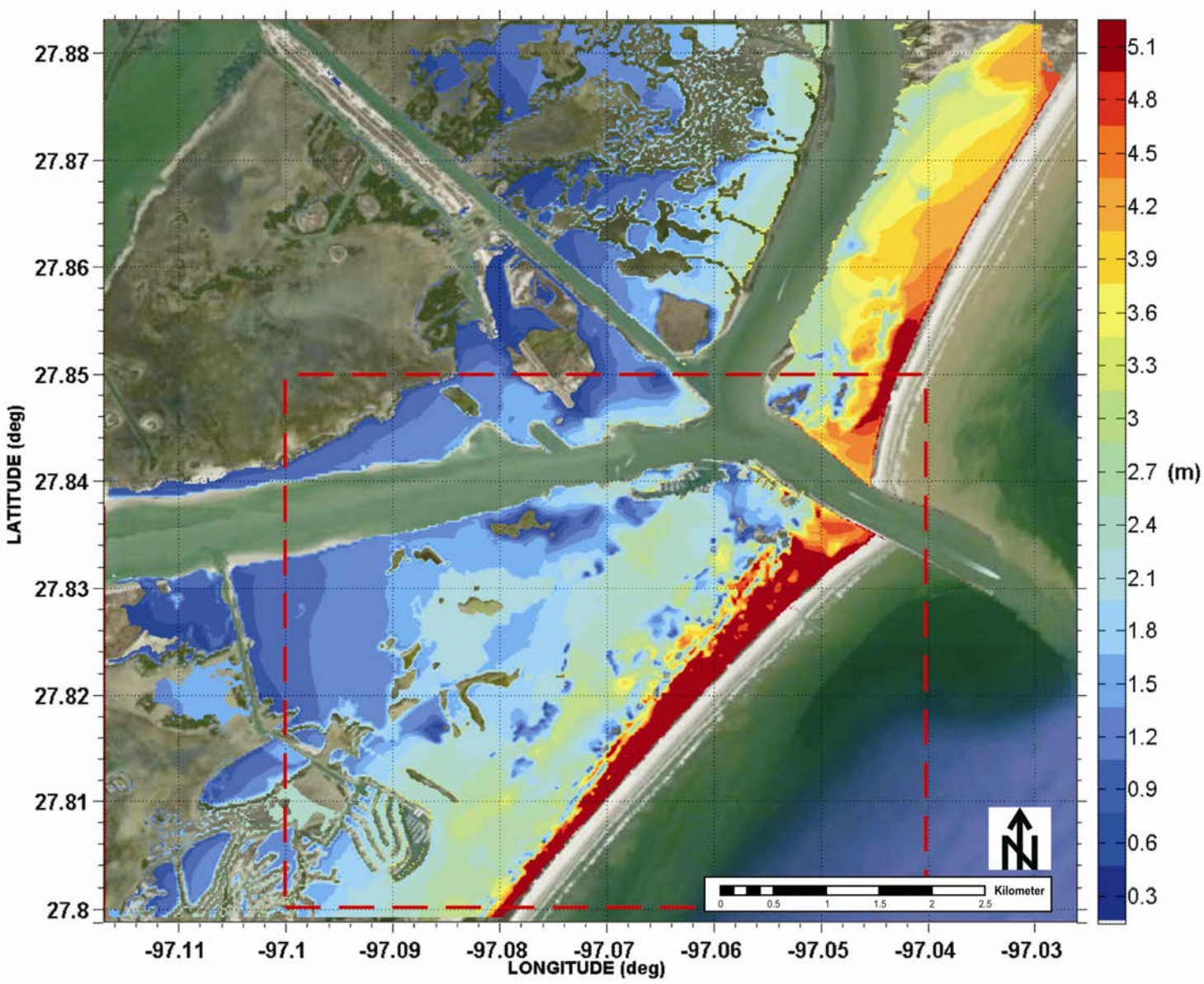


**Figure 34.** Tsunami inundation (water depth) caused by the Mississippi Canyon landslide in Port Aransas. Red rectangle encloses the populated area of Port Aransas.

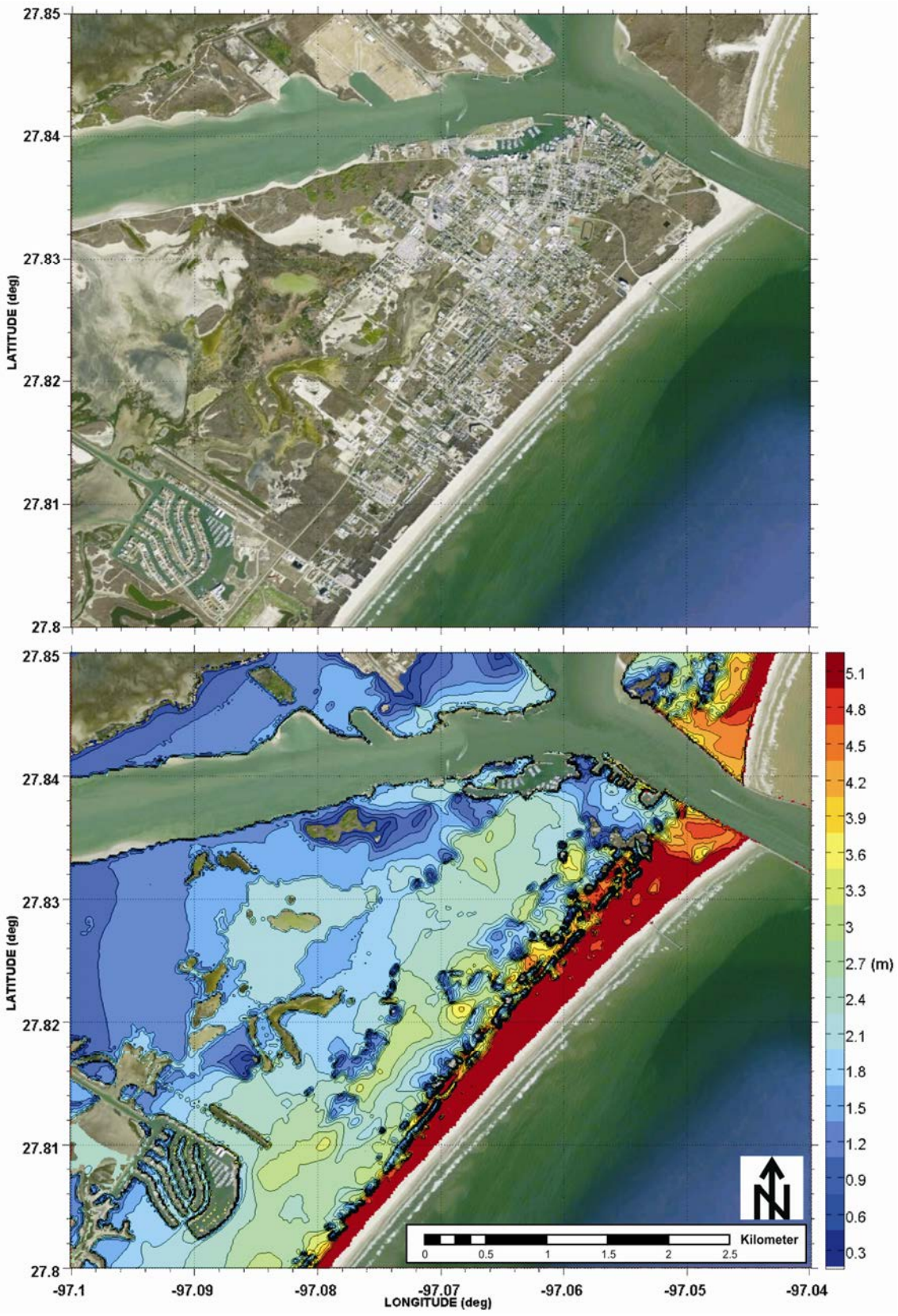


**Figure 35.** Zoom-in from Figure 34 Maximum water depth caused by the Mississippi Canyon landslide in Port Aransas.

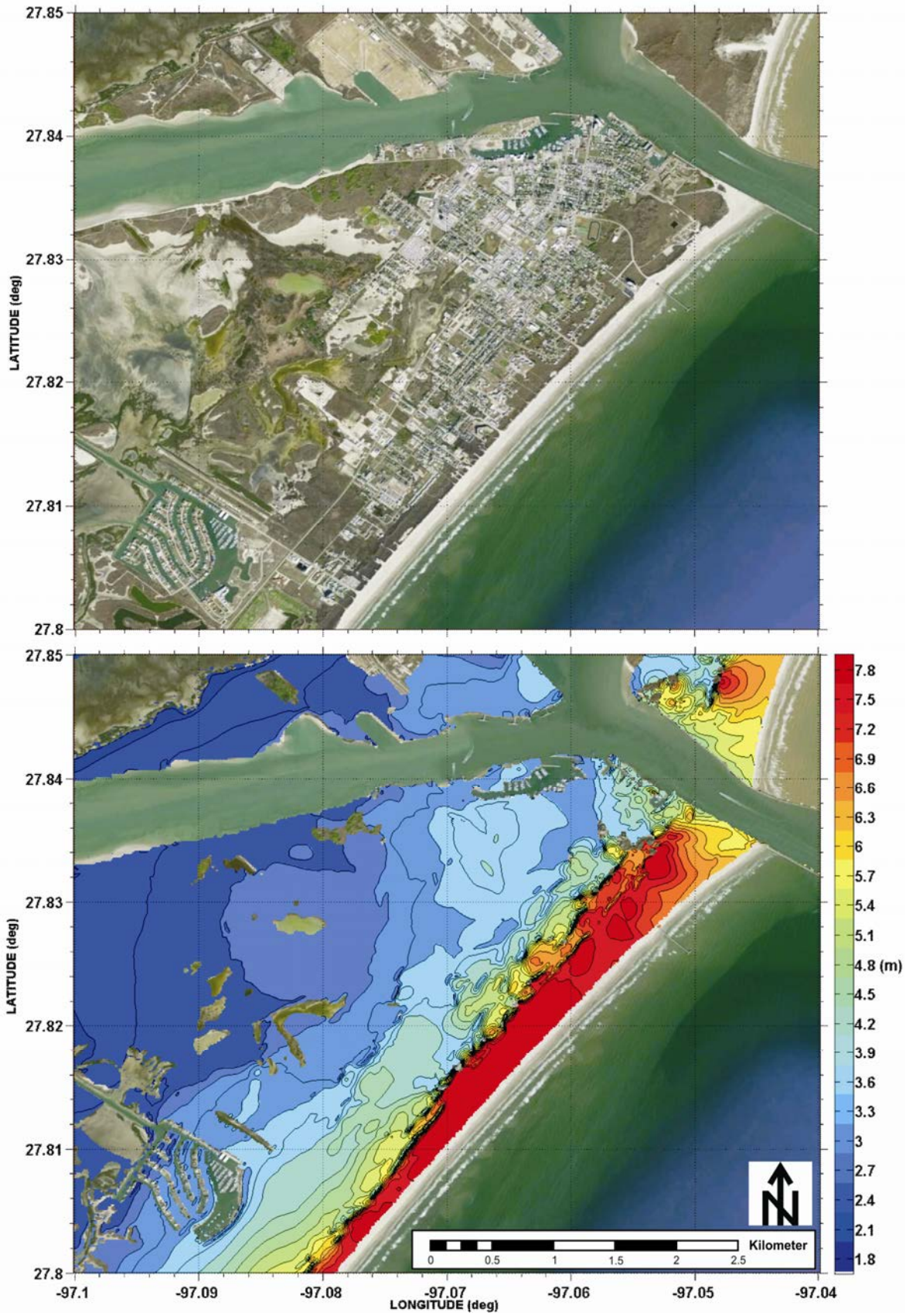


**Figure 36.** Maximum water elevation caused by the Mississippi Canyon landslide in Port Aransas.

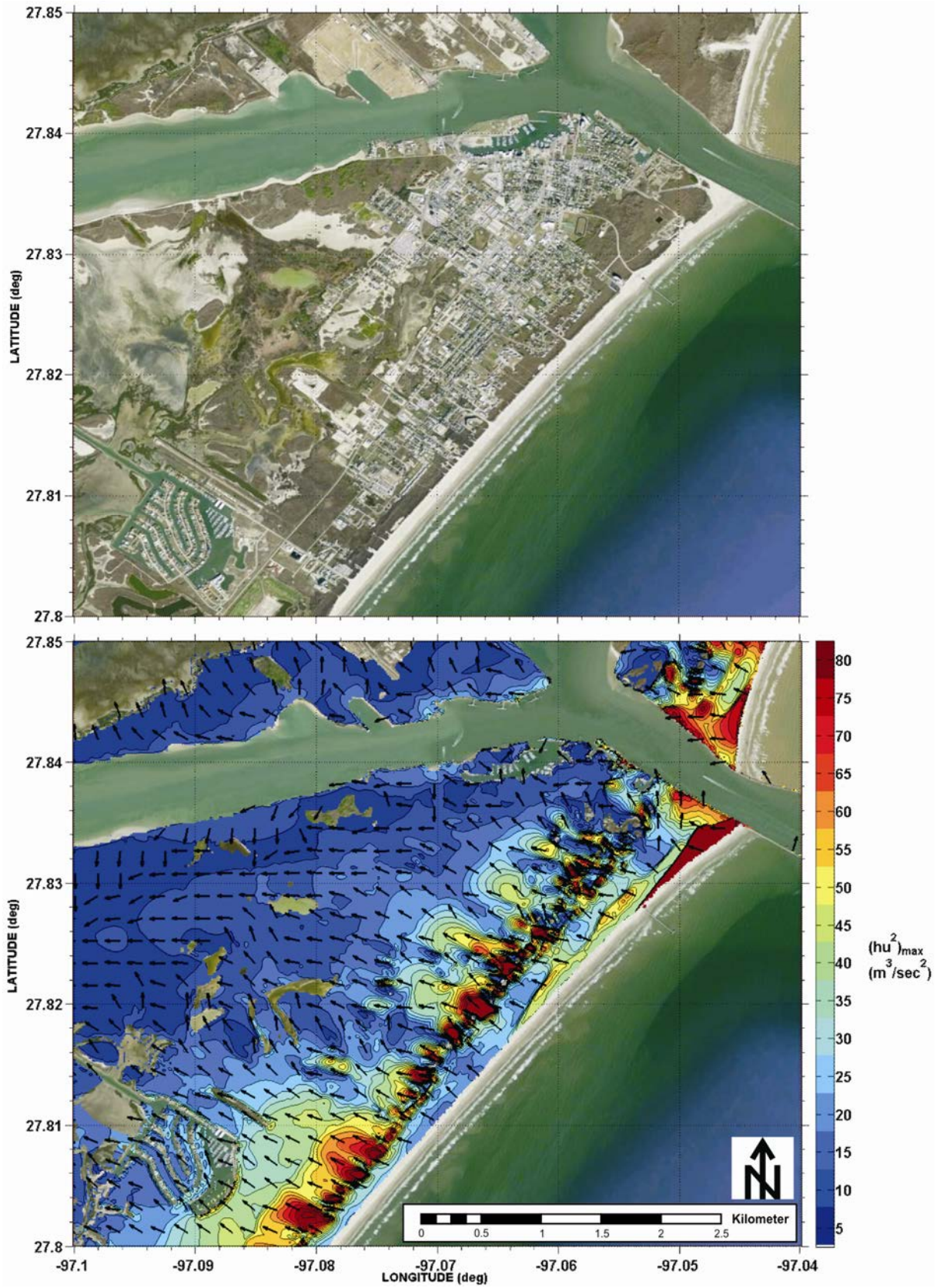


**Figure 37.** Maximum tsunami momentum flux caused by the Mississippi Canyon landslide in Port Aransas. Arrows represent momentum flux direction.

### West Florida Submarine Landslide Model Results

Figure 38 depicts qualitatively TSUNAMI3D numerical results for the West Florida initial tsunami source by using a sequence of snapshots. Model parameters, physical properties and computer performance used in the numerical simulation are given in Table 16.

**Table 16**. West Florida submarine landslide source model information

| Model Domain | |
|---|---|
| Number of Cells $x$-Direction | 360 |
| Number of Cells $y$-Direction | 360 |
| Number of Cells $z$-Direction | 120 |
| Total Number of Cells | 15'552,000 |
| $dx$ | 416 m |
| $dy$ | 464 m |
| $dz$ | Variable (minimum 2 m) |
| $dt$ | Variable (maximum 0.2 sec) |
| Physical Properties | |
| Water Density | 1025 Kg/ $m^3$ |
| Mud Density | 2000 kg/$m^3$ |
| Mud Angle of Repose | 0° |
| Slip Condition | Yes |
| Eddy Viscosity | 1e-5 $m^2$/sec |
| Computer Info. | |
| CPU Time | 96 hours |
| # of Processors | 4 |

A quantitative plot of the West Florida initial tsunami source is portrayed in Figure 39. As it can be gleaned from Figure 39, a maximum wave of approximately 114ft (35m) high is recorded after 2.1 minutes of the landslide initiation. The outgoing positive wave with amplitude of 52ft (16m) is followed by a negative wave or initial surface depression of 62ft (19m) caused by the landslide down slope motion.

Using the previous 3D results as an input on a coarse grid of 60 arc-seconds, a preliminary numerical simulation was carried out over the entire GOM to identify the effects of the West Florida submarine landslide along GOM's coastline, shallow and deep water regions. Maximum wave amplitude and

tsunami arrival time for the entire GOM domain were calculated. Model parameters, physical properties and computer performance used in the numerical simulation are given in Table 14.

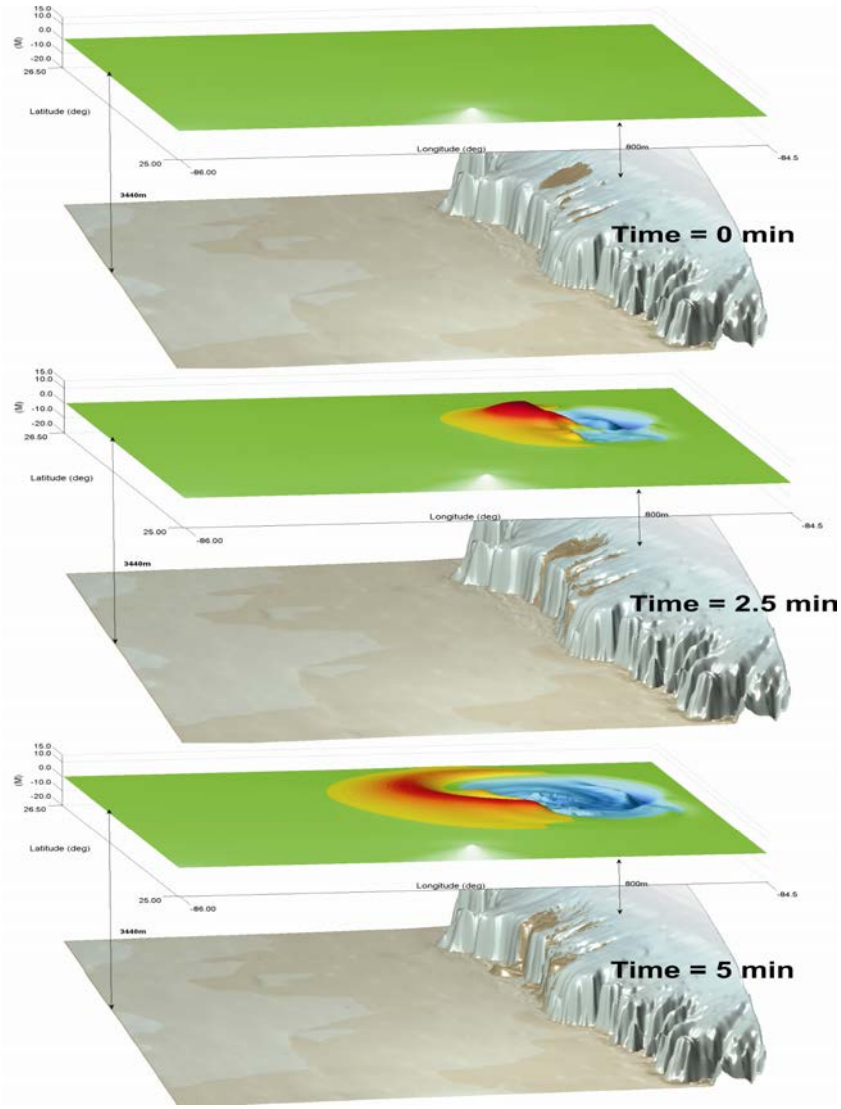


**Figure 38.** Sequence in perspective-view. TSUNAMI3D's numerical result for the determination of the initial tsunami source caused by the West Florida submarine landslide.

Figure 40 shows West Florida landslide maximum wave amplitude recorded after 4 hours of tsunami propagation. Tsunami waves of 3ft (1m) of amplitude are recorded just offshore of Port Aransas coast. Again, tsunami energy amplifications on coastal regions are observed in Port Aransas and South Padre Island, TX., Fort Walton Beach-to-Cape San Blas, FL. and in the northern region of the state of

Tamaulipas, Mexico. Offshore wave amplification is notorious on the Texas and Louisiana shelf breaks and on the northern shelf of the Yucatan Peninsula, Mexico.


**Figure 39.** TSUNAMI3D's numerical result side-view for the West Florida submarine landslide. Maximum wave height recorded at 2.1 minutes after the landslide initiation.

Figure 41 shows tsunami arrival time for the West Florida submarine landslide scenario. The West Florida scarp is approximately located at 763 miles (1228 Km) east of Port Aransas and the tsunami arrival time is estimated in 3.5 hours after the submarine landslide initiation.

Port Aransas is protected by a wide and shallow continental shelf and a strong dune system that encircles its eastern shoreline. It is evident that the West Florida landslide scenario is not a tsunami hazard for Port Aransas in terms of flooding. However, one meter tsunami wave approaching to Port Aransas can be considered a tsunami hazard as it might create strong currents in channels, basins, and marinas. In addition it is believed that owed to the US GOM's wide and shallow shelf, a tsunami approaching to the coast might develop bore like waves with a sharp and turbulent front that can impinge on structures causing severe damages.

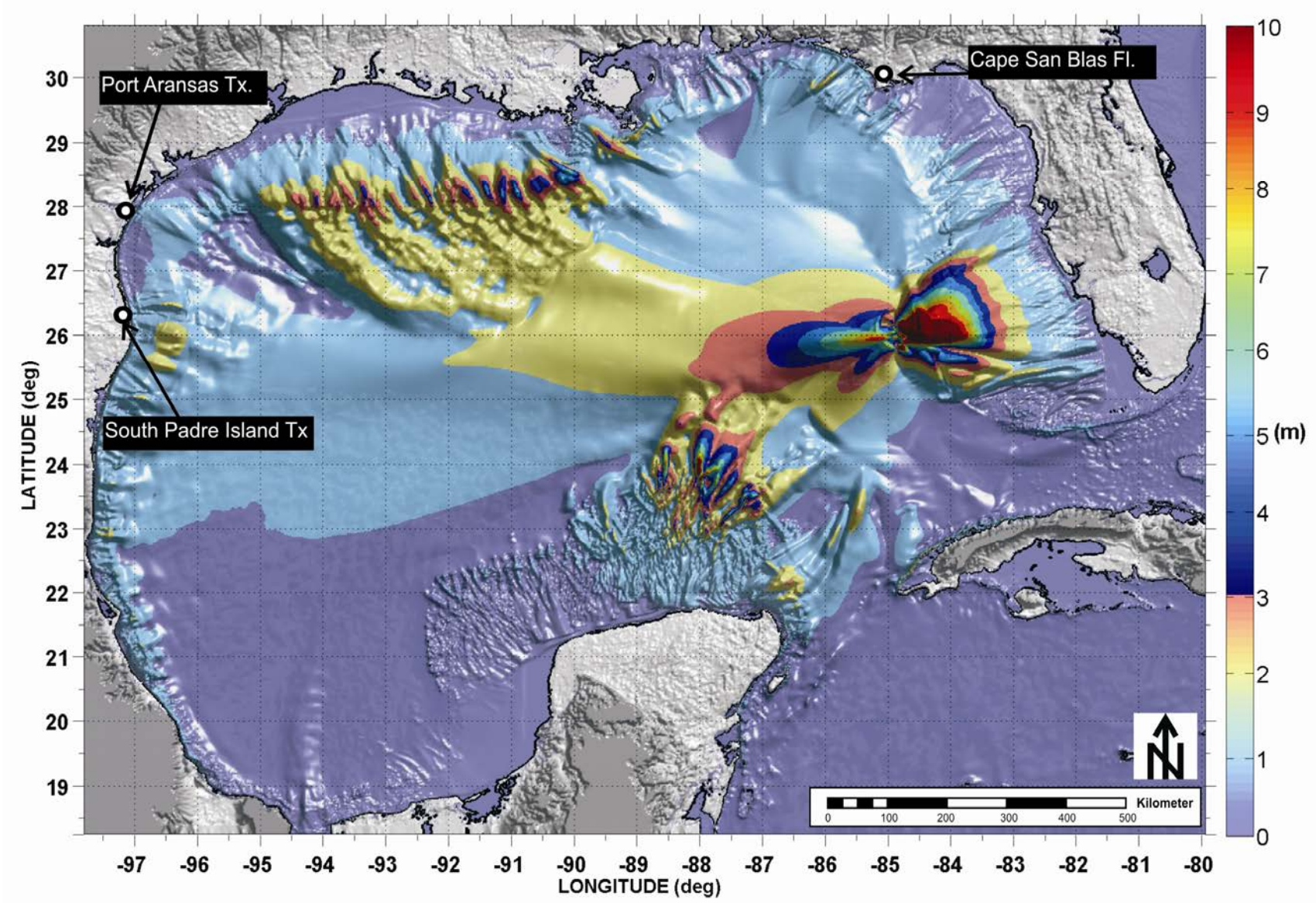


**Figure 40.** West Florida landslide maximum wave amplitude using 60 arc-seconds grid resolution.

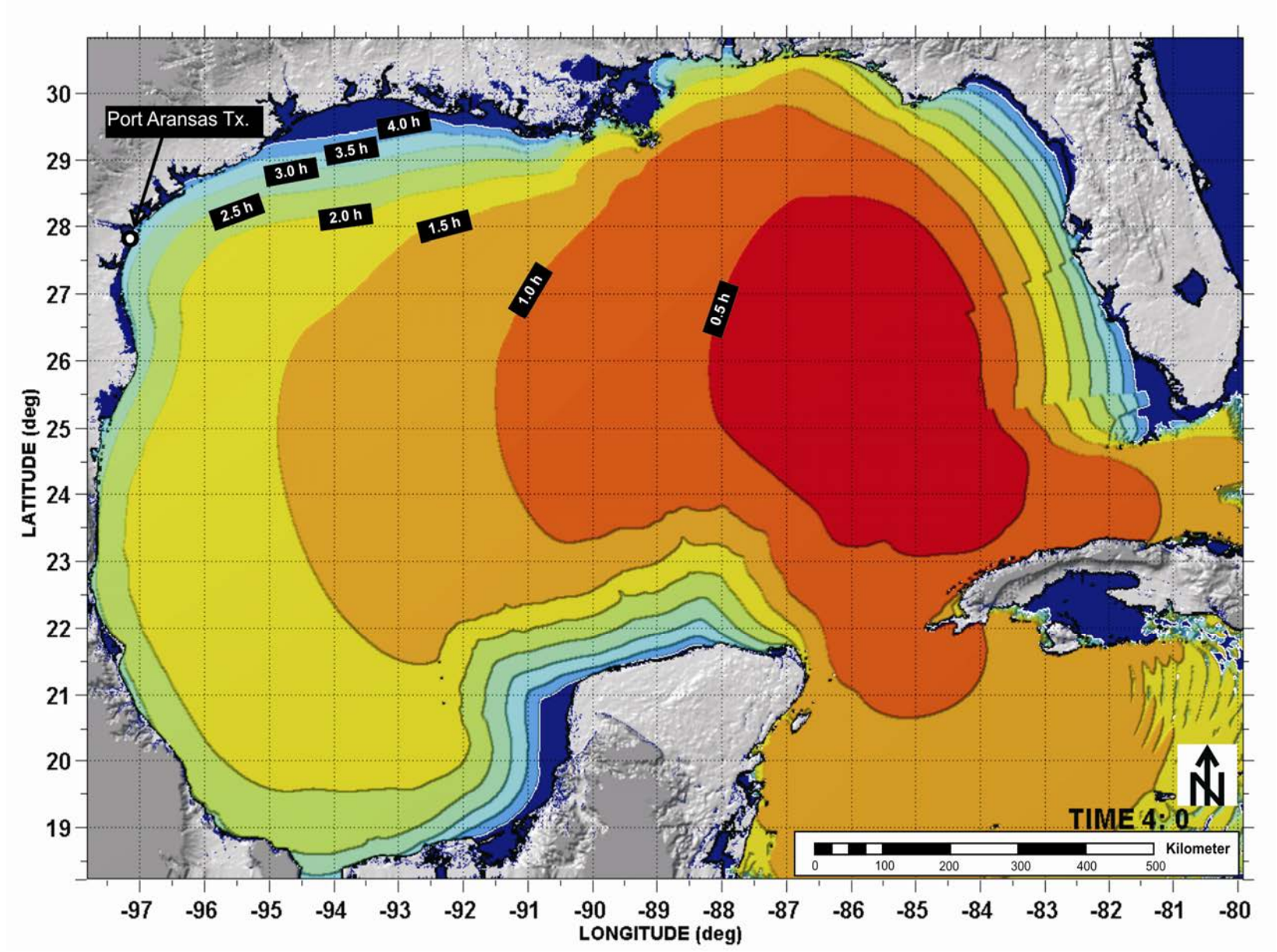


**Figure 41.** Tsunami Arrival time for the West Florida landslide.

## Future Work

The following step is to establish a systematic production of tsunami inundation maps along the US coast of the GOM aimed to provide guidance to state emergency managers and optimize real-time tsunami warnings to communities on the GOM coastline. The construction of tsunami maps will be based on identified past events of local submarine landslides (the same as in this study) and other local landslide sources determined by means of a probabilistic approach. Next generation of inundation maps for the GOM, must include, in addition to the worst case scenarios approach, a probabilistic analysis to identify potential submarine landslides with high risk of generating tsunami. The probabilistic analysis aims to estimate the hazard expressed in terms of slope failure, similar to the work described in Maretzki, Grilli and Baxter, 2007. The study will also include a complete description of ancient and probabilistic case landslide scenarios capable of producing a tsunami for risk assessment and planning purposes, which can then be included in the community model interface ComMIT. This implies that these new landslide sources can be used for future risk assessment analysis and planning purposes. The probabilistic approach results will be equally applicable to the oil industry as the recent deep water oil spill event in the GOM suggests that an established method to tsunami hazard assessment is warranted, as such hazards may put offshore rigs and pipelines located close to the landslide generation area or located in very shallow water at risk of failure, causing severe damage and oil spills. The same reasoning is applicable to the emergent field of energy generation by wind power unit, which is expected to grow in the near future in the GOM's waters.

In the model developing aspect, TSUNAMI3D model need to be implemented to cover the following features: 1- Spherical coordinates, 2- Coriolis, 3- Nesting capability (2D telescoping) and 4- turbulence closure.

## Discussion and Conclusion

Three submarine landslide scenarios, tsunamis generated by ancient landslides reported by the Tsunami Hazard Assessment Group (THAG), ten Brink *et.al*., 2009, have been used to obtained maximum tsunami amplitude, tsunami arrival time, inundation depth, inundation elevation, and momentum flux and direction in the Gulf of Mexico (GOM) and Port Aransas, TX. The three landslide scenarios are:

1. East Breaks
2. Mississippi Canyon
3. West Florida

For the construction of tsunami inundation maps for Port Aransas two numerical models were used:

1. The landslide generation (tsunami source) was taken by the 3D Navier-Stokes model developed by the University of Alaska Fairbanks (UAF) and Texas A&M University at Galveston (TAMUG) dubbed TSUNAMI3D for **T**sunami **S**olution **U**sing **N**avier-Stokes **A**lgorithm with **M**ultiple **I**nterfaces.
2. The tsunami wave propagation and inundation was carried out by the 2D non-hydrostatic/hydrostatic model developed by the University of Alaska Fairbanks (UAF) and the University of Hawaii (UH), NEOWAVE for **N**on-hydrostatic **E**volution of Ocean **WAVE**.

Our study has confirmed that these landslide scenarios have indeed the potential to cause severe flooding and damage to the GOM coastal communities. It is proved that such landslide sources can flood the entire town of Port Aransas with an average water elevation of 7 - 13ft (2.1 - 3.9m) or average water depth of 3 -8ft (0.9 - 2.4m). In term of flooding the tsunami generated by these landslide is comparable to storm surges originated by hurricanes of category 2 to 4.

Tsunami energy focusing is identified in several regions along the GOM coastline, as well. Regions most impacted are located at the southern tip of South Padre Island, TX., Grand Island, LA, Fort Walton Beach-to-Cape San Blas, FL, and the northern region of the state of Tamaulipas, Mexico. In light of this study, the possibility of the historical "tidal wave" event in Grand Island, LA. 09/1909 being a tsunami might gain some credibility and therefore needs further revision.

It is important to mention that storm surges and tsunamis are generated by different mechanism. While both can cause inundation and severe damage in coastal regions, they have quite different characteristics as well. For instance, a storm surge forces or piles up water onshore over a limited stretch of coastline. It will normally build up over a time frame of a few hours (often few fractions of a tide period). Normally wind-waves on top of the surge will contribute to cause extensive erosion and structural destruction due to the short wave period induced wave setup, current and cyclical load. On the other hand, a tsunami wave generated by a landslide often has a shorter time frame (~5-15 minutes period), can travel great distances across the basin/sea and affect vast areas of coastal land. The tsunami may develop a sharp wave front (bore like waves) as it propagates on very shallow water. The wave front may have a full-depth disturbance with greater momentum flux so the rushing flood may causes severe erosion and damage in housing stock and infrastructure in a shorter period of time. In addition tsunami waves entering into channels, marinas might create strong currents and damage.

## Acknowledgments

The study has been funded by the National Tsunami Hazard Mitigation Program under award NA09NWS4670006, ***Construction of inundation maps in the Gulf of Mexico.*** The authors thanks Professor Zygmunt Kowalik, University of Alaska Fairbanks for his input in the model development and Dr. Yoshiki Yamazaky, University of Hawaii for his unconditional support in the modeling settings and for sharing the numerical tsunami code NEOWAVE. Special thank you are due to Paul Whitmore for his

thorough reading and helpful suggestions to improve this report. The authors thanks Thomas LeBlanc for providing SLOSH results for Port Aransas, TX.

## References

2000 Census Data 2010 Retrieved October 11, 2010, 2010, from www.census.gov

Abadie S, D. Morichon, S. Grilli, S Glockner 2010 Numerical simulation of waves generated by landslides using a multiple-fluid Navier–Stokes model. *Coastal Engineering* 57 (2010) 779–794

Amante, C., & Eakins, B. W. 2009 *ETOPO1 1 Arc-Minute Global Relief Model: Procedures, Data Sources and Analysis.*

Chandrasekhar 1961 *Hydrodynamic and Hydromagnetic Stability.* Oxford : Clarendon Press.

Dunbar, P. K., & Weaver, C. S. 2008 *U.S. States and Territories National Tsunami Hazard Assessment: Historical Record and Sources for Waves.*

Gisler, Galen. 2006 Sage Calculations of the Tsunami Threat from la Palma, *Science of Tsunami Hazards*, Vol. 24, No. 4, page 288

Hirt, C.W., B.D. Nichols, 1981 Volume of Fluid (VOF) Method for the Dynamic of Free Boundaries, *J. Comput. Phys*. 39 201-225.

Horrillo J., Z. Kowalik and Y. Shigihara 2006 Wave Dispersion Study in the Indian Ocean-Tsunami of December 26, 2004. Marine Geodesy, 29:, 149-166.

Horrillo J., 2006 Numerical Method for Tsunami Calculation Using Full Navier-Stokes Equations and Volume of Fluid Method, thesis dissertation presented to the University of Alaska Fairbanks.

Kowalik Z., Horrillo J. and Kornkven E. 2006 Tsunami Runup onto a Plane Beach. In Advances in Coastal and Ocean Engineering. Advanced Numerical Models for Simulating Tsunami Waves and Runup. (ed. by F. L-F Liu, H, Yeh & C. Synolakis), vol. 10, pp. 0-5. World Scientific.

Kowalik Z., Horrillo J. and Kornkven E. 2006 Tsunami Propagation and Runup due to a 2D Landslide. In Advances in Coastal and Ocean Engineering. Advanced Numerical Models for Simulating Tsunami Waves and Runup. (ed. by P. L-F Liu, H, Yeh & C. Synolakis), vol. 10, pp. 0-4. World Scientific

Kowalik Z. and T.S. Murty,1993. Numerical Simulation of Two-Dimensional Tsunami Runup, *Marine Geodesy* 16:87-100.

Kuehne, C. M. (1973). *Hurricane Junction a history of Port Aransas*. San Antonio: St. Mary's University.

*Limits of Flooding City of Port Aransas*. 1971, U.S. Army Corps of Engineers.

Liu L-F P., P. Lynett and C.E., Synolakis 2003 Analytical solutions for forced long waves on a sloping beach, J. Fluid Mech. (2003), vol. 478, pp. 101–109.

Maretzki, S., Grilli, S.T. and Baxter, D.P. 2007. Probabilistic SMF Tsunami Hazard Assessment for the upper East Coast of the United States. In *Proc. 3rd Intl. Symp. on Submarine Mass Movements and their Consequences* (Santorini, Greece, October 2007) (Lykousis, V., Sakellariou, D., Locat, J., eds), Springer, 377-386.

Myers, T., Butman, A. E., & Brown, K. 2006 *Port Aransas Historic Resources Survey*: The Port Aransas Preservation and Historical Association.

Raichlen, F. and Synolakis, C.E. 2003 Runup from three dimensional sliding mass, in Proceedings *of the long wave Symposium 2003*, (eds. Briggs, M. Coutitas, Ch.) XXX IAHR Congress Proceedings, ISBN-960-243-593-3, 247-256.

Synolakis, C.E., E.N. Bernard, V.V. Titov, U. Kânoğlu, and F.I. González 2007 Standards, criteria, and procedures for NOAA evaluation of tsunami numerical models. NOAA Tech. Memo. OAR PMEL-135, NOAA/Pacific Marine Environmental Laboratory, Seattle, WA, 55 pp.

Synolakis, C.E., Raichlen, F. 2003 Waves and Runup generated by a three-dimensional sliding mass, in Submarine mass movements and their consequences, *Advances in Natural Hazards*, 19 eds. Locat, J. and Mienert, J. (Kluwer Academic publishers, Dordrect, 113-120)

Taylor, L. A., Eakins, B. W., Carignan, K. S., Warnken, R. R., Sazonova, T., & Schoolcraft, D. C. 2008 *Digital Elevation Model of Corpus Christi, Texas: Procedures, Data Sources and Analysis.*

ten Brink, U., D. Twichell, P. Lynett, E. Geist, J. Chaytor, H. Lee, B. Buczkowski, and C. Flores 2009 *Regional Assessment of Tsuami Potential in the Gulf of Mexico*: U.S. Geological Survey.

ten Brink, U.S., Geist, E.L., and Andrews, B.D. 2006 Size distribution of submarine landslides and its implication to tsunami hazard in Puerto Rico: *Geophysical Research Letters, v. 33,* p. doi:10.1029/ 2006GL026125.

U.S. Coastal Relief Model. (2010). 2010, from ww.ngdc.noa.gov/mgg/coastal/crm.html

Watson, R. L. (2009). Texascoastgeology.com. Retrieved July 2010, from www.texascoastgeology.com

Yamazaki, Y., Z. Kowalik and Kwok Fai Cheung, 2008 Depth-integrated, non-hydrostatic model for wave breaking and run-up, *Int. J. Numer. Meth. Fluids,* DOI: 10.1002/fld.1952

Yeh, Harry, 2007 Design Tsunami Forces for Onshore Structures. *Journal of Disaster Research* Vol.2 No.6.